VOLUME 44, NUMBER 1, MARCH 2021

# HADRONIC JOURNAL

HADRONIC JOURNAL Volume 44, Number 1, March 2021

Founded in 1978 by Prof. R. M. Santilli at Harvard University. Some of the past Editors include Professors S. L. Adler, A. 0. Barut, L. C. Biedenharn, N. N. Bogoliubov, M. Froissart, J.Lohmus, S. Okubo, Nobel Laureate Ilya Prigogine, M. L. Tomber, J. P.Vigier, J. Wess, Nobel Laureate Chen Ning Yang.

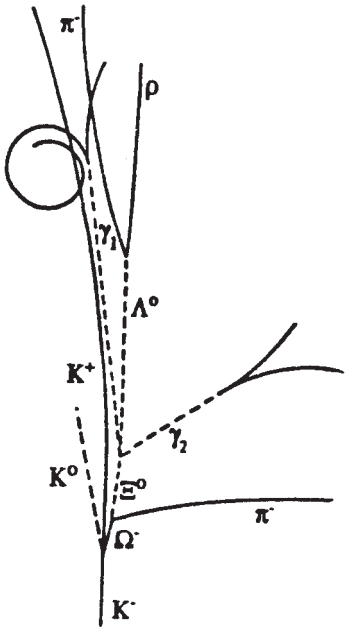


EDITORIAL BOARD

A.O.ANIMALU
A. K. ARINGAZIN
A. A. BHALEKAR
S. J. DHOBLE
J. DUNNING-DAVIES
T. L. GILL
L. P. HORWITZ
S. L. KALLA
S. I. KRUGLOV
M. NISHIOKA
R. F. O'CONNELL
Z. OZIEWICZ
E. RECAMI
M. SALEEM
B. G. SIDHARTH
S. SILVESTROV
H. M. SRIVASTAVA
E. TRELL
R.I. TSONCHEV
QI-REN ZHANG
C.A.WOLF
YI-ZHONG ZHUO

FOUNDER and
Editor In Chief
R. M. SANTILLI

H/P HADRONIC PRESS, INC.

# HADRONIC JOURNAL

## VOLUME 44, NUMBER 1, MARCH 2021

**ANALYTIC DISTORTED – WAVE APPROXIMATION FOR NUCLEONS QUASI – ELASTIC SCATTERING CALCULATIONS, 1**
**Mirteymur Mirabutalybov**
Physics Department,
Azerbaijan State Oil and Industrial University
Baku, Azerbaijan

**DISTORTED-WAVE APPROXIMATION THEORY FOR ELECTRON SCATTERING FROM ATOMIC, 19**
**Mirteymur M.M. and Resulova A.V.**
Physics Department
Azerbaijan State Oil and Industrial University
Baku, Azerbaijan

**MULTIPLE PARTON SCATTERING AT HIGH ENERGY PROTON-PROTON COLLISIONS, 27**
**M.Y. Hussein**
Department of Physics, University of Bahrain
P.O. Box 32038, Kingdom of Bahrain and
Search Center, Shaikh Ebrahim Bin Mohammed
Al Khalifa Center for Culture and Research
P.O. Box 13725, Muharraq, Kingdom of Bahrain

**HEAT MASS TRANSFER OF NANOFLUIDS FLOW WITH ABSORPTION IN THE PRESENCE OF THERMAL RADIATION, 35**
**S.Y. Zayyanu, I.J. Uwanta and M.M. Hamza**
Department of Mathematics
Usmanu Danfodiyo University
Sokoto, Sokoto, Nigeria

**NEW THERMODYNAMICS: INELASTIC COLLISIONS, LOST WORK, AND GASEOUS INEFFICIENCY, 67**
**Kent W. Mayhew**
68 Pineglen Cres.
Ottawa, Ontario, Canada, K2G 0G8
**CALCULATION OF THE EXACT RANGE OF THE MASS OF HIGGS BOSON IN THE LARGE HADRON COLLIDER (LHC) ON THE BASIS OF THE QUANTIZED SPACE AND TIME THEORY, 97**
**Hamid Reza Karimi**
Electrical Engineering Department, Islamic Azad University
South Tehran Branch, Tehran, 17776-13651, Iran

**HADRONIC JOURNAL 44**, 1 - 17 (2021)
DOI 10.29083/HJ.44.01.2021


# ANALYTIC DISTORTED – WAVE APPROXIMATION FOR NUCLEONS QUASI – ELASTIC SCATTERING CALCULATIONS

**Mirteymur Mirabutalybov**
Physics Department,
Azerbaijan State Oil and Industrial University
Baku, Azerbaijan
mmmteymur@yahoo.com

Received June 10, 2020
Revised June 29, 2020

## Abstract

On the basis of non-relativistic theory in the distorted-wave approximation in three dimensions, a theory of quasi-elastic knock-out of nucleons from nuclei by nucleons has been developed. On the basis of this theory the differential cross sections of quasi-elastic knock-out reactions of protons $1P$ and $1S$ in the with shells nucleus $^{16}O$ and $^{12}C$ have been calculated, which allows to determine the orbital moments of the nucleons in the nucleus before scattering by the angular distribution of emitted protons.

**Keywords:** Quasi-elastic nucleon scattering.

Excitation nucleus. Emitted protons

Copyright © 2021 by Hadronic Press, Inc., Palm Harbor, FL 34684, USA

## 1 Introduction

The reactions of knocking out nucleons from nuclei by protons, sometimes called quasi-elastic scattering, in the region of intermediate initial energies (*150-1000MeV*), the experiments in which it was studied, confirmed the correctness of the model of direct knocking out of a particle from the nucleus and the shell structure of nuclei.

When using protons with an energy of $\sim 1GeV$ as test particles, the difficulties in interpreting experimental data are much less than when using particles of lower energies. Despite the qualitative progress in understanding quasi-elastic processes, unresolved problems still remain. First of all, there is no quantitative description of the experimental differential cross sections ([1], [2]).

It is convenient to begin a qualitative description of knockout reactions with an idealized single-particle approximation in which the inelastic interaction of nucleons with nuclei can be represented as a sequence of independent intranuclear nucleon-nucleon collisions. When calculating the transition matrix element, the wave function of the nucleus is usually selected from the shell or cluster models of the nucleus.

The experimental data obtained in the study of knockout reactions undoubtedly contain information about the structure of the nucleus; however, the complexity of the interpretation of the reaction mechanism makes it difficult to extract it [3].

The peculiarity of the reaction of knocking out protons and neutrons under the action of nuclei of intermediate energies is that this process can occur mainly with the most weakly bound nucleons that are on the "surface" of the nucleus. Therefore, such a process is called direct or surface interaction ([4],[5]).

In the theory of direct interaction of a falling nucleon with a nucleus, it is assumed that some of the nucleons interact with the nucleus in such a way that it transfers a significant part of its energy to one (or several) nucleons that are emitted before the energy has time to be distributed over other degrees of freedom associated with a change in the state of many nucleons.

**2 The first part of the proposed theory**

The aim of this work is to obtain a general rigorous expression for the amplitude of quasi-elastic scattering of intermediate-energy nucleons on nuclei from a single position based on three-dimensional quasi-classics in the framework of the high-energy approximation.

Let us consider the derivation of a formula that determines the angular distribution of protons in the reaction of the surface interaction of incident neutrons on the target nucleus.

We write the differential cross section of the reaction A(n, np)B in the following form [6]:

$$d\sigma_{n,np} = (2\pi)^4 \frac{m}{k} d\mathbf{p}_f d\mathbf{p}_p \delta(E_i - E_f - E_p - E_N - E_R) \frac{1}{2J_i+1} \sum_{\sigma_i \sigma_f} \sum_{M_i M_f} |T_{if}|^2 \quad (1)$$

Here, $\mathbf{p}_f$, $\mathbf{p}_p$ the three-dimensional moment of scattered neutrons and knocked-out protons, and $E_i$, $E_f$ are the kinetic energies of incident and scattered neutrons. The energy of knocked-out protons is $E_p$, and the detachment energy of the least bound proton is - $E_N$. Finally, the recoil energy of the daughter nucleus is $E_R = \frac{P_R^2}{2M_{A-1}}$, which is determined using the recoil nucleus momentum ($\mathbf{P}_R$) and in turn, is associated with the missing mass ($M_R$) from the reaction based on the law of conservation of energy:

$$M_R = [(M_A - m_p + E_i - E_f - E_p)^2 - P_R^2]^{1/2} \quad (2)$$

For the missing mass, the connection between the nucleon separation energy ($E_N$) and the mass of the daughter nucleus ($M_{A-1}$), which is known from the experiment, is used.

$$E_N = M_R - M_{A-1} \quad (3)$$

Consider the derivation of the formula that determines the angular distribution of knocked-out protons in the reaction of the surface interaction of the incident neutron on the nucleus - $A$. For this case, we write the wave function of the initial state of the system $n + A$ in the following form:

$$\psi_{A-1}(\mathbf{r}) \psi_{nl}(r_p) Y_{lm}(\theta_p, \varphi_p) \psi_{\mathbf{k}_i}(\mathbf{r}'), \quad (4)$$

where $r_p, \theta_p, \varphi_p$ - are the polar coordinates of the proton in the nucleus - $A$, $\mathbf{r}$ -, are the coordinates of all other nucleons in the nucleus; $\mathbf{r}'$ and $\mathbf{k}_i$ - respectively, the coordinate and the wave vector of the incident neutron. After the proton emits a nucleus, the final state corresponds to a nucleus $A-1$, whose

wave function with a large distance of nucleons from the nucleus has the form:

$$\psi_{A-1}(\mathbf{r})\psi_{\mathbf{k}_f}(\mathbf{r}')\psi_{\mathbf{k}_p}(\mathbf{r}_p), \qquad (5)$$

where $\mathbf{k}_f$ and $\mathbf{r}'$ - are the wave vector and coordinate of the scattered neutron, respectively, and $\mathbf{k}_p$ - is the wave vector of the knocked-out proton.

The potential responsible for the direct interaction $v(|\boldsymbol{r}' - \boldsymbol{r}_p|)$ – represents the interaction of the incident neutron with the proton of the nucleus - $A$, a $U(|\mathbf{r}_p - \mathbf{r}|)$ is the potential of the interaction of the emitted proton with the nucleus of the residue, which is nonzero only on the "surface" of the nucleus, that is, under the condition $r_n = r_p = R$.

The matrix element of the transition of the nucleus is represented as ([8], [11]).

$$T_{if} = \langle f \left| \int d\mathbf{r}' d\mathbf{r}_p \Pi(r')\psi^{(+)}_{\mathbf{k}_i}(\mathbf{r}')M(r_p) \right| i \rangle, \quad (6)$$

here

$$\Pi(\boldsymbol{r}') = \psi^{(-)*}_{k_f}(\boldsymbol{r}')\psi^{*}_{k_p}(\boldsymbol{r}_p)v(|\boldsymbol{r}' - r_p|)$$

and

$$M(\boldsymbol{r}_p) = \psi_{nl}(\boldsymbol{r}_p)Y_{lm}W(\boldsymbol{r}_p)\delta(|\,\boldsymbol{r}_p - \boldsymbol{R}|)$$

where

$$W(\mathbf{r}_p) = \int \psi^{*}_{A-1}(\mathbf{r})U(|\mathbf{r}_p - \mathbf{r}|)\psi_{A-1}(\mathbf{r})d\mathbf{r} \qquad (7)$$

The wave functions of scattered nucleons obtained in [7] from the solution of the non-relativistic Schrödinger equation are written in the following form

$$\psi^{(-)*}_{\mathbf{k}_f}(\mathbf{r}')\psi^{(+)}_{\mathbf{k}_i}(\mathbf{r}') = e^{i[\mathbf{q}\mathbf{r}' + \phi(\mathbf{r}',\mathbf{q})]}, \qquad (8)$$

here $\phi(\mathbf{r}', \mathbf{q})$ it is a distorting function of scattered nucleons and depends on the distribution of nucleon density in the nucleus.

Expressing now in (6) the potential of two-nucleon interaction through the amplitudes of nucleon-nucleon scattering -

$$f_{NN}(\mathbf{q}') = -\frac{m_N}{4\pi\hbar^2}\int e^{i\mathbf{q}'\mathbf{r}'}\upsilon\ (|\mathbf{r}' - \mathbf{r}_N|)d\mathbf{r}', \quad (9)$$

using the Fourier transform, for the matrix element of the transition of the nucleus we get

$$T_{if} = \frac{-\hbar^2}{2\pi^2 m_p}\langle f | \int H_1 f_{NN}(q')\, M(\boldsymbol{r}_p)d\boldsymbol{r}'d\boldsymbol{q}'d\boldsymbol{r}_p | i \rangle \qquad (10)$$

here

$$H_1 = e^{i(qr'+\phi)} e^{-ik_p r_p} e^{-iq(r'-r_p)}.$$

In order to simplify the calculation, the wave function of the knocked-out proton is taken in the form of a plane wave.

To calculate the matrix element (10), replacing the variables in the phase $\mathbf{u} = \mathbf{r}' - \mathbf{r}_p$ after integration we obtain:

$$T_{if} = \frac{-4\pi\hbar^2}{m_p} \langle f | \int H_2 W(\boldsymbol{r_p}) \delta(|\boldsymbol{r_p} - \boldsymbol{R}|) d\boldsymbol{r_p} | i \rangle \tag{11}$$

here

$$H_2 = e^{i[qr_p + \phi(r_p) - ik_p r_p]} \psi_{nl}(\boldsymbol{r_p}) Y_{lm} f_{NN}(\boldsymbol{q_{eff}}).$$

Now, we choose the coordinate system in which $Oz \uparrow\uparrow \mathbf{q}$ . We denote $\cos(\hat{\mathbf{q}}\,\hat{\mathbf{r}}) = \mu$ where $\mathbf{r} = \{r\mu\varphi\}$. This allows taking into account the energy loss, the momentum transmitted by the incident nucleon to the target nucleus can be written as:

$$|\mathbf{q}| = |\mathbf{k}_i - \mathbf{k}_f| = \sqrt{k_i^2 + k_f^2 - 2k_i k_f \cos\vartheta} =$$
$$= (\frac{2m}{\hbar^2})^{1/2} \sqrt{E_i + E_f - 2E_i^{1/2} E_f^{1/2} \cos\vartheta} \tag{12}$$

The scattering angle $\vartheta = \vartheta_1 + \vartheta_2$ and the deflection angles of the incident ($\vartheta_1$) and scattered particles relative to the axis OX and $\vartheta_3 = (\hat{\mathbf{k}}_i \hat{\mathbf{k}}_j)$ the scattering angle of the knocked out particle in a three-dimensional coordinate system are related as follows :

$$\cos(\hat{\mathbf{r}}\hat{\mathbf{k}}_i) = \mu \sin\vartheta_1 + \cos\vartheta_1 \sqrt{1-\mu^2} \cos\varphi$$
$$\cos(\hat{\mathbf{r}}\hat{\mathbf{k}}_f) = -\mu \sin\vartheta_2 + \cos\vartheta_2 \sqrt{1-\mu^2} \cos\varphi \tag{13}$$
$$\cos(\hat{\mathbf{r}}\hat{\mathbf{k}}_j) = -\mu \sin(\vartheta_3 - \vartheta_1) + \cos(\vartheta_3 - \vartheta_1) \sqrt{1-\mu^2} \cos\varphi$$

$$tg\vartheta_1 = \frac{E_i^{1/2}}{E_f^{1/2}} \frac{1}{\sin\vartheta} - ctg\vartheta$$

We immediately note that the angles $\vartheta$ and $\vartheta_3$ are determined from the experiment.

Now, to calculate the integral expression (10), we apply the recurrence formula obtained in [7]. In this case, the amplitude of the free nucleon – nucleon interaction is selected in the following parameterized form [9]:

$$f_{n,p}(q') = \frac{ik\sigma_{p,n}}{4\pi} (1 - i\varepsilon_{p,n}) \ell^{-\frac{\beta_0^2 q'^2}{2}} \tag{14}$$

Immediately, we note that in the calculations for the parameters of free - interaction, the following values are taken in expression (14).

$$\sigma_p = 4.75 \ \phi M^2, \quad \varepsilon_p = -0.05, \quad \beta_0^2 = 0.21 \ \phi M^2;$$
$$\sigma_n = 4.04 \ \phi M^2, \quad \varepsilon_n = -0.5; \tag{15}$$

After that, the amplitude of the process, simplifying, takes the following form:

$$T_{if} = \frac{-\hbar^2 k \sigma_{NN}}{2m_p}(i+\varepsilon_0)\ell^{\frac{-\beta_0^2 q^2}{2}} W(R)\sum_{n=0}^{3} a_n \frac{\partial^n I(q)}{\partial q^n} \quad (16)$$

where

$$I(q) = \int \ell^{i(\mathbf{q}-\mathbf{k}_p)\mathbf{R}} \psi_{nl}(R) Y_{lm}(\theta_p, \varphi_p) d\Omega \quad (17)$$

$$W(R) = \langle f | \int \psi^*_{A-1}(\mathbf{r})\ U(|\mathbf{R}-\mathbf{r}|)\psi_{A-1}(\mathbf{r}) d\mathbf{r} | i \rangle \quad (18)$$

An explicit expression of the potential at the center of the nucleus is $U(0)$, functions $a_n(q)$ and distorting parameters $a, b$ that depend on the distribution of nucleon density in nuclei are given in [10].

When calculating the integral (17), we use the expansion of a plane wave in spherical functions [11]:

$$\ell^{i(\mathbf{q}-\mathbf{k_p})\mathbf{R}} = \sum_{L=0}^{\infty} i^L \sqrt{4\pi(2L+1)}\ j_L(|\mathbf{q}-\mathbf{k}_p|R) Y^*_{L0}(\theta), \quad (19)$$

after taking into account the orthogonality condition in (17), we obtain

$$I(q) = \sum_{L=0}^{\infty} i^L \sqrt{4\pi(2L+1)}\ j_L(|\mathbf{q}-\mathbf{k}_p|R)\psi_{nL}(R), \quad (20)$$

here $j_L(|\mathbf{q}-\mathbf{k}_p|R)$ is the Bessel function and

$$|\mathbf{q}-\mathbf{k}_p| = \sqrt{q^2 - 2|\mathbf{q}||\mathbf{k}_p|\cos(\tfrac{\pi}{2}+\vartheta_3-\vartheta_1)+k_p^2}\ . \quad (21)$$

It is known that experiments on the angular distribution of the products of the reaction of direct interaction make it possible to judge the properties of the energy levels of nuclei. Therefore, expression (20) allows determining from the angular distribution – $L$, of the emitted protons.

Finally, we proceed to the calculation of the integral (7). Moreover, in the interaction potential of a knocked-out proton with nucleons of the residual nucleus, the two-particle interaction potential is taken into account in an asymptotic form due to single-peon exchange, which allows us to write:

$$W(R) = -\frac{4\pi\ \hbar^2}{m}\gamma \int \frac{\ell^{-k_0|\mathbf{R}-\mathbf{r}|}}{|\mathbf{R}-\mathbf{r}|}\rho(\mathbf{r})d\mathbf{r}, \quad (22)$$

here $\gamma = g^2/\hbar c = 0.081 \pm 0.002$ the coupling constant, which determines the potential obtained by analyzing scattering $\pi$- mesons at nucleons $k_0 = \frac{m_\pi c}{\hbar}$, whose inverse value corresponds to the radius of action of nuclear forces.

To calculate the integral (22), the density distribution of nucleons in the ground state of the residual nucleus is selected in the form of a Fermi - function:

$$\rho_N(r) = \rho_0(1+\ell^{\frac{r-R}{d}})^{-1} \quad (23)$$

Moreover, using the pole method [7] of calculating the integral (22), we have

$$W = W_0(d)\ell^{-k_0 R}[\cos(dk_0) - i\sin(dk_0)] \quad (24)$$

where $W_0(d) = i(2\pi)^3 \frac{8\hbar^2\gamma}{m} dR\rho_0\{1+\frac{3i}{2}\frac{\pi d}{R} - \frac{1}{2}(\frac{\pi d}{R})^2\}$ (25)

We examined the knocking out of protons from nuclei by scattering of nucleons, i.e. reaction $(n,np)$ type, however, the results can be directly applied to reactions $(p,np)$, $(p,2p)$ and $(n,2n)$ as well because the Coulomb interaction is not taken into account. Since direct interaction is significant at medium and higher nucleon energies, the effect of the Coulomb interaction on the angular distribution is not significant.

Thus, the final expression of the differential cross section for quasi-elastic scattering of nucleons on nuclei can be writ

$$\frac{d^3\sigma}{d\Omega_1 d\Omega_2 dE_f} = \aleph_0(q)\sum_{L=0}^{\infty} i^{2L}(2L+1)\left|\psi_{n'L}(R)\sum_{n=0}^{3} a_n(q)\frac{\partial^n j_L(|\mathbf{q}-\mathbf{k}_p|)}{\partial q^n}\right|^2 \quad (26)$$ where

$$\mathcal{N}_0(q) = (2\pi)^5\hbar^4 m_p^2\sigma_{NN}^2(1+\varepsilon_0^2)e^{-\beta_0^2 q^2}\overline{W} \quad (27)$$

here

$$\overline{W} = |W(R)|^2 E_f^{1/2}\,(E_i - E_f - E_N - E_R)^{1/2}$$

Since in the future these reactions will be studied on light nuclei, it is desirable to give explicit expressions of the radial wave functions of nucleons for the $\psi_{n'L}(R)$ для $1s$ and $1p$ states in the nuclei obtained from the solution of the non-relativistic Schrödinger equation for a spherically symmetric potential [12]:

$$\psi_{1s}(R) = 2\frac{R}{a_0}\pi^{-\frac{1}{4}} exp(-\frac{R^2}{2a_0^2}) \quad (28)$$

$$\psi_{1p}(R) = \left(\frac{8}{3}\right)^{\frac{1}{2}}\frac{R^2}{a_0^2}\pi^{-\frac{1}{4}} exp(-\frac{R^2}{2a_0^2}) \quad (29)$$

## 3 The results of the first part of theoretical calculations

The proposed approach allows one to calculate the differential cross section by knocking out nucleons with protons with energy $E_i = 1GeV$, using a variation of the parameter characterizing the thickness of the surface layer $(d)$ of the nucleus.

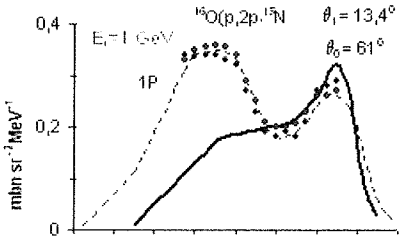

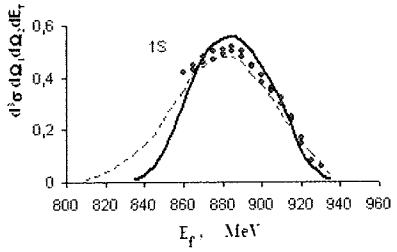


Fig.1: Experimental (dots) and theoretical (solid line) differential cross sections for quasi-elastic proton knockout reactions from sub shells $1p$ and $1s$ nucleus $^{16}O$ at angles $\vartheta_1 = 13{,}4^\circ$, $\vartheta_0 = 61^\circ$. The dashed curves are the results of [12] calculated with Hartree – Fock wave functions taking into account the excitation of the nucleus.

The results of specific calculations of the reactions A(p, 2p)B on nucleus $^{16}O$ and $^{12}C$ in comparison with experimental data are shown in Fig. 1 and 2.

The calculations were mainly performed for different angles of release of slow protons at a fixed scattering angle ($\vartheta_3 = 61^\circ, 64^\circ, 67^\circ, 73^\circ$) of fast protons $\vartheta = 13{,}4^\circ$. The figures show the results only for the emission angle $\vartheta_3 = 61^\circ$ of slow protons [13]. An analysis of the results shows that the scattering cross section weakly depends on the angles of the knocked out protons.

Nuclei $^{16}O$ and $^{12}C$ can emit protons from levels $1p, 1s$ therefore the differential cross section is calculated for each of these cases. In the experiment, slow protons were recorded at energies $E_p = (60 \div 105) MeV$ (the theoretical cross section coincides with those measured by the registration of fast protons at precisely these energies of slow protons).

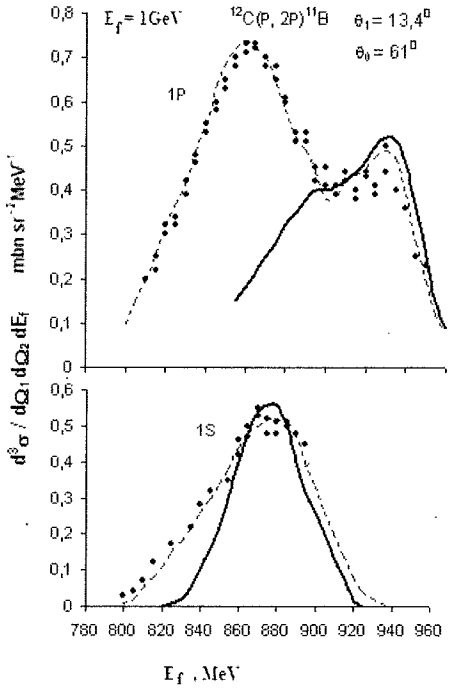


Fig.2: The same as in fig.1, but for the nucleus $^{12}_{6}C$.

As can be seen from Fig. 1 and 2, the theoretical curves obtained in this work for knocking out protons from the level $1p$, unlike the experiment, have only one maximum. Apparently, this is a consequence of the fact that the process considers absolute quasi-elastic proton knockout, that is, the residual nucleus is not excited. However, the shift of the maximum toward higher energies is due to the fact that distortion is not taken into account in the wave function of the knocked-out proton.

For comparison, the figures also show theoretical curves calculated in the distorted-wave pulse approximation, where the Hartree - Fock wave functions were used for nuclear nucleons. Moreover, the authors of [12] also took into account the excitation of the residual nucleus.

**4 Analysis of the results**

Based on the above-developed theory, the calculated differential cross sections for quasielastic proton knockout reactions from subshells $1p$ and $1s$ in nuclei $^{16}$O and $^{12}$C make it possible to determine the orbital moments of these nucleons in nuclei before scattering from the angular distribution of emitted protons.

Thus, we can come to the conclusion that such calculations are convenient for practical use with analytical wave functions of the nucleus.

From an analysis of the results obtained, it follows that the knockout reaction requires a more rigorous consideration of intranuclear wave functions, in particular, a more accurate consideration of the excitation of the residual nucleus, i.e. single-particle [14] and collective ([15],[16]) also distortions in the wave functions of knocked out nucleons from nuclei.

## 5 The second part of the proposed theory

*Knocking out nucleons from nuclei taking into account excitation of the residual nucleus*

Nucleons of medium and higher initial energies participating in nuclear reactions have a wavelength shorter than the size of the nucleus, which allows us to consider their motion quasiclassically and talk about the "location" of the nucleon entering the nucleus, as well as the "trajectory" of its motion inside the nucleus, which makes it convenient accounting for changes in the phase of the incident and outgoing waves.

In addition, for these incident nucleons the "transparency" of the nucleus increases and it becomes possible to interact with the transfer of energy to one nucleon sufficient to remove it outside the nucleus, not only with "surface" loosely coupled nucleons, but also with "deep" nucleons. This leads to a rearrangement of nucleons at energy levels on the surface of the target nucleus, i.e. excitation of the nucleus.

Considering the above, we consider the reaction of quasielastic knocking of protons by nucleons from the nucleus, and with the transition of nucleons in the nucleus of the residue to the upper energy level.

We write down the wave functions of the system for the reaction. In this case, the wave function of the initial state has the form [11]:

$$\psi_{A-1}(\mathbf{r},r_2)\varphi_{jm_2}(\theta_2,\varphi_2)\psi_{nl}(r_3)\varphi_{lm_3}(\theta_3,\varphi_3)\chi_{1/2\mu}\psi_{\mathbf{k}_i}(\mathbf{r}') \quad (30)$$

where is the $r_3$ - coordinate, $\varphi_{lm_3}(\theta_3,\varphi_3)$ - is the spin is the angular function of the knocked out proton in the nucleus-$A$, $r_2$ - is the coordinate and $\varphi_{jm_2}(\theta_2,\varphi_2)$ - is the spin is the angular function of the underlying proton in this nucleus; $\mathbf{r}'$, $\mathbf{k}_i$ and $\chi_{1/2\mu}$ - , are the coordinate, wave vector, and spin function of the incident nucleon, respectively. The final state corresponds to the nucleus, which is obtained after filling in the nucleus $A$, with the underlying proton ($\mathbf{r}_2$) of the proton emitted by the nucleus. The wave function of this state takes the following form

$$\psi_{A-1}(\mathbf{r},r_2)\varphi_{j'm'_2}(\theta_2,\varphi_2)\psi_{\mathbf{k}_3}(\mathbf{r}_3)\chi_{1/2m'_1}\psi_{\mathbf{k}_f}(\mathbf{r}')\chi_{1/2\mu'} \quad (31)$$

where $\varphi_{j'm'_2}$ is the spin - angular function occupying the underlying proton in the nucleus - $B$, $\mathbf{k}_3,\mathbf{r}_3$ and $\chi_{1/2m'_1}$ - are the wave vectors, coordinates, and spin function of the knocked-out proton, respectively; $\mathbf{k}_f$, $\mathbf{r}'$ and $\chi_{1/2\mu''}$ - correspond to the scattered nucleon.

*If there is only one nucleon outside the closed shells A and B, then the* spin - angular functions that determine the angular dependence of the wave functions of the initial and final states of the nucleus will take the form :

$$\varphi_{lm_3} = \sum_{m_3''} (l\,½ m_3'', m_3 - m_3'' \Big| jm_3) Y_{lm_3''} \chi_{½, m_3 - m_3''} \quad (32)$$

The transition matrix element is now written

$$T_{if} = \sum_{\sigma_N \sigma_p} \langle f \Big| \int \psi^{(-)*}_{k_f}(\mathbf{r}') \psi^*_{\mathbf{k}_3}(\mathbf{r}_3) \varphi^*_{j'm'}(\theta_2, \varphi_2) \chi^*_{½ m_3'} \chi^*_{½ \mu'} v(|\mathbf{r}' - \mathbf{r}_3|)$$

$$\psi^{(+)}_{\mathbf{k}_i}(\mathbf{r}') \varphi_{jm}(\theta_2, \varphi_2) \psi_{nl}(\mathbf{r}_3) \varphi_{im_3}(\theta_3, \varphi_3) \chi_{½ \mu} d\mathbf{r}_3 W(\mathbf{r}_3) \delta(|\mathbf{r}_3 - R|) \Big| i \rangle,$$

here the summation is carried out over the spin variables of the scattered nucleon and the knocked-out proton, and

$$W(\mathbf{r}_3) = \int \psi^*_B(r_2, \mathbf{r}) U(|\mathbf{r}_3 - \mathbf{r}|) \psi_{A-1}(r_2, \mathbf{r}) d\mathbf{r} \quad (33)$$

After a similar conduct of all mathematical operations applied above, the matrix element, simplifying, takes the form

$$T_{if} = \frac{-\hbar^2 k \sigma_{NN}}{m} (i + \varepsilon_0) e^{-\beta_0^2 q^2} W(R) \sum_{\sigma_N \sigma_p} \sum_{n=0}^{3} a_n(q, \beta) \frac{\partial^n J(q)}{\partial q^n} \quad (34)$$

$$J(q) = S(J) \sum_{L=0}^{\infty} i^L \sqrt{4\pi(2L+1)} \;\; j_L(|\mathbf{q} - \mathbf{k}_3| R) \psi_{nL}(R) \quad (35) \quad \text{here}$$

$$S(J) = \sum_{M=-J}^{J} \int \varphi^*_{j'm'}(\theta_2, \varphi_2) Y_{JM}(\theta) \varphi_{i\mu}(\theta_1, \varphi_1) \varphi_{jm}(\theta_2, \varphi_2) d\Omega$$

Now, a few words about the calculation of the integral expression- $S(J)$. Moreover, the product of two spherical functions of the same angular variables $(\theta_2, \varphi_2)$ is expressed through a linear combination of spherical functions of the same variables. The calculation of the sum of the magnetic quantum numbers of the products of the vector addition coefficients is carried out according to the Raka method [11].

So, the differential cross section for quasi-elastic knocking out of nucleons by single-particle excitation of the residual nucleus can be written as follows:

$$\frac{d^3\sigma}{d\Omega_1 d\Omega_2 dE_f} = \aleph(q) S^2(J_1, J, J_2) \sum_{\sigma_i \sigma_f} \sum_{L=0}^{\infty} i^{2L} (2L+1) \times$$

$$\times \left| \psi_{n'L}(R) \sum_{n=0}^{3} a_n(q) \frac{\partial^n j_L(|\mathbf{q} - \mathbf{k}_3| R)}{\partial q^n} \right|^2, \quad (36)$$

where

$$S^2 = (2L_2 + 1)(2L_1 + 1)(2J_1 + 1) W_R^2(L_2 J_2 L_1; \tfrac{1}{2} J) \quad (37)$$

The coefficient Raka - $W_R(L_2 J_2 L_1; \frac{1}{2} J)$, is given in [11].

The energy of a knocked out nucleon is determined using the following expression

$$E_p = E_i - E_f - E_N - E_R - E^*_{A-1}, \quad (38)$$

which is determined through the recoil energy of the residual core

$$E_R = \frac{P_R^2}{2M_{A-1}} \qquad (39)$$

and the law of conservation of momentum

$$\mathbf{P}_R = \hbar\mathbf{k}_i - \hbar\mathbf{k}_f - \hbar\mathbf{k}_3 \qquad (40)$$

Here $E^*_{A-1}$ is the energy of the excited states of the daughter nucleus and is determined by the formula:

$$E^*_{A-1} = E_N - B_N, \qquad (41)$$

where $B_N$ - is the separation energy of the least bound nucleon in the daughter nucleus.

As noted above, the wave function of the slow nucleon (in this case, the knocked-out proton) is determined from the solution of the non-relativistic Schrödinger equation for a spherically symmetric potential, taking into account the spin-orbit interaction. The radial part of these functions for the studied nuclei is given in (28) and (29). The Eigen values $E_N = E_{nlj}$ of this equation, for specific nuclei, is defined as

$$E_{nlj} = E_{nl} + \Delta_{(n)l}. \qquad (42)$$

Here $\Delta_{(n)l} = |U_{ls}|(2l+1)/2$ is the distance between the split levels, which is determined from the following well-known expression [17]:

$$\Delta_{(n)l} = -20\mathbf{ls}A^{-2/3}\,MeV, \qquad (43)$$

where

$$\mathbf{ls} = \frac{1}{2}\{j(j+1) - l(l+1) - s(s+1) - \text{takes values}$$

$\frac{l}{2}$ for $j = l + \frac{1}{2}$ and $\frac{l(l+1)}{2}$ for $j = l - \frac{1}{2}$.

$$E_{nl} = \hbar\varpi(2n + l + 3/2) \qquad (44)$$

where

$$\hbar\varpi = \frac{\hbar^2}{ma_0^2}. \qquad (45)$$

During quasi-elastic knocking out of nucleons, the recoil nucleus has a hole in the shell from which the proton is emitted, and the separation energy is equal to the energy of this single-particle state. Since at the beginning the core $A$ was at rest, the momentum of the nuclear nucleon $(\mathbf{q}_0)$ before the interaction is assumed to be equal in magnitude, but opposite in direction to the momentum of the recoil nucleus in the final state, so its value can be found from the momentum conservation law (40),

$$\mathbf{q}_0 = -\mathbf{P}_R = -\hbar\mathbf{k}_{A-1}, \qquad (46)$$

$$\mathbf{q}_0 = \mathbf{k}_i - \mathbf{k}_f - \mathbf{k}_3 = \mathbf{q} - \mathbf{k}_3, \qquad (47)$$

equal in magnitude to the momentum of the nuclear nucleon before the act of

interaction.

Here, $\mathbf{q}=\mathbf{k}_i-\mathbf{k}_f$ the momentum of the transfer of the scattered proton $\mathbf{k}_3$ – is the momentum of the knocked out nucleon.

It should be noted that when calculating the cross section for the sum over the spinors $\chi_i$ and $\chi_f$ - corresponding to the nucleon moment $\mathbf{k}_i$ and $\mathbf{k}_f$ before and after scattering, we obtain

$$\sum_{\sigma_i\sigma_f}\left|\chi_f^*\chi_i\right|^2=\cos^2(\vartheta/2) \quad . \qquad (48)$$

However, taking into account the above, for the sum over the spins of the knocked-out protons we get unity. Therefore, for the factor in (40) we obtain

$$\aleph(q)=\aleph_0(q)\cos^2\vartheta/2 \qquad (49)$$

In the residual nucleus, the proton transition occurs between states characterized by certain values of the angular momentum and parity. In this case, the selection rules arising from the law of conservation of moments and parity allow us to determine possible values $L$ from the so-called triangle relation.

$$\left|J_1-J_2\right|-\frac{1}{2}\le L\le J_1+J_2+\frac{1}{2}$$

$L_1+L_2+L$ - even number

**6 Applying Theory to Individual Nucleus**

The nucleus $^{16}0$ can emit protons from the levels $1P_{3/2},1P_{1/2},1S_{1/2}$ and the nucleus $^{12}C$ – from the $1P_{3/2}$ and $1S_{1/2}$ levels. Therefore, the differential cross sections calculated for each of these cases are shown in Fig.3 and 4, respectively. In addition, in these figures, for comparison, the theoretical curves calculated in [12] with the Hartree – Fock wave functions are given.

Thus, knowing the energies of the emitted nucleons and the angles of their escape, we can directly determine the energies and momentum distributions of single-particle states in specific shells of the nucleus.

The differential cross section for quasi-elastic scattering of protons with an energy of 1GeV was

calculated for $^{16}0$ and $^{12}C$. The analysis was mainly reduced to studying the shape of the correlation distributions and relative yields of protons from various nuclear shells.

The calculations were mainly performed for the emission angle $\theta_p=61^0$ of slow protons at a fixed scattering angle $\theta_1=13.4^0$ of the fast proton. In this case, the oscillator parameter was "free" with the help of which a noticeable similarity of the theoretical differential cross section with the experimental ones was obtained.

As can be seen from Fig.3, the proton energy distribution for the levels $P_{1/2}$ and $P_{3/2}$, corresponds to two maxima in the energy range of *865MeV* and *925MeV*, which can be explained on the basis of the momentum distribution of protons at the corresponding single-particle level.

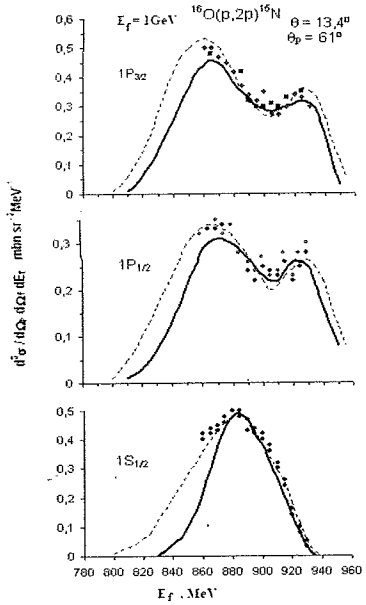


Fig.3: Differential cross sections for quasi-elastic proton knockout reactions from shells $1P_{3/2}$, $1P_{1/2}$ and $1S_{1/2}$ nuclei $^{16}_{8}O$. The points are experimental data [12], the solid line is the theoretical calculations, the dashed line is the theoretical results with the Hartree-Fock wave functions.

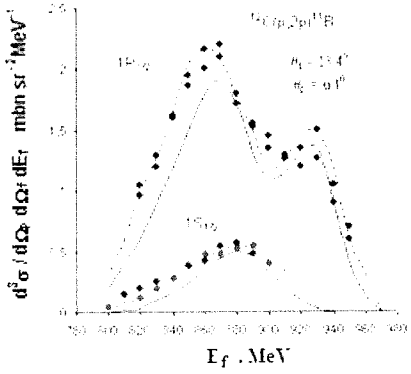


Fig.4: The same as in fig.3,
but for the nucleus $^{12}_{6}C$.

The first maximum corresponds to the population of the ground state $(1/2-)$ and $(3/2-)$.The second maximum corresponds to the excited state in the core of the residue $^{15}_{7}N$.

This figure also shows a curve describing the knockout of a proton from a state with a maximum in the energy region of *875MeV*.

In the case of a nucleus (Fig. 3and 4), the theory reproduces well the relative course of differential cross sections upon transition from one nuclear shell to

another ($1P_{3/2}$,$1S_{1/2}$).The experiment for this nucleus was performed in a wide range of kinematic allowable energies - $E_p$, therefore, it becomes possible to analyze in more detail the behavior of the correlation distributions of the emitted fast and slow protons.

As can be seen from the figures, the theoretical values of the cross sections at the maxima and minima are in good agreement with the experimental cross sections. This agreement is also achieved by correctly taking into account

This agreement is also achieved by correctly taking into account the distortion in the wave functions of protons, which are manifested in a shift in the position of the minima to the region of high energies $E_p$.

As can be seen from the figures, the theoretical values of the cross sections at the maxima and minima are in good agreement with the experimental cross sections. This agreement is also achieved by correctly taking into account the distortion in the wave functions of protons, which are manifested in a shift in the position of the minima to the region of high energies $E_p$.

Calculated and experimental energies
single-particle states in nuclei.

| Nucleus | Conditin | $a$ (Fm) | $E_{nlj}$ (MeV) | $E^*_{nlj}$ (MeV) | $E_{nlj}$ (exp.) (MeV) |
|---|---|---|---|---|---|
| $^{16}_{8}O$ | $1P_{3/2}$ | 2.27 | 18.6 | 15.98 | 19.6 |
| | $1P_{1/2}$ | 2.55 | 12.8 | 10.74 | 13.0 |
| | $1S_{1/2}$ | 1.28 | 38.1 | 33.19 | 39.2 |
| $^{12}_{6}C$ | $1P_{3/2}$ | 2.43 | 15.6 | 12.53 | 16.0 |
| | $1S_{1/2}$ | 1.33 | 35.2 | 29.09 | 33.9 |

Table1

Table-1 shows the energies calculated for single-particle levels in the nuclei $^{16}_{8}O$ and $^{12}_{6}C$ for the corresponding values of the oscillator parameter, and the energy of the excited hole state. In addition, for comparison, the experimental values of the energy of single-particle levels are also given [18].

**7 Conclusion**

It should be noted that the obtained values of the energy of single-particle excitations of residual nuclei are somewhat overestimated. This is possibly due to the fact that the contributions from collective excitations were not taken into account in the residual nuclei.

Thus, we can conclude that a satisfactory description of the shape of the

correlation distributions and relative proton yields, on the one hand, indicates that the method of accounting for wave distortions and the mathematical methods used in calculating the process amplitude are quite accurate. On the other hand, the agreement of single-particle energy spectra with both experimental data and cross-section curves calculated with the Hartree-Fock wave functions allows us to conclude that this theoretical mechanism describes well the *A(p,Np)B* reactions, as well as and core structures. Therefore, it can be used for the quantitative analysis of differential cross sections of quasi-elastic interaction of nucleons in a number of nuclei.

The effective $NN$- interaction, reconstructed from data on elastic scattering, allows one to obtain a qualitative description of quasi-free scattering and other inelastic processes. The results of a theoretical analysis of the data on quasi-elastic scattering of protons in the region of intermediate energies shows that the peripheral nature of the interaction of protons with nuclei at these energies makes this process a powerful tool for studying the surface modes of nuclear excitation.

Having made certain conclusions, it can be said that the experimental data obtained to date do not allow an exhaustive analysis and preference for one or another theoretical model of the interaction of intermediate-energy nucleons with nuclei.

**References**

[1]J.I.Johanson,H.S.Sherif,F.Ghoddoussi. Orthogonalty effects in relativistic models of nucleon knockout reactions. Nuclear Physics A, 665 (2000), 403-415.

[2] Toshmi Suda, Haik Simon, Progress in Particle and Nuclear Physics, Available online 24 April (2017).

[3] P.K. Deb, B.C. Clark, Comparison of optical model results from a microscopic Schrödinger approach to nucleon-nucleus elastic scattering with those from a global Dirac phenomenology . Phys. Rev. C. 72 (2005), 014608/25.

[4] Yahiro Massanobu, Minomo Kosho Prog,
A New Glauber Theory Based on Multiple Scattering Theory Theor. Phys. 120 (2008),757-763.

[5] M.M. Mirabutalybov, Analytic Disorted- Wave Approximation for Intermadate Energy Proton Scattering Calculations. Materialy VIII Mezinarodni Vedecko-Prakticka Konference, "Dny Vedy-2014", Dil 83 Fyzika, Praha, 3-7.

[6] M.M. Mirabutalybov, Reaction of quasi-elastic knock-out of nucleon from nuclei by protons. The LX International Conference on Nuclear Physics, (Saint Petersburg, Russia-2010),325.

[7] M.M. Mirabutalybov, Nonrelativistic descripton of nucleon-nuclear scattering. Phys. of Atomic Nuclei RAS 67 (2004), 2171-2177.

[8] M.M. Mirabutalybov, The new theory of quasielastic knock-out of protons from nuclei by nucleons. ANA of Sciences Journal of Radiation Researches, 4 (2017), 31-34.

[9] G.D. Alkhazov, A. Vorobyov, Investigation of the spatial distribution of nucleons in nuclei by the method of elastic and inelastic scattering of protons

with an energy of 1 GeV / Leningrad Nuclear Physics Preprint 969 (1984), 25-32.

[10] M.M. Mirabutalybov, Investigation of atomic nuclei by scattering particles, German, (2011). [11]

A.S. Davydov, Theory of atomic nucleus, Moscow (1958).

[12] A.V. Vorobyev, Yu.V. Dotsenko, Analysis of the nuclear correlation-structural functions in quasi-free knockout reactions of nucleons on light nuclei at T = 1 GeV Leningrad Institute of Physics PNPI, Preprint 1076 (1985), 38-45.

[13] M.M. Mirabutalybov, Reaction of Quasi-Elastic Knock-Out out of Nucleons From Nuclei by Protons, Cumhuriyet Science Journal 37 (2016),71-78.

[14] M.I. Gorenstein, W.Greiner, A. Rustamov, Strangeness Production in Light and Intermediate size Nucleus-Nucleus Collisions. Phys. Lett. B, 731 (2014). 302-306.

[15] G. Bonasera, S.Shiomo, D.H Yougblood, Isoscalar and isovector giant resonances in $^{92}$Mo and $^{90}$Zr Nuclear Physics A 992 (2019),121612.

[16] M.M. Mirabutalybov, The study of giant resonances in nuclei by inelastic electron scattering. Materialy VIII Mezinarodni Vedecko-Prakticka Konference, "Dny Vedy-2014", Dil 83 Fyzika, Praha, 49-56.

[17] V.G. Soloviev, Theory of the atomic nucleus. Nuclear models, Moscow (1981).

[18] Yu.A. Berezhnoy, Analysis of elastic proton-nuclear scattering in the Glauber-Sitenko approach, taking into account intermediate excitations of nuclei Physics of Atomic Nuclei 63(2000), 852-856.

**HADRONIC JOURNAL 44**, 19 - 25 (2021)
DOI 10.29083/HJ.44.01.2021



# DISTORTED-WAVE APPROXIMATION THEORY FOR ELECTRON SCATTERING FROM ATOMIC

**Mirteymur M.M. and Resulova A.V.**
Physics Department
Azerbaijan State Oil and Industrial University
Baku, Azerbaijan
mmmteymur@yahoo.com

Received June 20, 2020
Revised July 4, 2020

## Abstract

***Abstract:*** The expression for differential cross section of elastic and inelastic scattering of relativistic electrons from atoms has been obtained analytically on the basis of distorted-wave theory. Differential section of elastic scattering of electrons from free atoms $_{49}$In and $_{20}$Ca calculated in incident energy of electrons ~ 100 eV has been compared with experiments. Thickness of surface layer and root-mean square radius of density distribution of electron in that atoms have been determined.

***Key words:*** Distorted Electron Wave, Differential sections, Atomic Structure

Copyright © 2021 by Hadronic Press, Inc., Palm Harbor, FL 34684, USA

## 1. Introduction

At present there are many experimental and theoretical methods to investigate surfaces and surface area of atoms and solid bodies among which the reactions followed by electrons scattering should be indicated [1,2,3].

Analyses of a number of experimental data of differential cross-section of on atom nuclear showed that good conformation is obtained in the cases, when wave functions of scattered electrons are distorted both on the phase and amplitude.

These effects bring to the displacement of diffraction minimums to the side of small angles and partially fill these minimums.

Apparently these phenomena are conditioned with that distorted functions are the functions of the distribution of charges density in the nuclear [4,5,6,7].

At present for modeling of the processes of electrons scattering from free atom or atomic crystallic lattice various set up models of calculation based on Monte-Carlo method are widely used [4].

Another widely used calculation method of differential cross section of elastic and inelastic electrons scattering is Mott's method of partial waves with screened atom potential of Dirac-Hartree-Fock where phase shift of scattered waves is determined from the number integration of differential equation [5]. Application of these calculation methods in analyzing of scattering from free atoms or the atoms in crystals in big energy of incident electrons is rather labour-consuming.

It is important to consider distortion of incident and scattering waves in coulomb field of atom nuclear and electrons screening this nuclear. However it complicates calculation of scattering amplitude.

Differential cross section of elastic scattering of electron beam from free atom in work [6] has been calculated analytically considering distortions, only in phase functions of scattered spherical waves which brought to the improvement of the agreement with the results obtained by numerical methods.

Rather precise numerical method to consider distortions in the phase and in the amplitude of scattered electrons in coulomb field was obtained in the frame of high energetic approximation in work [7] by Yennie, Boss and Ravenhall from quasi-classic solution of Dirac equation.

It should be noted that such approach of calculation of distorted phase function and amplitude of scattered waves depending on distribution density of charges in the target gave satisfactory results obtained in a number of calculations of differential sections on elastic and inelastic scattering of high-energetic electrons in nuclear [8].

## 2. The proposed theory

The aim of the work is to get expression in the analytical form for the amplitude of elastic and inelastic scattering of electrons from free atom or from the crystals developing this distorted-wave theory of electrons scattering.

Moreover in the frame of terms kR>>1 and E>>V, where E- is energy of incident particle, V- is atomic potential, R- is area of potential effect; more adequate in the given work is high energetic approximation. These terms allow developing various approaches in the theory of electrons scattering.

Differential cross section of electrons scattering is determined by standard form [8]:

$$\frac{d\sigma_{if}}{d\Omega} = \frac{E_i E_f}{(2\pi)^2} \cdot \frac{k_f}{k_i} \frac{1}{2} \cdot \frac{1}{2J_i + 1} \sum_{\sigma_i \sigma_f} \sum_{M_i M_f} \left| T_{if} \right|^2 \qquad (1)$$

Matrix element of atom transition from initial state ($i$) into final ($f$) in distorted-wave high energetic approximation is presented in the form

$$T_{if} = \left\langle J_f M_f \left| \int d\mathbf{r} \Psi_f^{(-)+}(\mathbf{r}) V(\mathbf{r}) \Psi_i^{(+)}(\mathbf{r}) \right| J_i M_i \right\rangle \qquad (2)$$

For wave functions of incident and scattered electrons the following expression has been obtained

$$\Psi^{(\pm)}(\mathbf{r},\mathbf{k}) = u^{(\pm)}(\mathbf{r},\mathbf{k}) \exp[i\mathbf{kr} - i\frac{E}{k}\int_0^\infty V(\mathbf{r} \mp \hat{k}s)ds] \qquad (3)$$

where $u^{(\pm)}$ (r, k) -are spinor functions.

Wave function of atomic state $|\mathrm{JM}\rangle$ is determined in the frame of this or that atom model. Coulomb interaction of incident electron with point nuclear and atom electrons with distribution density $\rho(r)$ is chosen in the form [9]:

$$V(\mathbf{r}) = -\frac{Ze^2}{\hbar c}\frac{1}{|\mathbf{r}|} + \frac{Ze^2}{\hbar c}\int \frac{\rho(\mathbf{x})\, d^3\mathbf{x}}{|\mathbf{r}-\mathbf{x}|} \qquad (4)$$

Product of wave functions of scattered electrons is presented as

$$\Psi_f^{(-)*}\Psi_i^{(+)} = g(\mathbf{r}, \upsilon_f^+ \upsilon_i) \exp[i\mathbf{qr} + i\phi(\mathbf{r})] \qquad (5)$$

Thus, for matrix element get

$$T_{if} = \langle J_f M_f \left| -\frac{Ze^2}{\hbar c}\int d^3r g(\boldsymbol{r}) \frac{e^{i[qr+\phi(r)]}}{|r|} + \frac{4\pi Ze^2}{\hbar}\int dx \frac{g(x)e^{i[qx+\phi(x)]}}{q_{eff}^2(x)}\rho(x) \right| J_i M_i \rangle \qquad (6)$$

where

$$q_{eff}(\mathbf{x}) = \mathbf{q} + \nabla_u \phi(\mathbf{u}+\mathbf{x})_{u=0}.$$

Let's indicate function of electrons density distribution in the atom through radial transition density

$$< J_f M_f | \rho(\mathbf{x}) | J_i M_i > = \sum_{LM} \rho_L(x) Y_{LM}^*(\hat{x}) \left\langle J_i L M_i M \middle| J_f M_f \right\rangle$$

$\rho_L(x)$ –is called radial transition density of atom.Now let's indicate section through form factor

$$\frac{d\sigma}{d\Omega} = \left(\frac{d\sigma}{d\Omega}\right)_0 \frac{E_f}{E_i}\frac{k_f}{k_i}\frac{2J_f+1}{2J_i+1}\sum_{LM}\frac{1}{2L+1}|F_{LM}|^2 \qquad (7)$$

Where

$$\left(\frac{d\sigma}{d\Omega}\right)_0 = \left(\frac{2Ze^2k_i}{q^2}\right)^2 \cos^2 \theta/_2$$

for form-factor - $F_{LM}(\mathbf{q})$ get

$$F_{LM} = -\int g_0(\boldsymbol{r})\frac{e^{i[qr+\phi(r)]}}{|r|}d^3r + +q^2\int \frac{g(x)}{q_{eff}^2(x)} e^{i[qx+\phi(x)]}\rho_L(x)Y_{LM}^*(\hat{x})d^3 \qquad (8)$$

Here $\boldsymbol{q} = \boldsymbol{k}_i - \boldsymbol{k}_f$ is the impulse of electrons transfer to the target atom.

Let's write evident expression for distorting functions g(**x**) and ϕ(**x**). First of all let's write coulomb potential (4) for spherical symmetric distribution of electrons density $\rho(x)$ and present it in the form of

$$V_e(r) = -4\pi\gamma\left\{\frac{1}{r}\int_0^r \rho(x)x^2dx + \int_r^\infty \rho(x)xdx\right\}$$

here, $\gamma = e^2/(\hbar c) = 1/137$

Now, expressing distorting terms in the phase and amplitude of scattered waves through these parameters one can get:

$$\phi(\mathbf{x},\gamma) = -(\mathbf{qx})\frac{V(0)}{k} + a(3/2\,k^2x^2\mathbf{qx} - (\mathbf{k}_i\mathbf{x})^3 + (\mathbf{k}_f\mathbf{x})^3) - b([\mathbf{xk}_i]^2 + [\mathbf{xk}_f]^2)$$

$$g(\mathbf{x}) = (1-\frac{V(0)}{k})\{1 + a((\mathbf{k}_i\mathbf{x})^2 - [\mathbf{k}_i\mathbf{x}]^2 + (\mathbf{k}_f\mathbf{x})^2 - [\mathbf{k}_f\mathbf{x}]^2) + 3b((\mathbf{k}_i\mathbf{x}) - (\mathbf{k}_f\mathbf{x}))$$

Here parameter $a$, describing radial dependence of coulomb potential in the atom center is proportional to charge density

$$a = -4\pi\gamma + \frac{4\pi\gamma}{3k^3}\rho(0),$$

parameter $b$- giving curviness to wave front of the incident wave has the form

$$b = \frac{\pi\gamma}{k^2}\int_0^\infty \rho(x)dx$$

but potential in the centre of the atom have the form:

$$V(0) = -4\pi\gamma + 4\pi\gamma\int_0^\infty \rho(x)xdx$$

Before calculating integrals in form-factor (8), after applying the mathematical method of calculating the distorted-wave form-factor proposed by us in [8], then form-factor takes the following expression

$$F_{LM}(q) = -\int G_0(r)e^{iqr}d^3r + q^2\int G_{LM}(x)e^{iqx}\rho_L(x)Y^*_{LM}d^3x, \quad (9)$$

where amplitude functions $G_0(\mathbf{r})$ and $G_{LM}(\mathbf{x})$ accept the following form

$$G_0(\boldsymbol{r}) = \left(1-\frac{V(0)}{k}\right)\left\{1 + a((\boldsymbol{k}_i\boldsymbol{r})^2 - [\boldsymbol{k}_i\boldsymbol{r}]^2 + \left((\boldsymbol{k}_f\boldsymbol{r})^2 - [\boldsymbol{k}_f\boldsymbol{r}]^2\right) + \right.$$
$$\left. + b((\boldsymbol{k}_i\boldsymbol{r}) - -(\boldsymbol{k}_f\boldsymbol{r}))\right\},$$

$$G_{LM}(\mathbf{x}) = \frac{g(\mathbf{x})\{1 + i\phi(\mathbf{x}) - \frac{1}{2}\phi^2(\mathbf{x})\}}{q^2_{eff}(\mathbf{x})}$$

Thus further research both elastic and inelastic scattering of electrons from the free atom brings to the calculation of form-factor.

### 3. Application of the theory

As the form-factor of the atom is experimentally measured value in elastic scattering of electrons, then its theoretical calculation with the help of obtained analytical expression by these or other methods is of great significance.

With this purpose let's choose the following coordinate system in calculating three-dimensional integral (9). Choosing axis $oz$ $\uparrow\uparrow \mathbf{q}$ and indicating, $\cos(\hat{qx}) = \mu$, where $\mathbf{x} = \{x\mu\varphi\}$ and $d\mathbf{x} = x^2dxd\mu d\varphi$ disregarding loss of electron energy $\Delta E << E_i$, that is $|\mathbf{k}_i| = |\mathbf{k}_f| = k$ supposing that for impulse of transfer of scattered electrons we get $q = 2k\sin 9/2 = 2k\alpha$

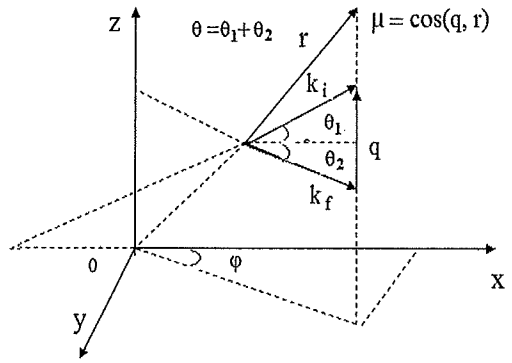


Fig.1. Impulse of incident ($\mathbf{k}_i$)and scattered ($\mathbf{k}_f$) electrons in three-dimension Decart coordinate system with transfer impulse $\mathbf{q} = \mathbf{k}_i - \mathbf{k}_f$

$$\cos \hat{x}\hat{k}_i = \mu\alpha + \sqrt{1-\mu^2}\sqrt{1-\alpha^2}\cos\varphi$$

$$\cos \hat{x}\hat{k}_f = -\mu\alpha + \sqrt{1-\mu^2}\sqrt{1-\alpha^2}\cos\varphi$$

After integration into (9) on the angles, the obtained form-factor for elastic scattering ($L=0$) can be brought to one-dimensional integral, which is the functional of Born form-factor

$$F_{L=0}(q) = \frac{2\pi i R^3}{(1-\frac{V(0)}{k})}\{F_B(q) - \frac{V(0)}{kR}\frac{\partial F_B(q)}{\partial q} -$$

$$-i3b\ [1+\frac{2(4k^2-q^2)}{3q^2R(1-\frac{V(0)}{k})}]\frac{\partial F_B(q)}{\partial q}\}.$$

However, in calculating Born form-factor - $F_B(q)$, it is necessary to choose the function of electrons density distribution in the atom.

It is known that scattered electrons on the atom surface "feel" thin structure well. Thin structure in the distribution of electrons density is revealed in three-parametric Fermi-functions with the help of parameter- $\omega$

$$\rho_e(x) = \rho_0(\omega_0 + \omega\frac{x^2}{R^2})(1+\exp(\frac{x-R}{d})^{-1} \qquad (10)$$

Pole method is used for calculation of radial integral-

$$F_B(q) = \frac{3}{4\pi R^5[1+(\frac{\pi d}{R})^2]}\sum_{\varepsilon=\pm1}\varepsilon\int_0^\infty \ell^{iqx\varepsilon}\frac{\omega_0+\omega\frac{x^2}{R^2}}{1+e^{\frac{x-R}{d}}}xdx,$$

which is shown in [8].

Final expression of differential cross section of elastic scattering of electrons from free atom has the following form:

$$\frac{d\sigma}{d\Omega} = (\frac{d\sigma}{d\Omega})_0\{|\mathrm{Re}\,F_0(q)|^2 + |\mathrm{Im}\,F_0(q)|^2\} \qquad (11)$$

where

$$\mathrm{Re}\, F_0(q) = F_B(q) - \frac{V(0)}{kR}\frac{\partial F_B(q)}{\partial q}$$

$$\mathrm{Im}\, F_0(q) = -3b\ [1 + \frac{2(4k^2 - q^2)}{3q^2R(1 - \frac{V(0)}{k})}]\ \frac{\partial F_B(q)}{\partial q}$$

$$F_B(q) = -4\frac{\pi d}{R}\cdot e^{-\pi dq}\left\{[\omega_0 + \omega(1 - 3\pi(\frac{d}{R})^2)]\sin(qR - \frac{\pi d}{R}) + \right.$$

$$\left.\left[\frac{\pi d}{R}(\omega_0 + \omega(3 - (\frac{\pi d}{R})^2))\right]\cos(qR - \frac{\pi d}{R})\right\}$$

After determination of evident expression of form-factor, elastic scattering of electrons from free atoms let's calculate differential cross section.

## 4. Results and discussions

Compactness of the obtained analytic expression of differential cross section (11) allows checking above developed theory in high accuracy level. Such examination has been carried out on the example of elastic scattering of electrons from atomics of $_{49}In$ and $_{20}Ca$ in the energy of incident electrons ~100 eV.

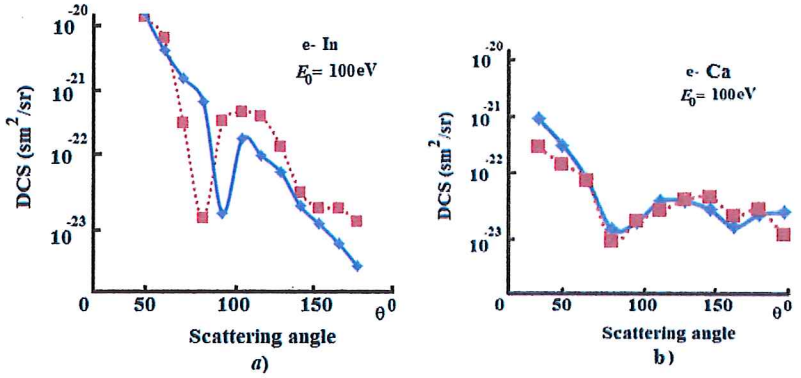


Fig.2. Differential cross section( DCS) of elastic scattering of electrons from $_{49}$In (a) and $_{20}$Ca (b) atomics by the comparison with experiments [12,13].

In fig. 2 comparison has been shown, calculated differential section with the data experiment. As it is seen from this figure-2 though in these calculations various approaches have been made while choosing potentials in this case function of electrons density distribution in the atom according to Fermi-Dirac statistics has been chosen in the form of Fermi function movement of curved differential cross sections is in a good agreement.

Thickness of surface layer of distribution of electrons density in the atom is determined with the help of the expression

$$\Delta r = r_2(0{,}1\ \rho_{max}) - r_1(0{,}9\ \rho_{max}) = 0{,}167\cdot 10^{-8}\mathrm{sm}$$

For radius of root-mean-square distribution of electrons density in atom $_{49}In$ - $< r >^{1/2} = 0{,}12 \cdot 10^{-8}\ sm$ has been found in atom radius

$R = 1{,}27 \cdot 10^{-8}\ sm$, also for atom $_{20}Ca$- $< r >^{1/2} = 0{,}12 \cdot 10^{-8}\ sm$, $R = 1{,}16 \cdot 10^{-8}\ sm$ , ($\omega_0$ =0,3; $\omega$ =0,6).

## 5. Conclusion

Thus carried out calculations and comparisons of charged atoms form-factors with the results obtained by experiments show that calculation of amplitude of elastic scattering process of electrons obtained in distorted wave high energy approximation is both convenient and precise method. This makes possibility to apply this theory to study the electronic structure of crystals by means elastic and inelastic electron scattering.

## References

[1].Tosic S.D. Measurements of differential cross sections for elastic electron scattering and electronic excitation of silver and lead atoms, Journal of Physics: Conference Series 399 (2012) p.1-6

[2]. Foram M. Joshi, Joshipura K.N., Scattering of electrons with atomic Mo: free and metallic phases, Journal of Physics: Conference Series 399 (2015) p.1-3

[3]. Salvat F., Martinez J.D, Mayol R., Parellada J. Analytical Dirac-Hatree-Fock-Slater screening function for atoms (Z=1-92), Physical Review A, v. 36, N 2 (1987) p.467-474

[4]. Saltvat F , Workshop F., Salvat J., Femandes-Varea M., Sempau J. Proc. Barcelona, Spain, 4-7 June 2006, OECD(2006), NEA N 6222

[5].Tot N. "Theory of atom Mott H., Messi G. red.Ya.I. Frenkel 2-edition M. Foreign Literature (1965) p.752

[6]. Stolyar V.A., Khuey N.Ch.T. "Analytical approach to the calculation of cross of elastic electron scattering on atom New of Volgograd State Technical University №3,3,(2009) p.15-19

[7].Yennie D.R., Boss F.L., Jr., Ravenhall D.G. Analytic distorted-wave approximation for high-energy electron scattering calculations Phys.Rev.B, v.137, N 4,(1965) p. 882-903

[8]. Mirabutalybov M.M. Study of atomic nuclei by scattering particles . Academic Publishing Cm bHCoKG, Germany, (2011) p. 246

[9]. Mirabutalybov M.M., Aliyeva M.Kh, Verdiyeva N.A., Rasulova A.V. Investigation of atom properties on the basis of distorted wave theory of scattering. VII International scientific-practical conference "Problems and perspectives of modern science" Moscow, (2016) p.85-87

[10]. Mirteymur M., Alieva M., Rasulova A., SaricanovaV.,Analytical method of calculation the cross section of elastic scattering of electrons on atom, IX.International Workshop on Nuclear structure properties, 1-3 September, (2016), Sivas,Turkey, p.61-62

[11]. Smolar V.A., Hieu N.T.T., Electrons elastic scattering in solids, News of Volgograd State Technical University, №5, v. 6, (2011) p.11-16

[12]. Maja S., Rabasovic J. Physics Cobf. ser. 565 (2014)012006

[13]. Milisavljevic S., SevicD., Chauhan R.K. Differential and integrated cross sections for the elastic electron scattering by calcium atom, Journal of Physics B:Atomic, Molecular and Optical Physics, №14, v.38, (2005)p.3-7

**HADRONIC JOURNAL 44**, 27 - 34 (2021)
DOI 10.29083/HJ.44.01.2021



# MULTIPLE PARTON SCATTERING AT HIGH ENERGY PROTON-PROTON COLLISIONS

**M.Y. Hussein**
Department of Physics, University of Bahrain
P.O. Box 32038, Kingdom of Bahrain
and
Search Center, Shaikh Ebrahim Bin Mohammed
Al Khalifa Center for Culture and Research
P.O. Box 13725, Muharraq, Kingdom of Bahrain
myhussein81@gmail.com

Received September 25, 2020
Revised October 25, 2020

## Abstract

Multiple parton scattering occurs when two or more independent identified hard particle from each proton takes place in the same proton-proton collision. The multiparton scattering mechanism got a new impulse at the LHC, where the high energy provides access to a very small value at the fractional momentum.Double parton scattering (DPS) and triple parton scattering (TPS), are expected to occur frequently in the proton-proton collision at the LHC and future high-energy colliders. This can give rise to a sizeable background to certain rare single parton scattering (SPS) and an interesting signal process in their own right.In this article, we discuss the total cross sections in both double and triple parton scattering mechanism for different process.

Copyright © 2021 by Hadronic Press, Inc., Palm Harbor, FL 34684, USA

## 1. Introduction

The multiple parton scattering got a new impulse with the operation of the LHC, extended nature of hadrons and their growing parton densities probed at increasingly higher energies, make it possible to simultaneously produce multiple particles in independent multiparton interactions in $(pp, p\bar{p})$ collisions [1-3].

The interest of MPI has increases in the last years not only as a source of particle production at hadron colliders, but due to information on partonic behavior observed in $pp$ collisions.

Recently, double parton scattering mechanism is consider to be as an important sourse of background in searches for new physics. In the process such as $pp \to HZ + X \to b\bar{b}Z + X$, one hard scatter can produce the Z and the other a continuum $b\bar{b}$ pair [1]. The same holds for $pp \to HW + X \to b\bar{b}W + X$, where the DPS contribution to the background has been studied in detail for Tevatron kinematics in [2]. A process with DPS contributions of prominent size is the like charge weak gauge boson $W^+W^+$or $W^-W^-$ production at hadron colliders [4-9].

The associated production of a Higgs boson with a $t\bar{t}$ pair at the LHC, $pp \to t\bar{t}h$, will play a very important role in the Higgs boson mass range, both for discovery and for precision measurements of the Higgs boson couplings. This process will provide a direct measurement of the top quark Yukawa coupling which could help to distinguish a SM Higgs boson from more complex Higgs sector and shed light on the details of the generation of fermions masses [7-9].

The $b\bar{b}$ channel is the most favorite Higgs boson decay mode when the Higgs boson mass is below the $W^+W^-$ threshold . The confidence in the capability of identifying efficiently the b quark jets has therefore addressed towards the detection of $b\bar{b}$ pairs to observe the Higgs boson production at the LHC.

To reduce the huge QCD background to the $b\bar{b}$ pair production, the $b\bar{b}$ pair is detected in association with an isolated lepton from the decay of a W boson. The process of interest to detect the Higgs boson production through the $b\bar{b}$ decay channel is therefore $pp \to WH + X, W \to l\nu$and $H \to b\bar{b}$, where $l$ is $e, \mu$.

The purpose of the present note is to point out that to a sizeable background to certain rare single parton scattering (SPS) and an interesting signal process in their own right, namely by a double parton mechanism (DPS) process and triple parton scattering mechanism (TPS). In fact as a result of the present analysis we find that double and triple parton scatterings may represent a rather sizeable source for some processes and background to other different processes.

## 2. Single Parton Scattering Mechanism

The Drell–Yan process occurs in high-energy $pp$ scattering as shown in Fig. (1). It takes place when a quark of one proton and an antiquark of another proton annihilate, creating a virtual photon or Z boson which then decays into a pair of oppositely-charged leptons.

Importantly, the energy of the colliding quark-antiquark pair, can be almost entirely transformed into the mass of new particles [10].

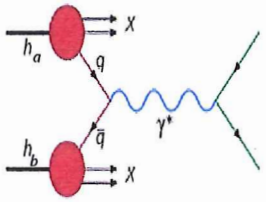


**Figure 1** Drell–Yan process: a quark from one quark and an antiquark from another hadron annihilate to create a pair of leptons through the exchange of a virtual photon.

The distribution of the fractional momenta of quarks in hadrons is described by the structure functions, which were obtained from lepton-nucleon scattering experiment.

The total cross section for particle production in the Drell-Yan scattering, can be written in the form:

$$\sigma(p\bar{p} \rightarrow V + X) = \sum \int_0^1 d\, x_a dx_b \;\; G_{a/p}(x_a, Q^2) G_{a/\bar{p}}(x_b, Q^2)\, \hat{\sigma}_{q\bar{q}} \rightarrow V \;, \qquad (1)$$

Where $\hat{\sigma}_{q\bar{q}} \rightarrow V$ is the sub process cross-section and, $V$ is the production of virtual particle.

## 3. Double Parton scattering Mechanism

The multiple parton scattering occurs when two or more different pairs of parton scattering independently in the same hadronic collision, as shown in Fig. (2).

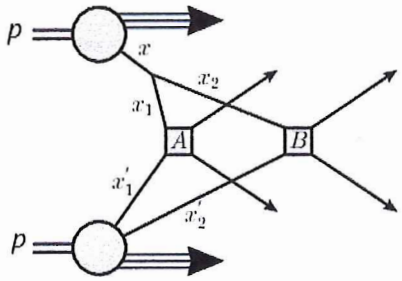


**Figure 2** Mechanism od Double Parton Scattering in which two quarks from one hadron and two antiquarks from another hadron annihilate [11].

With the only assumption of factorization of the two hard parton processes A and B, the inclusive cross section of a double parton-scattering in a hadronic collision is expressed by [11-13]:

$$\sigma_{(A,B)}^{DPS} = \frac{m}{2} \sum_{i,j,k,l} \int \Gamma_{i,j} \;\; (x_1, x_2 : b) \hat{\sigma}_{ik}^{A} (x_1, x_1') \, \hat{\sigma}_{jl}^{B}(x_2, x_2') \, \Gamma_{k,l}(x_1', x_2' ; b) \, dx_1 dx_1' \, dx_2 dx_2' \, d^2 b. \qquad (2)$$

Where $\Gamma_{i,j}(x_1, x_2: b)$ are the double parton distribution functions which depends on $x_1, x_2$ the fractional momenta, and the relative transverse separation b of the two parton undergoing the hard processes A and B, the indices $i$ and $j$ refer to the different parton species and $\hat{\sigma}^A_{ik}$ and $\hat{\sigma}^B_{jl}$ are the partonic cross sections. The factor $m$ is for symmetry, specifically $m = 1$ for indistinguishable parton processes and $m = 2$ for distinguishable processes.

The double distributions $\Gamma_{i,j}(x_1, x_2: b)$ are the main reason of interest in multiparton collisions. This distribution contains in fact all the information of probing the hadron in two different points contemporarily through the hard processes A and B.

The cross section for multiparton process is sizable when the flux of parton is large, namely at small x. Given the large flux one may hence expect that correlations in momentum fraction will not be a major effect and partons to be rather correlated in transverse space. Neglecting the effect of parton correlations in x one writes the double distributions $\Gamma_{i,j}(x_1, x_2: b)$:

$$\Gamma_{ij}(x_1, x_2; b) = \Gamma_i(x_1)\Gamma_j(x_2)F^i_j(b) \tag{3}$$

Where $\Gamma_{ij}(x_1)$ the usual one body parton distribution is function and $F^i_j(b)$ is a function normalized to one and representing the pair density in transverse space. The inclusive cross section hence simplifies

$$\sigma^{DPS}_{(A,B)} = \frac{m}{2}\sum_{ijkl}\Theta^{ij}_{kl}\hat{\sigma}_{ij}(A)\hat{\sigma}_{kl}(B), \tag{4}$$

Where $\hat{\sigma}_{ij}(A)$ and $\hat{\sigma}_{kl}(B)$ are the hadronic inclusive cross section for the two partons labeled $i$ and $j$ undergoes the hard interaction labeled A and for two partons $k$ and $l$ to undergo the hard interaction labeled B;

$$\Theta^{ij}_{kl} = \int d^2b F^i_k(b)F^j_l(b) \tag{5}$$

are the geometrical coefficients with dimension an inverse cross section and depending on various parton processes. These coefficients are the experimentally accessible quantities carrying the information of the parton correlation in transverse momentum. The cross section for multiple parton collisions has been further simplified as:

$$\sigma^D_{(A,B)} = \frac{m}{2}\frac{\hat{\sigma}(A)\hat{\sigma}(B)}{\sigma_{eff}} \tag{6}$$

Where all the information on the structure of the hadron in transverse space is summarized in the value of the scale factor. The experimental value measured by CDF yields [15] $\sigma_{eff} = 14.5 \pm 1.7^{+1.7}_{-2.3} mb$.

Fig. 4 shows effective cross sections measured by different experiments and energies.

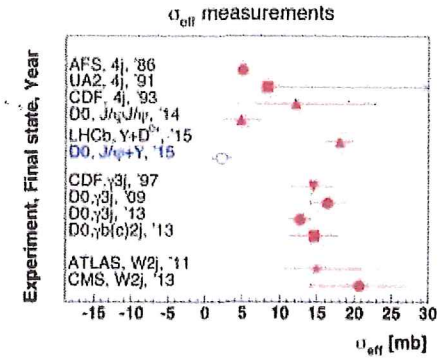


**Figure 4** $\sigma_{eff}$ measured by different experiments using different process. This figure was obtained from [15].

## 4. Triple Parton Scattering Mechanism

The triple parton scattering mechanism for $pp \rightarrow abc + X$ reaction is schematically illustrated in Fig. 3. The corresponding inclusive TPS cross section in a general form [16] can be written as follows:

$$\sigma^{TPS}_{pp\rightarrow abc}=\left(\frac{1}{3!}\right) \sum \int \Gamma^{qqq}_{p}(x_1, x_2, x_3;\ b_1, b_2, b_3) \times \hat{\sigma}^{qq}_{a}(x_1, x_1') \hat{\sigma}^{qq}_{b}(x_2, x_2') \hat{\sigma}^{qq}_{c}(x_3, x_3') \times \Gamma^{qqq}_{p}(x_1', x_2', x_3';\ b_1, b_2, b_3) \times dx_1\, dx_2\, dx_3\, dx_1'\, dx_2'\, dx_3'\, d^2b_1\, d^2b_2\, d^2b_3 . \quad (7)$$

where $x_i, x_i'$ are the longitudinal momentum fractions, scales, $\hat{\sigma}^{qq}_{a}(x_i, x_i')$ are the partonic cross sections for $qq \rightarrow a$ mechanism and $\frac{1}{3!}$ is the combinatorial factor relevant for the case of the three identical final states. The above TPS hadronic cross section is expressed in terms of the so-called triple-gluon distribution functions $\Gamma^{qqq}_{p}(x_1, x_2, x_3;\ b_1, b_2, b_3)$ that contain additional information about positions of the three corresponding partons in the transverse plane of the colliding protons.

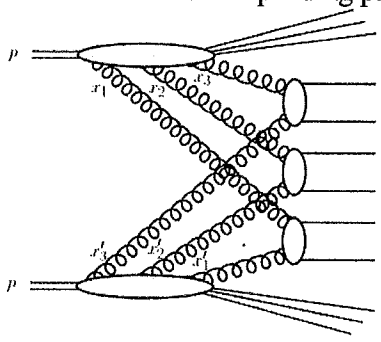

**Figure**.3. A diagrammatic illustration of the triple-parton scattering mechanism for triple production in proton–proton scattering. Only the dominant at high-energies [16].

Therefore, in practice one usually follows the so-called factorized Ansatz, where the correlations between partons are neglected and longitudinal and transverse degrees of freedom are separated.

Taking all together, the formula for inclusive TPS cross section can be simplified to the pocket form [16]:

$$\sigma^{TPS}_{pp\rightarrow abc} = \frac{1}{3!} \frac{\sigma^{SPS}_{pp\rightarrow a} \cdot \sigma^{SPS}_{pp\rightarrow b} \cdot \sigma^{SPS}_{pp\rightarrow c}}{\sigma^{2}_{eff,TPS}} \quad (8)$$

where the triple-parton scattering normalization factor $\sigma^{2}_{eff,TPS}$ contains only information about proton transverse profile and can be related to the overlap function from via the following expression:

$$\sigma^{2}_{eff,TPS} = [\int d^2b\ T^3(b)]^{-1} \quad (9)$$

The normalization factor $\sigma^{2}_{eff,TPS}$ contains all unknowns about the TPS dynamics. Its pure geometrical interpretation comes from the practical approximations of the factorized Ansatz mentioned above.

## 5. n-Parton Scattering Mechanism

In a hadronic collision, the inclusive cross section to produce n hard particles in n independent parton scattering, $hh' \rightarrow a_1 \ldots . a_n$, can be written as of a generalized n-parton distribution functions and elementary partonic cross sections over all involved partons [17]:

$$\sigma^{NPS}_{hh' \rightarrow a_1 \ldots\ldots a_n} = \frac{m}{n!} \sum_{i_1,\ldots i_n, i'_1 \ldots i'_n} \int \Gamma_h^{i_1 \ldots\ldots i_n}(x_1, \ldots\ldots x_n; b_1 \ldots\ldots b_n) \times$$
$$\hat{\sigma}^{i_1 i'_1}_{a_1}(x_1, x'_1) \ldots\ldots \hat{\sigma}^{i_n i'_n}_{a_n}(x_n, x'_n,) \times \Gamma_{h'}^{i'_1 \ldots\ldots i'_n}(x'_1, \ldots\ldots\ldots x'_n; b_1, \ldots\ldots b_n) \times$$
$$dx_1 \ldots dx_n dx'_1, \ldots\ldots dx'_n \, d^2 b_1, \ldots\ldots d^2 b_n d^2 b, \qquad (10)$$

Here, $\Gamma_h^{i_1 \ldots\ldots i_n}(x_1, \ldots\ldots x_n; b_1 \ldots\ldots b_n)$ are n parton generalized distribution functions on the momentum $x$and energy $Q$ scales at transverse $b$ of $i$ parton, producing final states $a$ with subprocess cross sections $\hat{\sigma}$. $\frac{m}{n!}$ Factor takes into account the different cases final states.

follows the so-called factorized Ansatz, where the correlations between partons are neglected and longitudinal and transverse degrees of freedom are separated. The n-parton cross section cross section can be expressed as the nth product of the corresponding SPS cross sections for the production of each single final-state particles, normalized by the $(n-1)$ power of an effective cross section

$$\sigma^{NPS}_{hh' \rightarrow a_1 \ldots\ldots a_n} = \frac{m}{n!} \frac{\sigma^{SPS}_{hh' \rightarrow a_1 \ldots\ldots} \sigma^{SPS}_{hh' \rightarrow a_n}}{\sigma^{n-1}_{eff,NPS}} \qquad (11)$$

Where all the information on the structure of the hadron in transverse space is summarized in the value of the scale factor.

## 6. Cross section calculation

**Table 1.** The SPS and DPS cross sections for different processes at the LHC

| Final State | $\sigma^{SPS}_{pp \rightarrow a+X}$ | $\sigma^{DPS}_{(qq)(qq) \rightarrow ab+X}$ |
|---|---|---|
| $\sigma\ (W^+W^- +X)$ | 6 (pb) | 1.06 (pb) |
| $\sigma\ (ZZ +X)$ | 1 (pb) | 0.28 (pb) |
| $\sigma\ (W^+W^+ +X)$ | 5 (pb) | 3.2 (pb) |
| $\sigma\ (W^-W^- +X)$ | 2 (pb) | 1.2 (pb) |
| $\sigma\ (W^{\pm}H +X)$ | 1 pb | 1.4 (nb) |
| $\sigma\ (ZH +X)$ | 0.5 pb | 0.17 (nb) |
| $\sigma\ (b\bar{b}H +X)$ | 2 pb | 0.12 (fb) |
| $\sigma\ (t\bar{t}H +X)$ | 380 fb | 120 (fb) |

**Table2.** The SPS and TPS cross sections for different processes at the LHC

| Final State | $\sigma^{SPS}_{pp\to a+X}$ | $\sigma^{DPS}_{(qqq)(qqq)\to abc+X}$ |
|---|---|---|
| $\sigma\ (b\bar{b}$ +X) | 0.50 (mb) | 0.12 (μb) |
| $\sigma\ (WWW$ +X) | 0.1 (pb) | 0.28 (pb) |
| $\sigma\ (WWZ$ +X) | 0.08 (pb) | 3.2 (pb) |
| $\sigma\ (WZZ$ +X) | 0.03 (pb) | 1.2 (pb) |
| $\sigma\ (ZZZ$ +X) | 0.008 (pb) | 0.5 (pb) |
| $\sigma\ (ZH$ +X) | 0.28 fb | 0.03 (fb) |
| $\sigma\ (b\bar{b}H$ +X) | 2 pb | 0.12 (fb) |
| $\sigma\ (t\bar{t}H$ +X) | 600 fb | 120 (fb) |

## 7. Discussion

When looking at extrapolation of the cross section at high energies, one finds that the results is effected by several uncertainties, as the knowledge of the parton structure functions at very small $x$ and the values of the heavy quark mass and of the running coupling constant.

The study presented that Double and Triple parton scattering are a non-negligible source of perturbative particle production in pp collision at increasingly higher energyies at the LHC. The formula derived for Double, triple and n-Parton scattering yields for any final state of interest. More integrated luminosity needed for the new chanal, also higher center of mass energy would increase multiple parton scattering mechanism.

**References**

1. Campbell J, Dawson S, Dittmaier S, Jackson S, Kramer M, Maltani F, Reina L, Spira M, Wackeroth D and Willenbrock S, hep-ph/0405302.
2. Landshoff P V and polkinghorne J C, Phys. Rev. **D18**, 3344(1987); Goebel C, Halzen F and scott D H. Phys. Rev. **D22**, 2789(1980); Halzen F, Hoyer P and Striling W J Phys. Lett. **B188**, 375 (1987).
3. Paver N and Treleani D, Nuovo Cimento **A70**, 215 (1982); M. Broun and D. Treleani, Eur. Phys. J. **C18**, 511 (2001).
4. Han T and Willenbrock S, Phys. Lett. **B273**, 167 (1991):. Han T, Valencia G and Willenbrock S, Phys. Rev. Lett. **69**, 3274 (1992).
5. Dittmaier S, Kramer M and Spira M, Phys. Rev. **D70**, 0704010 (2004); Dawsen S, Jakson C B, Rena L and Wackeroth D, Phys. Rev. **D69**, 074027 (2004).
6. Dawson S, Nucl. Phys. **B359**, 283 (1991).
7. Djouadi A, Spira M, and Zerwas P M, Phys. Lett. **B264**, 440 (1991).
8. Grandenz D, Spira M, and Zerwas P M, Phys. Rev. Lett. **70**, 1472 (1993).
9. Spira M, Djouadi A,. Grandenz D and Zerwas P M, Phys. Lett. **B264**, 440 (1991).
10. Cartiglia N, arXiv:1305.6131 [hep-ex].
11. Maciula R and Szczurek A, Phys. Rev. **D90**, no. 1, 014022 (2014) [arXiv:1403.2595 [hep-ph]].
12. Calucci G and Treleani D, Phys. Rev. **D83**, 016012 (2011) [arXiv:1009.5881 [hep-ph].
13. Chatrchyan S *et. al.* [CMS Collaboration], JHEP 1403, **032** (2014) [arXiv:1312.5729 [hep-ex]].
14. Chatrchyan S *et al.* [CMS Collaboration], JHEP 1403, **032** (2014) [arXiv:1312.5729 [hep-ex]].
15. UA2 Collaboration 1991 Phys. Lett. B **268** 145; AFS Collaboration 1987 Z. Phys. C **34** 163; Abe F*et et. al.* and CDF Collaboration 1993 Phys. Rev. D **47** 4857; CDF Collaboration 1997 Phys. Rev. D **56** 3811: Abazov V M *et al* and D0 Collaboration 2010 Phys. Rev. D **81** 052012 [arXiv:0912.5104 [hep-ex]]; G. Aad *et al.* and ATLAS Collaboration 2013 New J. Phys. **15** 033038 arXiv:1301.6872 [hep-ex].
16. Maciula R and Szczurek [arXiv:1703.07163 [hep-ph]; A Snigirev A M, Phys. Rev. **D 94** (2016) 034026.
17. d'Enterria D and Snigirev A, arXiv:1708.07519; A Alekhin S *et al.*, arXiv:1609.03327.

**HADRONIC JOURNAL 44**, 35 - 65 (2021)
DOI 10.29083/HJ.44.01.2021


# HEAT MASS TRANSFER OF NANOFLUIDS FLOW WITH ABSORPTION IN THE PRESENCE OF THERMAL RADIATION

**S.Y. Zayyanu, I.J. Uwanta and M.M. Hamza**
Department of Mathematics
Usmanu Danfodiyo University
Sokoto, Sokoto, Nigeria

Received December 16, 2019

## Abstract

*This study investigates the effects of chemical absorption on Heat Mass transfer of nanofluids flow over an infinite vertical plate in the presence of thermal radiation and applied magnetic field. the fluid is assumed to be electrically conducting water based Cu-nanofluid. The Tiwari and Das model is used to model the nanofluid, whereas Rosseland approximation is used for thermal radiation effect. Solutions for time dependent velocity, temperature and concentration equations are obtained using Laplace transform technique. The physical quantities of engineering interest such as skin friction, Nusselt number and Sherwood number are also computed. The obtained analytical solutions satisfy all imposed initial and boundary conditions. The effect of various parameters controlling the physical situation is discussed with the aid of line graphs. During the course of computation, excellent result was found from various physical parameters embedded in the problem.*

**Keywords**: Nanofluid, Chemical absorption, Thermal radiation, Heat transfer, Mass transfer.

Copyright © 2021 by Hadronic Press, Inc., Palm Harbor, FL 34684, USA

**List of Constants**

| | |
|---|---|
| $C$ | Dimensionless Concentration |
| $C_f$ | Skin friction coefficient |
| $C_p$ | Specific heat capacity of fluid (J/KgK) |
| $g$ | Acceleration due to gravity |
| $Kr$ | Chemical reaction parameter |
| $Ka$ | Chemical absorption parameter |
| $K$ | Thermal conductivity |
| $K^*$ | Rosseland mean absorption coefficient |
| $M$ | Magnetic parameter |
| $Nu$ | Nusselt number |
| Pr | Prandtl number |
| $Q_o$ | Chemical absorption coefficient |
| $Grc$ | Solutal grashof number |
| $Grt$ | Thermal grashof number |
| $q_r$ | Radiative heat flux |
| $R$ | Radiation parameter |
| $Sc$ | Schmidt number |
| $Sh$ | Sherwood number |
| $t$ | Dimensionless time |
| $T$ | Dimensional temperature |
| $\theta$ | Dimensionless temperature |
| $u^*$ | Dimensional velocity |
| $u$ | Dimensionless velocity |
| $t^*$ | Dimensional time |
| $y^*$ | Cartesian coordinate along the plate |
| $D_{nf}$ | Mass diffusion coefficient |

$K_o^*$ Chemical reaction coefficient

**Greek Symbols**

$\nu$ Kinematic viscosity

$\mu_{nf}$ Dynamic viscosity( $Kg/m^{-1}s^{-1}$)

$\varphi$ Nanoparticle volume fraction

$\sigma^*$ Stefan-Boltzmann constant

$\sigma$ Electric conductivity of fluid

$\rho$ Density

$\beta$ Thermal expansion coefficient

$q$ Laplace parameter

**Subscript**

$f$ Based fluid

$s$ Solid nanoparticle

$w$ At the wall condition

$\infty$ Far from the wall

## 1.0 Introduction

Recent advances in nanotechnology have allowed the development of a new category of fluids termed nanofluids. A nanofluid refers to the suspension of nanosize particles, which are suspended in the based fluid with low thermal conductivity, these particles also called nanoparticles, have a diameter of less than 100nm. The base fluid or dispersing medium can be aqueous or non-aqueous in nature. Nanofluids or so called smart fluids research has attracted considerable attention in recent years owing to their significance in engineering application and technology. The broad range of current and future applications have been given in the studies by, Wang and Mujumdar [1], Kakac and Pramuanjaroenkij [2], Eapen *et al.* [3] and Fan and Wang [4].Recently, Sheikholeslami and gamji [5] studied the MHD effects on Nanofluid flow in a permeable channel. Kuznetsov and Nield [6] critically analyzed the natural convection flow of a Nanofluid past a vertical plate .The problem of transient MHD free convection flow of a Nanofluid over a rotating vertical plate is addressed by Hamad and Pop [7]. They solved the governing equations analytically using the perturbation method and found that, the inclusion of nanoparticles into the based fluid is capable of varying the flow pattern. Turkyilmazoglu [8] reported the exact solution for heat and mass transfer of magnetohydrodynamic flow of nanofluid. Further, Turkyilmazoglu and Pop [9] have examined the heat and mass transfer of unsteady natural convection flow of nanofluid past a vertical plate with thermal radiation. Das [10] discussed the

problem of free convection flow of nanofluid bounded by moving vertical plate with constant heat source and convective boundary condition in a rotating frame of reference. He found that, the skin friction coefficient increases with an increase in nanoparticle volume fraction. However, Sheikholeslami *et al.* [11] have presented the heat and mass transfer behavior of unsteady flow of Nanofluid between parallel plates in the presence of thermal radiation. They concluded that, the solutal boundary layer thickness increases with increase in radiation parameter. Giresha *et al.*[12] have studied the effect of nanoparticles on flow and heat transfer of dusty fluid. Das and Jana [13] studied the MHD flow past a moving vertical plate in the presence of thermal radiation using Laplace transform method for closed form expressions of flow fields, they found that, the sheer stress at the plate for $Cu$ - water nanofluid is found to be lower. Heat transfer in flow of nanofluid with heat source/sink and an induced magnetic field is addressed by Giresha *et al.*[14]. The boundary layer in newtonian and porous media filled by nanofluids over fixed and moving boundaries have been studied by Mahdy and Elshehabey [15].

In many industrial and engineering applications, the heat and mass transfer is a consequence of buoyancy caused by thermal diffusion and chemical species, therefore, the study of heat and mass transfer is needed for improving many technologies such as polymer and ceramic production, food processing, gas production, geothermal reservoirs, thermal insulations and so on. The heat and mass transfer flow of nanofluids in the presence of magnetic field also find a variety of applications such as energy saving, reduction of production time and also a

greater quality of the final product. Heat and mass transfer under the influence of chemical reaction has also attracted considerable attention of many authors due to wide range of applications. in view of these ,conjugate heat and mass transfer flow past a vertical permeable plate with thermal radiation and chemical reaction is investigated by Pal and Talukdar [16]. They found that, the thermal radiation and chemical reaction effect decrease the velocity and concentration profiles. Numerical investigation of heat and mass transfer of an electrically conducting fluid over a moving surface with first order chemical reaction is carried out by Chamkha [17]. Uwanta and Omokhuale [18] have analyzed the influence of radiation and chemical reaction effect on heat and mass transfer of a viscoelastic fluid in a mixed plane. Later, the combined effects of radiation and chemical reaction on the MHD free convection flow of an electrically conducting viscous fluid over an inclined plate have been studied by Ali *et al.*[19] and have obtained a closed form solution by employing laplace transform technique. Fetecau *et al.*[*20*], studied natural convection flow of fractional nanofluids over an isothermal vertical plate.

Motivated by aforementioned studies, we intend to investigate/extend the study reported by Fetecau *et al.*[20], the effect of heat and mass transfer on natural convection flow over a vertical plate, the effects of chemical

absorption, chemical reaction are also considered, to best of our knowledge, this study has not been considered by any author, our interest here, is to obtain the closed form solution for the present problem by employing Laplace Transform technique, the basic partial differential equations are derived by using Boussinesq approximation and then are transformed to dimensionless equations using suitable non-dimensional parameters. The resultant equations have been solved analytically.

## 2.0 Mathematical Formulation and Solution

Consider the natural convection flow, heat and mass transfer of nanofluid, past an infinite vertical plate situated in the $(x^*, z^*)$-plane of a fixed Cartesian coordinate system $Ox^*y^*z^*$.The plate is at rest initially with constant ambient temperature and concentration $T_\infty$ and $C_\infty$ respectively, uniform transverse magnetic field of strength $(\beta_0)$ and radiative heat flux $(q_r)$ are applied perpendicular to the plate. It is assumed that the pressure gradient is neglected and the fluid is electrically conducting, water based nanofluid embedded with copper nanoparticles. Since the plate is infinite, all of the physical quantities describing the fluid motion are functions of $y^*$ and $t^*$.

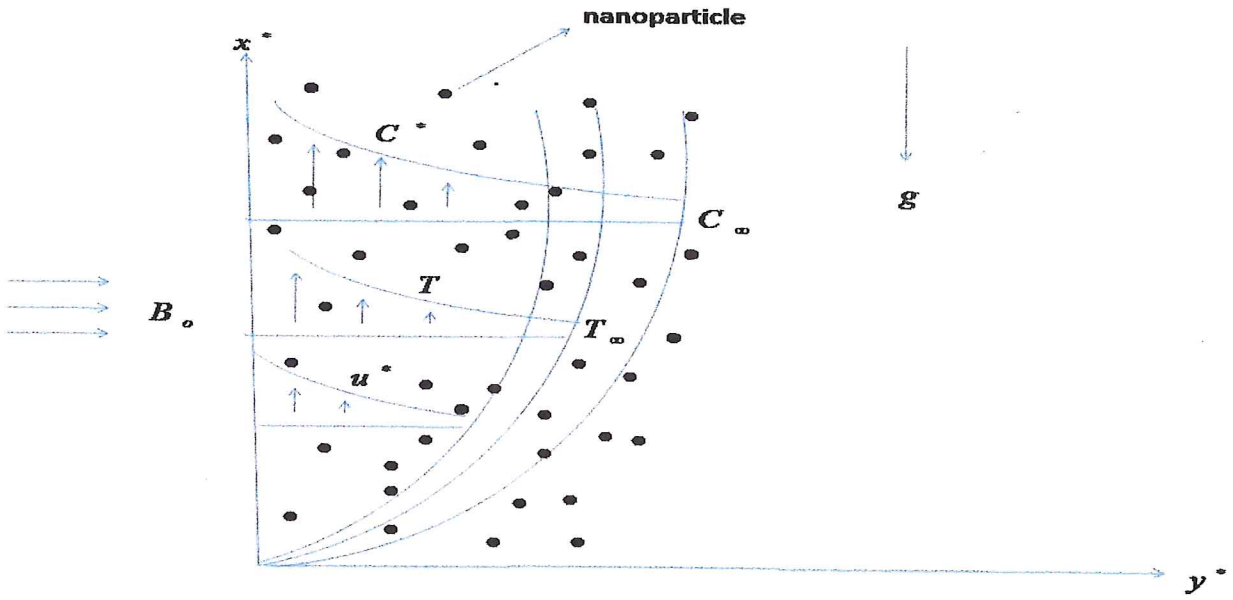


Fig.1: GEOMETRY OF THE PROBLEM

The thermophysical properties of copper $(Cu)$ are given in table1 (Oztop and Abu-nada [22]).

| Physical properties | base fluid | $Cu$ |
|---|---|---|
| $\rho\ (kg/m^3)$ | 997.1 | 8933 |
| $C\rho\ (J/kgK)$ | 4179 | 385 |
| $K\ (W/mK)$ | 0.613 | 401 |
| $\beta_t \times 10^5 (K^{-1})$ | 21 | 1.67 |
| $\beta_c \times 10^6 (m^2/h)$ | 298.2 | 3.05 |

| $\varphi$ | 0.0 | 0.05 |
|---|---|---|
| $\sigma\ (s/m)$ | $5.5\times10^{-6}$ | $59.6\times10^{6}$ |

**TABLE 1:** Thermophysical properties of copper $(Cu)$

Assuming small differences between the temperature $T(y^*,t^*)$ and the stream temperature $T_\infty$, and adopting the Rosseland approximation [5], the radiative heat flux $q_r(y^*,t^*)$ can be linearized to :

$$q_r(y^*,t^*) = -\frac{16\sigma^* T_\infty^3}{3K^*}\frac{\partial(y^*,t^*)}{\partial y^*} \tag{1}$$

Where $\sigma^*$ is the Stefan-Boltzman constant and $K^*$ is the mean absorption coefficient. In view of the above assumption and taking into account the nanofluid model proposed by Tiwari and Das [21], the governing equations can be written as:

$$\rho_{nf}\frac{\partial u^*}{\partial t^*} = \mu_{nf}\frac{\partial^2 u^*}{\partial y^{*2}} + g(\rho\beta)_{nf}(T-T_\infty) + g(\rho\beta)_{nf}(C^*-C_\infty) - \sigma_{nf}\beta_0^2 u^* \tag{2}$$

$$(\rho Cp)_{nf}\frac{\partial T}{\partial t^*} = K_{nf}\left(1+\frac{16\sigma^* T_\infty^3}{3K_{nf}K^*}\right)\frac{\partial^2 T}{\partial y^{*2}} + Q_O(C^*-C_\infty) \tag{3}$$

$$\frac{\partial C^*}{\partial t^*} = D_{nf}\frac{\partial^2 C^*}{\partial y^{*2}} - K_0^*(C^*-C_\infty) \tag{4}$$

In the above equations, $u^*(y^*,t^*)$ is the fluid velocity in the $x^*$ direction , $T_w$ is constant plate temperature ($T_w > T_\infty$ or $T_w < T_\infty$ corresponds to the Heated or cooled plate respectively ), $g$ is the acceleration due to gravity , $\sigma_{nf}$ is the effective thermal conductivity, $K_0^*$ the chemical reaction coefficient, $D_{nf}$ is the diffusion coefficient and $Q_O$ is chemical absorption coefficient, $\rho_{nf}$ is the density of the nanofluid, $\mu_{nf}$ is the dynamic viscosity of the nanofluid , $\beta_{nf}$ is the thermal expansion coefficient of the nanofluid. The effective properties of nanofluid are given by the following co-relations (see Das and Jana [13]):

$$\mu_{nf} = \frac{\mu_f}{(1-\varphi)^{2.5}} \quad , \quad \rho_{nf} = (1-\varphi)\rho_f + \varphi\rho_s \, , (\rho C_p)_{nf} = (1-\varphi)(\rho C_p)_f + \varphi(\rho C_p)_s \, ,$$

$$(\rho\beta)_{nf} = (1-\varphi)(\rho\beta)_f + \varphi(\rho\beta)_s \, , \sigma_{nf} = \sigma_f \left( 1 + \frac{3(\sigma-1)\varphi}{(\sigma+2)-(\sigma-1)\varphi} \right), \; \sigma = \frac{\sigma_s}{\sigma_f},$$

$$\frac{K_{nf}}{K_f} = \frac{K_s + 2K_f - 2\varphi(K_f - K_s)}{K_s + 2K_f + \varphi(K_f - K_s)} \tag{5}$$

Where $\varphi$ the volume fraction of nanoparticles, $\rho_f$ and $\rho_s$ are density of base fluid and nanoparticles respectively, $C_{pf}$ and $C_{ps}$ are specific heat of the base fluid and nanoparticles respectively, $\sigma_f$ and $\sigma_s$ are electrical conductivity of base fluid and nanoparticles correspondingly, $\beta_f$ and $\beta_s$ are thermal expansion coefficient of the

base fluid and nanoparticles respectively, $K_f$ and $K_s$ are thermal conductivity of base fluid and nanoparticles.

If no slipping exists between the fluid and the plate, the appropriate initial and boundary conditions are:

$$\begin{aligned} &u^*(y^*,0)=0,\ T(y^*,0)=T_\infty,\ C^*(y^*,0)=C_\infty; y^*>0 \\ &u^*(0,t^*)=0,\ \ T(0,t^*)=T_w,\ \ C^*(0,t^*)=C_w; t^*>0 \\ &u^*(y^*,t^*)=0,\ T(y^*,t^*)=0,\ C^*(y^*,t^*)=0; y^*\to\infty \end{aligned} \tag{6}$$

The non-dimensional quantities introduced in the above equations are defined as :

$$y=\frac{y^*}{L}\ ,\quad t=\frac{v_f t^*}{L^2}\ , u=\frac{u^* L}{v_f}, L^3=\frac{v_f^2}{g\beta_f(T_w-T_\infty)}, \theta=\frac{T-T_\infty}{T_w-T_\infty}\ ,\quad C=\frac{C^*-C_\infty}{C_w-C_\infty}\ ,$$

$$Kr=\frac{K_0^* L^2}{v_f}\ ,\quad Sc=\frac{v_f}{D_{nf}}\ ,\ \Pr=\frac{v_f}{K_f}\ ,\ Ra=\frac{16\sigma^* T_\infty^3}{3K^* K_f}\ ,\ Ka=\frac{L^2(C_w-C_\infty)}{v_f(T_w-T_\infty)(\rho Cp)_f}\ ,$$

$$M^2=\frac{\sigma_f\beta_0^2 L^2}{\rho_f v_f}\ , G_{rc}=\frac{g\beta(C_w-C_\infty)}{v_f^2},\quad G_{rt}=\frac{g\beta(T_w-T_\infty)}{v_f^2} \tag{7}$$

On substituting these dimensionless variables into equations (2),(3) and (4) , one can get ;

$$\frac{\partial u}{\partial t}=\frac{1}{a_1}\frac{\partial^2 u}{\partial y^2}+a_2\theta+a_3 C-a_5 u \tag{8}$$

$$\frac{\partial \theta}{\partial t} = \frac{1}{a_6}\frac{\partial^2 \theta}{\partial y^2} + a_7 C \tag{9}$$

$$\frac{\partial C}{\partial t} = \frac{1}{Sc}\frac{\partial^2 \theta}{\partial y^2} - KrC \tag{10}$$

With initial and boundary conditions

$$\begin{aligned} &u(y,0) = 0, \theta(y,0) = 0, \ C(y,0) = 0; y > 0 \\ &u(0,t) = 0, \ \theta(0,t) = 1, \quad C(0,t) = 1; t > 0 \\ &u(y,t) = 0, \ \theta(y,t) = 0, \ C(y,t) = 0; y \to \infty \end{aligned} \tag{11}$$

By applying the Laplace Transform on both sides of equations (8) – (11), we have

$$\frac{d^2 \bar{u}}{dy^2} - (a_1(q + a_5))\bar{u} + a_1 a_2 \bar{\theta} + a_1 a_3 \bar{C} = 0 \tag{12}$$

$$\frac{d^2 \bar{\theta}}{dy^2} - a_6 q \bar{\theta} + a_6 a_7 \bar{C} = 0 \tag{13}$$

$$\frac{d^2 \bar{C}}{dy^2} - (Sc(q + Kr))\bar{C} = 0 \tag{14}$$

With corresponding initial and boundary conditions

$$\begin{aligned} &\bar{u}(y,0) = 0, \ \bar{\theta}(y,0) = 0, \ \bar{C}(y,0) = 0; y > 0 \\ &\bar{u}(0,q) = 0, \bar{\theta}(0,q) = \frac{1}{q}, \ \bar{C}(0,q) = \frac{1}{q}; q > 0 \\ &\bar{u}(y,t) = 0, \ \bar{\theta}(y,q) = 0, \ \bar{C}(y,q) = 0; y \to \infty \end{aligned} \tag{15}$$

Where $\bar{u} = \int_0^\infty u(y,t)\ell^{-qt}dt$ , $\bar{\theta} = \int_0^\infty \theta(y,t)\ell^{-qt}dt$ , $\bar{C} = \int_0^\infty C(y,t)\ell^{-qt}dt$ and $q > 0$.Now

by solving the above system ,one can have ;

$$\bar{C}(y,q) = \frac{1}{q}\ell^{-y\sqrt{(q+Kr)Sc}} \tag{16}$$

$$\bar{\theta}(y,q) = \frac{\ell^{-y\sqrt{a_6 q}}}{q} + \frac{V_2}{V_1}\left(\frac{\ell^{-y\sqrt{(q+Kr)Sc}}}{q-V_1} - \frac{\ell^{-y\sqrt{(q+Kr)Sc}}}{q} - \frac{\ell^{-y\sqrt{a_6 q}}}{q-V_1} + \frac{\ell^{-y\sqrt{a_6 q}}}{q}\right) \tag{17}$$

$$\begin{aligned}\bar{u}(y,q) = {} & \frac{b_9\ell^{-y\sqrt{(q+a_5)a_1}}}{q-V_4} + \frac{b_{10}\ell^{-y\sqrt{(q+a_5)a_1}}}{q} + \frac{b_{11}\ell^{-y\sqrt{a_1 q}}}{q-V_4} + \frac{b_{12}\ell^{-y\sqrt{a_1 q}}}{q} \\ & + \frac{b_4\ell^{-y\sqrt{a_1 q}}}{q-V_1} - \frac{b_{13}\ell^{-y\sqrt{(q+a_5)a_1}}}{q-V_1} + \frac{b_{14}\ell^{-y\sqrt{(q+Kr)Sc}}}{q+V_7} + \frac{b_6\ell^{-y\sqrt{(q+Kr)Sc}}}{q+V_1} \\ & + \frac{b_{15}\ell^{-y\sqrt{(q+Kr)Sc}}}{q} + \frac{b_{16}\ell^{-y\sqrt{(q+a_5)a_1}}}{q+V_7}\end{aligned} \tag{18}$$

In order to determine, the flow fields in the time domain, by applying Inverse Laplace Transform on both sides of equations (16) - (18) , we get;

## 2.1 Velocity Equation

$$u(y,t) = b_9 I_1 + b_{10} I_2 + b_{11} I_3 + b_{12} I_4 + b_4 I_5 - b_{13} I_6 + b_{14} I_7 + b_6 I_8 + b_{15} I_9 + b_{16} I_{10} \tag{19}$$

## 2.2 Temperature Equation

$$\theta(y,t) = I_4 + c_2 I_{12} - c_2 I_9 - c_2 I_5 + c_2 I_4 \tag{20}$$

## 2.3 Concentration Equation

$$C(y,t) = I_9 \tag{21}$$

In order to determine the three entities of physical interest, namely the skin friction coefficient ($C_f$),Nusselt number ($Nu$) and Sherwood number ($Sh$),we use the relations;

## 2.4 Skin Friction ($C_f$)

The Skin friction coefficient at the plate y=0 is given by;

$$C_f = \frac{1}{(1-\varphi)^{2.5}} \left.\frac{\partial u}{\partial t}\right|_{y=0} \tag{22}$$

$$\left.\frac{\partial u}{\partial t}\right|_{y=0} = \left( b_9 \frac{\partial I_1}{\partial y} + b_{10} \frac{\partial I_2}{\partial y} + b_{11} \frac{\partial I_3}{\partial y} + b_{12} \frac{\partial I_4}{\partial y} + b_4 \frac{\partial I_5}{\partial y} - b_{13} \frac{\partial I_6}{\partial y} + b_{14} \frac{\partial I_7}{\partial y} + b_6 \frac{\partial I_8}{\partial y} + b_{15} \frac{\partial I_9}{\partial y} + b_{16} \frac{\partial I_{10}}{\partial y} \right)_{y=0}$$

## 2.5 Nusselt Number ( $Nu$ )

The Nusselt number ( $Nu$ ) at the plate y=0 is given by;

$$Nu = -\frac{K_{nf}}{K_f}\frac{\partial\theta}{\partial y}\bigg|_{y=0} \tag{23}$$

$$\frac{\partial\theta}{\partial y}\bigg|_{y=0} = \left(\frac{\partial I_4}{\partial y} + c_2\frac{\partial I_{12}}{\partial y} - c_2\frac{\partial I_9}{\partial y} - c_2\frac{\partial I_5}{\partial y} + c_2\frac{\partial I_4}{\partial y}\right)_{y=0}$$

## 2.6 Sherwood Number ( $Sh$ )

The Sherwood number ( $Sh$ ) at the plate y=0 is given by;

$$Sh = -\frac{\partial I_9}{\partial y}\bigg|_{y=0} \tag{24}$$

## 3.0 Results and Discussion

In the present study, the Laplace Transform technique has been employed to obtain the analytical expressions for Velocity, Temperature and Concentration profiles as well the Skin friction coefficient, Nusselt number and Sherwood number. In order to have the clear insight of the problem, a numerical computation has been carried out for different values of pertinent parameters. Throughout our numerical computation, the value of Prandtl number ( Pr ) has been taken to be 6.2 which corresponds to $Cu$ water, Radiation parameter ( $R$ ) has been taken as 1 (Fetecau *et al.*[20]), Schmidt number ( $Sc$) is taken to be 0.6

which correspond to water vapor, other parameters are varied over the range which are listed in the figures legend.

**Fig.2** is prepared to show that, an increase in chemical reaction parameter ( $Kr$ ) decreases the concentration profile and vice-versa. The reason behind this is that, the number of solute molecules undergoing chemical reactions gets increased as chemical reaction parameter increases, which lead to decrease in concentration profile. While **Fig.3** shows that an increase in Schmidt number corresponds to a weaker solute diffusivity which allows a shallower penetration of solutal effect, as consequence, the concentration decreases with increase in $Sc$. It is observed in **Fig.4** that, an increase in the chemical absorption parameter $(Ka)$ leads to increase in the temperature of the fluid and vice-versa, it is also noted that in the absence of chemical absorption $(Ka = 0)$ the temperature reduces drastically, these is in excellent agreement with the work of Fetecau *et al.*[20].

In **Fig.5**, the effect of chemical reaction on velocity is shown when other parameters are considered as constants. It is noticed from the Figure that there is marked effect of increasing the value of chemical reaction parameter ( $Kr$ ) on velocity profile in the boundary layer. It is highlighted that the velocity decreases with increase in the rate of chemical reaction, this is due to the fact that increase in chemical reaction rate leads to a fall in the momentum boundary layer. **Fig.6**, highlighted the effects of chemical absorption parameter on velocity

profile, it is observed that the increase in chemical absorption parameter leads to decrease in the velocity profile significantly and vice-versa. **Fig.7** depicts the effects of Solutal grashof number ($Grc$), it is described as the ratio of the species buoyancy force to the viscous hydrodynamic force. As solutal grashof number increases, the viscous hydrodynamic force decreases, as a result, the momentum boundary layer thickens and vice-versa. In **Fig.8**, it is observed that the fluid velocity decreases as the magnetic field parameter increases, this is due to the fact that, the application of transverse magnetic field to an electrically conducting fluid gives rise to resistive type of force called Lorentz force. This force has the tendency to slow down the motion of the fluid, consequently, the fluid velocity reduced significantly; this result is consistently agreed with that of Sheikholeslami and Gamji [5]. **Fig.9**, is prepared to show the influence of Schmidt number on Sherwood number versus chemical reaction parameter ( $Kr$ ), an increase in Schmidt number decreases the Sherwood number in the interval $0 \le Kr \le 2$.It is evidence from **Fig.10** that, an increase in chemical absorption parameter ( $Ka$ ) leads to decrease in the rate of heat transfer and vice-versa.

Also **Fig.11**, shows the effect of chemical reaction parameter on Nusselt number( $Nu$ ),it is observed from the figure that an increase in chemical reaction parameter decreases the rate of heat transfer and vice-versa, reverse trend is observed in **Fig.12**, as an increase in chemical reaction parameter decreases the rate of heat transfer.

However, **Fig.13** delicates effect of magnetic parameter on the skin friction coefficient, it is observed that increase in magnetic parameter decrease the skin friction coefficient ( $C_f$ ), and vice-versa.

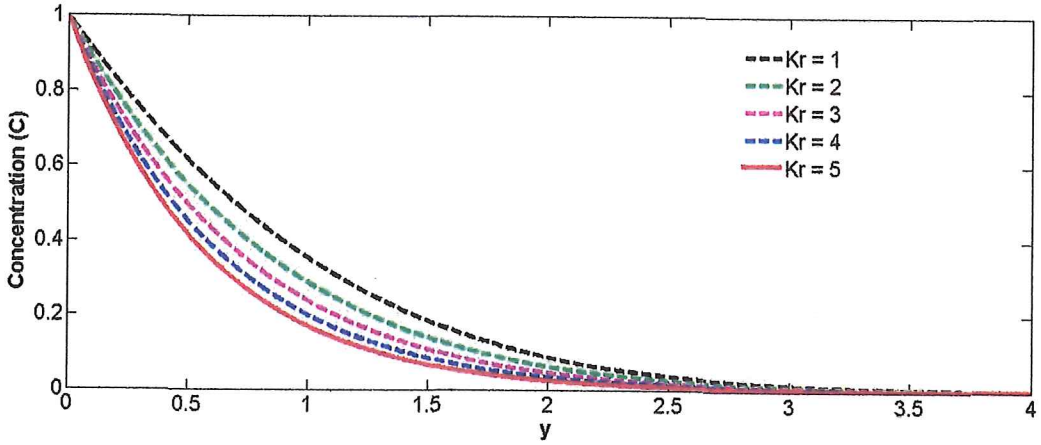


**Fig.2** Effects of chemical reaction parameter $(Kr)$ on concentration profile when $Sc = 0.6,\ t = 0.5.$

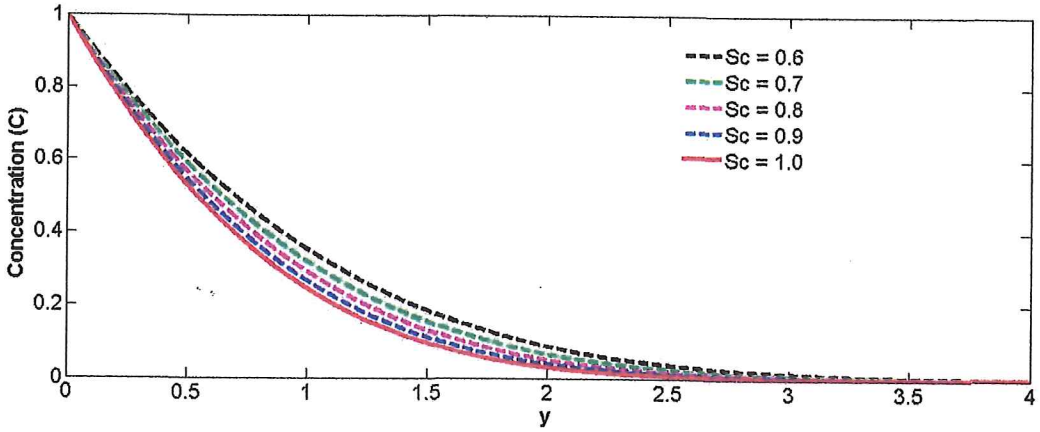


**Fig.3** Effects of Schmidt number $(Sc)$ on concentration profile when $Kr = 1,\ t = 0.5.$

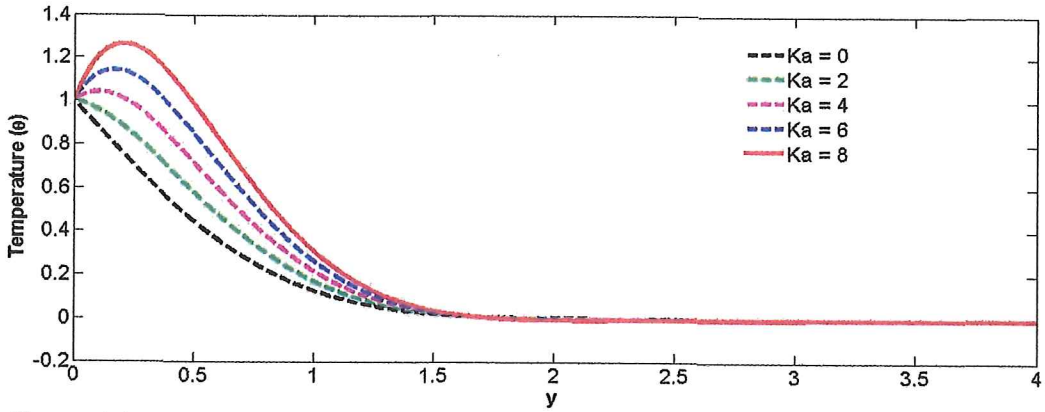


**Fig.4** Effects of chemical absorption parameter ( $Ka$ ) on temperature profile when $Kr = 10$,

$t = 0.5, R = 1, \varphi = 0.2, \text{Pr} = 6.2, Sc = 0.6.$

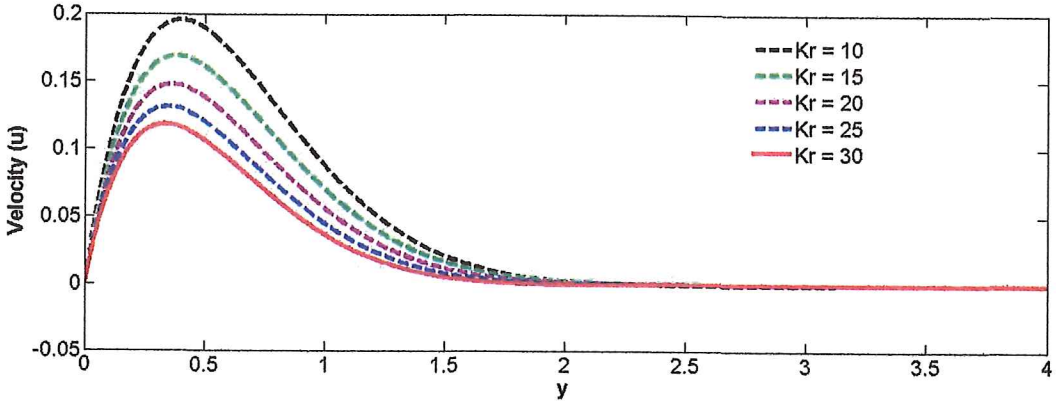


**Fig.5** Effects of chemical reaction parameter ( $Kr$ ) on velocity profile when $t = 0.5$, $R = 1$

$\varphi = 0.2, \text{Pr} = 6.2, Sc = 0.6, M = 0.1, Grc = 1, Grt = 0.1.$

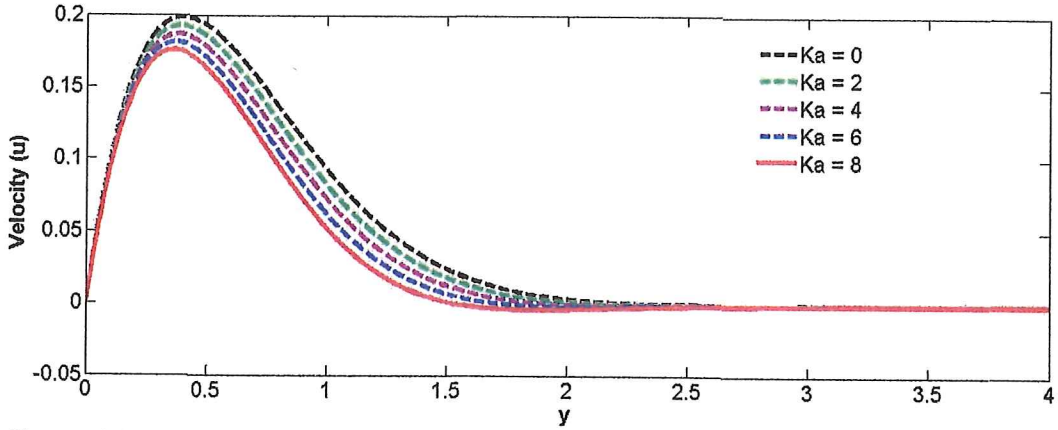


**Fig.6** Effects of chemical absorption parameter ( $Ka$ ) on velocity profile when

$t = 0.5,\ R = 1$

$\varphi = 0.2,\ \mathrm{Pr} = 6.2, Sc = 0.6,\ M = 0.1,\ Grc = 1,\ Grt = 0.1,\ Kr = 10$

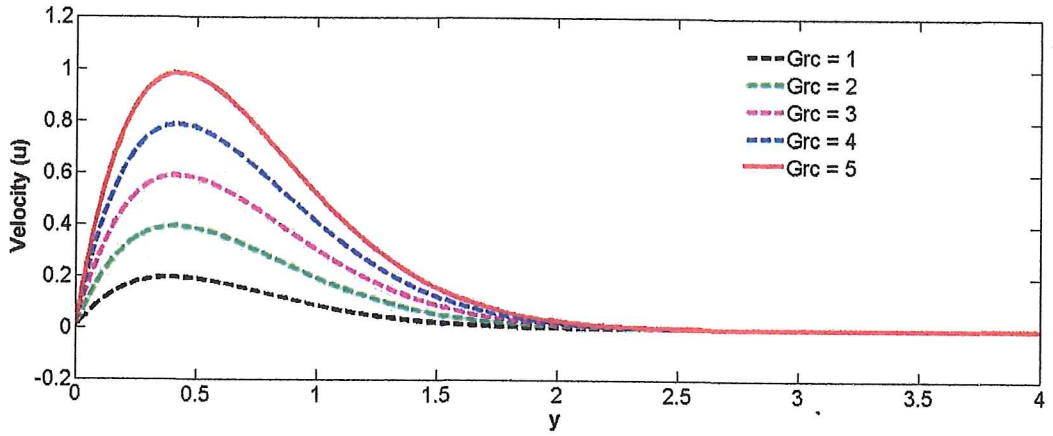


**Fig.7** Effects of Solutal grashof number ( $Grc$ ) on velocity profile when $Kr = 10$,

$t = 0.5,\ R = 1$,

$\varphi = 0.2$ , $\mathrm{Pr} = 6.2$, $Sc = 0.6$, $M = 0.1$, $Ka = 1$ , $Grt = 0.1$.

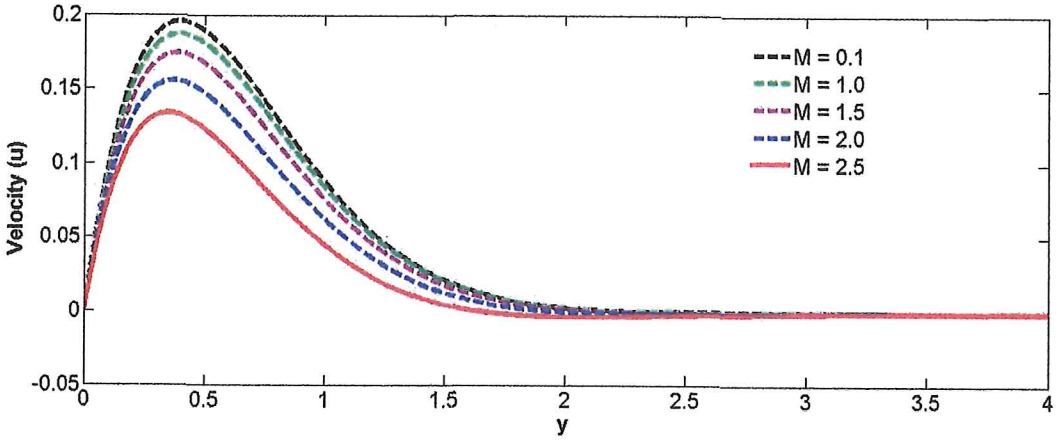


**Fig.8** Effects of Magnetic parameter ( $M$ ) on velocity profile when $Kr = 10$, $t = 0.5$, $R = 1$,

$\varphi = 0.2$, $\mathrm{Pr} = 6.2$, $Sc = 0.6$, $Ka = 1$, $Grc = 1$, $Grt = 0.1$.

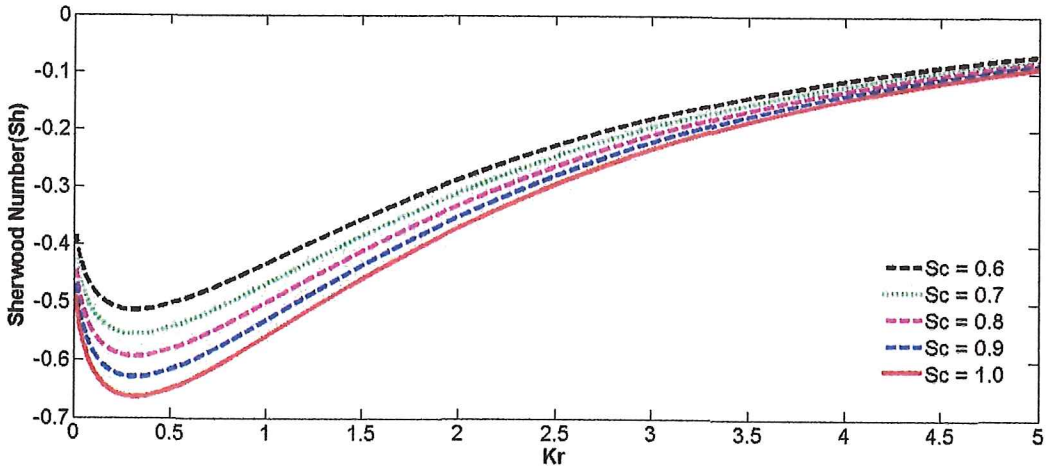


**Fig.9** Effects of Schmidt number ( $Sc$ ) on Sherwood number when $t = 0.5$.

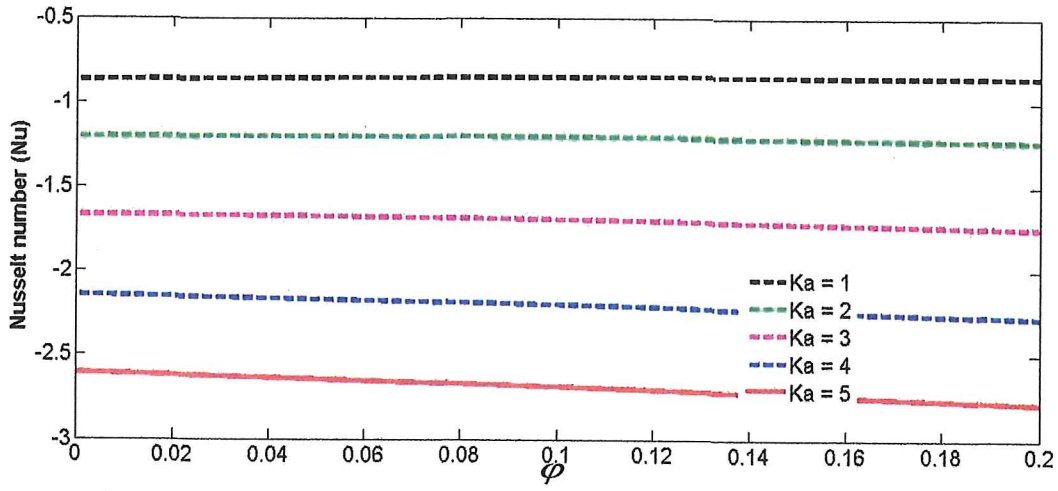


**Fig.10** Effects of chemical absorption parameter ( $Ka$ ) on Nusselt number when $Kr = 10,\ t = 0.5$

$R = 1,\ \varphi = 0.2, \Pr = 6.2,\ Sc = 0.6$ .

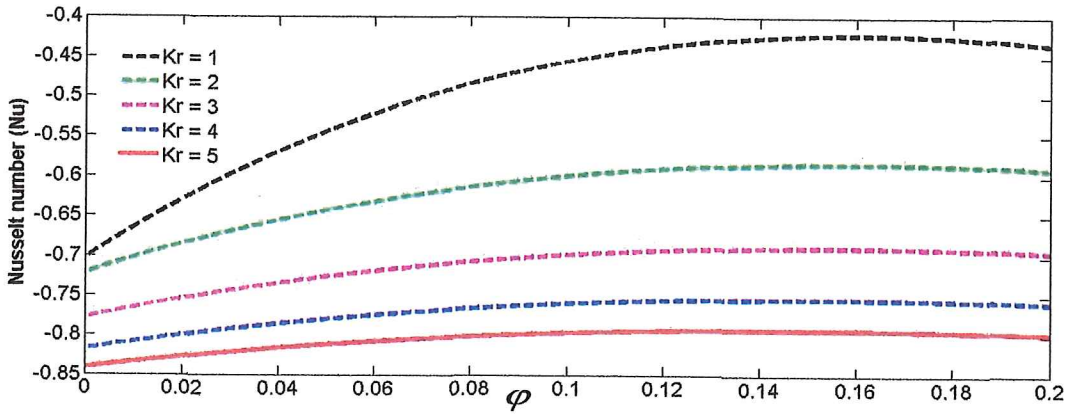


**Fig.11** Effects of chemical reaction parameter ( $Kr$ ) on Nusselt number when

$t = 0.5, R = 1, Sc = 0.6, \Pr = 6.2, Ka = 1.$

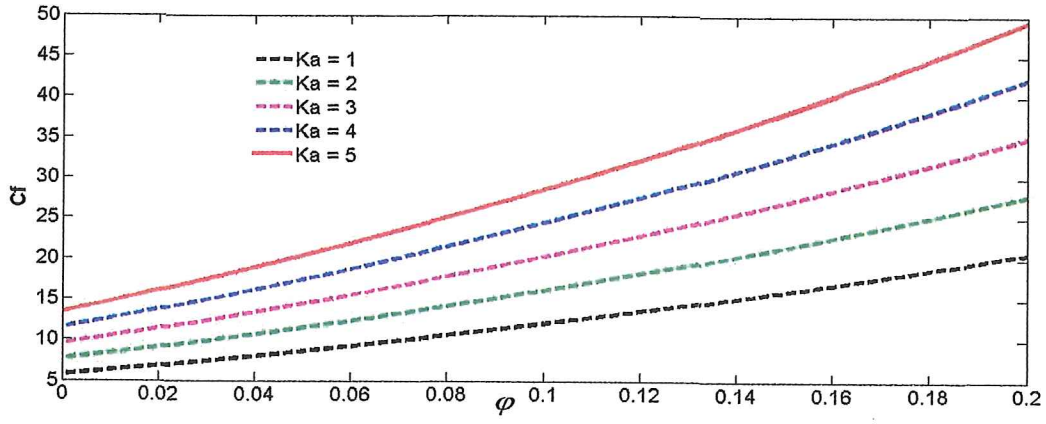


**Fig.12** Effects of chemical absorption parameter ( $Ka$ ) on Skin friction when

$Kr = 10,\ t = 0.5,\ R = 1,\ \Pr = 6.2,\ Sc = 0.6,\ Ka = 1,\ Grc = 1,\ Grt = 0.1.$

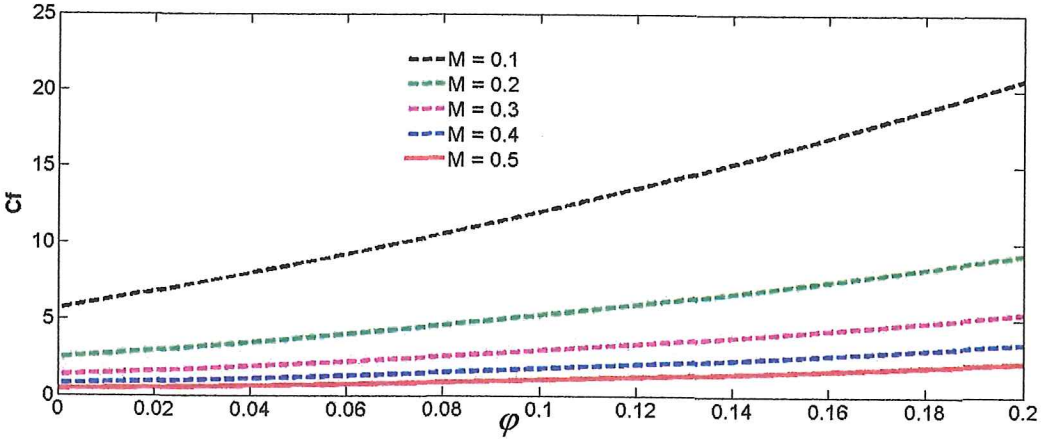


**Fig.13** Effects of Magnetic parameter ( $M$ ) on Skin friction profile when $Kr = 10,$

$t = 0.5,\ R = 1,$

$\Pr = 6.2,\ Sc = 0.6,\ Ka = 1,\ Grc = 1,\ Grt = 0.1.$

## 4.0 Conclusion

The heat mass transfer of nanofluids flow with absorption in the presence of thermal radiation has been studied, the set of governing equations has been solved analytically using Laplace transform technique, the effects of pertinent parameters on the nanofluid concentration, temperature, velocity, rate of mass transfer, rate of heat transfer and skin friction are investigated and analyzed with the help of their graphical representations. Based on the results, the following conclusions are drawn:

- The presence of Chemical reaction reduces the concentration and velocity of the fluid.
- Chemical absorption parameter causes to increase the temperature of the fluid and causes to decrease the velocity of the fluid.
- Intensifying magnetic field strength stabilizes the velocity of the fluid.
- The influence of solutal grashof number and chemical absorption parameter are opposite on velocity field.
- As a result of chemical reaction and chemical absorption, the rate of the flow enhances.
- An increase in chemical reaction parameter decreases the rate of heat transfer of the fluid.

**References**

[1] Wang, X.Q and Mujumdar, A.S.(2008).A review on nanofluids .part 1:theoretical and numerical investigations.*Brazilian Journal of Chemical Engineering,* ***25*****(4)**,613-630.

[2] Kakaç, S., and Pramuanjaroenkij, A. (2009). Review of convective heat transfer enhancement with nanofluids.*International Journal of Heat and Mass Transfer*, ***52*****(13-14)**, 3187-3196.

[3] Eapen, J., Rusconi, R., Piazza, R., and Yip, S. (2010). The classical nature of thermal conduction in nanofluids. *Journal of heat transfer*, ***132*****(10)**, 102402.

[4] Fan, J., and Wang, L. (2011). Review of heat conduction in nanofluids. *Journal of Heat Transfer*, ***133*****(4)**, 040801.

[5] Sheikholeslami, M., and Ganji, D. D. (2014). Magnetohydrodynamic flow in a permeable channel filled with nanofluid. *Scientia Iranica. Transaction B, Mechanical Engineering*, ***21*****(1)**, 203.

[6] Kuznetsov, A. V., and Nield, D. A. (2010). Natural convective boundary-layer flow of a nanofluid past a vertical plate.*International Journal of Thermal Sciences*, ***49*****(2)**, 243-247.

[7] Hamad, M. A. A., and Pop, I. (2011). Unsteady MHD free convection flow past a vertical permeable flat plate in a rotating frame of reference with constant heat source in a nanofluid.*Heat and mass transfer*, ***47*****(12)**, 1517.

[8] Turkyilmazoglu, M. (2012). Exact analytical solutions for heat and mass transfer of MHD slip flow in nanofluids. *Chemical Engineering Science*, ***84***, 182-187.

[9] Turkyilmazoglu, M., and Pop, I. (2013). Heat and mass transfer of unsteady natural convection flow of some nanofluids past a vertical infinite flat plate with radiation effect. *International Journal of Heat and Mass Transfer*, ***59***, 167-171.

[10] Das, K. (2014). Flow and heat transfer characteristics of nanofluids in a rotating frame. *Alexandria engineering journal*,***53*****(3)**, 757-766.

[11] Sheikholeslami, M., Ganji, D. D., and Rashidi, M. M. (2015). Ferrofluid flow and heat transfer in a semi annulus enclosure in the presence of magnetic source considering thermal radiation. *Journal of the Taiwan Institute of Chemical Engineers*, ***47***, 6-17.

[12] Gireesha, B. J., Mahanthesh, B., and Gorla, R. S. R. (2014). Suspended particle effect on nanofluid boundary layer flow past a stretching surface. *Journal of nanofluids*, ***3*****(3)**, 267-277.

[13] Das, S., and Jana, R. N. (2015). Natural convective magneto-nanofluid flow and radiative heat transfer past a moving vertical plate. *Alexandria Engineering Journal*, ***54*****(1)**, 55-64.

[14] Gireesha, B. J., Mahanthesh, B., Shivakumara, I. S., and Eshwarappa, K. M. (2016). Melting heat transfer in boundary layer stagnation-point flow of nanofluid toward a stretching sheet with induced magnetic field. *Engineering Science and Technology, an International Journal*, ***19*****(1)**, 313-321.

[15] Mahdy, A., and ElShehabey, H. M. (2012). Uncertainties in physical property effects on viscous flow and heat transfer over a nonlinearly stretching sheet with nanofluids. *International Communications in Heat and Mass Transfer*, ***39*****(5)**, 713-719.

[16] Pal, D., and Talukdar, B. (2010). Perturbation analysis of unsteady magnetohydrodynamic convective heat and mass transfer in a boundary layer slip flow past a vertical permeable plate with thermal radiation and chemical reaction.*Communications in Nonlinear Science and Numerical Simulation*, ***15*****(7)**, 1813-1830.

[17] Chamkha, A. J. (2003). MHD flow of a uniformly stretched vertical permeable surface in the presence of heat generation/absorption and a chemical reaction. *International Communications in Heat and Mass Transfer*, ***30*****(3)**, 413-422.

[18] Uwanta, I. J., and Omokhuale, E. (2012). Viscoelastic fluid flow in a fixed plane with heat and mass transfer. *Research Journal of Mathematics and Statistics*, ***4*****(3)**, 63-69.

[19] Ali, F., Khan, I., and Shafie, S. (2013). Conjugate effects of heat and mass transfer on MHD free convection flow over an inclined plate embedded in a porous medium. *PloS one*, ***8*****(6)**, e65223.

[20] Fetecau, C., Vieru, D., and Azhar, W. A. (2017). Natural convection flow of fractional nanofluids over an isothermal vertical plate with thermal radiation. *Applied Sciences*, ***7*****(3)**, 247.

[21] Tiwari,R.K.,and Das,M.K.(2007).Heat transfer augment in a two-sided Lid-driven DifferentiallyHeated square cavityUtilizing Nanofluids,*Int.J.Heat MassTransfer,**50**,2002-2018.*

[22] Oztoz,H.F.,and Abu-Nada,E.(2009).Numerical study of natural convection in partiallyheated rectangular enclosuresfilled with nanofluids,*Int.J.Heat Fluid Flow,**29**,1326-1336.*

**APPENDICES**

$$x_1 = \left(1-\varphi+\varphi\frac{\rho_s}{\rho_f}\right),$$

$$x_2 = (1-\varphi)^{2.5},$$

$$x_3 = \left(1-\varphi+\varphi\frac{(\rho\beta)_s}{(\rho\beta)_f}\right),$$

$$x_4 = \left(1+\frac{3(\sigma-1)\varphi}{(\sigma+2)-(\sigma-1)\varphi}\right)$$

$$x_5 = \left(1-\varphi+\varphi\frac{(\rho Cp)_s}{(\rho CP)_f}\right),$$

$$x_6 = \frac{K_{nf}}{K_f},$$

$$a_1 = x_1 x_2,$$

$$a_2 = \frac{x_3}{x_1},$$

$$a_3 = \frac{a_2 G_{re}}{G_{rt}},$$

$$a_4 = \frac{x_4}{x_1},$$

$$a_5 = a_4 M^2.$$

$$a_6 = \frac{\Pr x_5}{x_6+R},$$

$$a_7 = \frac{Ka}{x_5}$$

$$V_1 = \frac{KrSc}{a_6-Sc},$$

$$V_2 = \frac{a_6 a_7}{a_6-Sc},$$

$$V_3 = \frac{a_1 a_2}{a_6-a_1},$$

$$V_4 = \frac{a_1 a_5}{a_6-a_1},$$

$$V_5 = \frac{a_6 a_1 a_2 a_7}{(a_6-a_1)(a_6-Sc)}$$

$$V_6 = \frac{a_6 a_1 a_2 a_7}{(a_6-Sc)(a_1-Sc)},$$

$$V_7 = \frac{a_1 a_5 - KrSc}{(a_1-Sc)},$$

$$V_8 = \frac{a_1 a_4}{a_1-Sc}.$$

$$b_1 = \frac{V_3}{V_4},$$

$$b_2 = \frac{V_5}{V_1 V_4},$$

$$b_3 = \frac{V_5}{(V_4-V_1)V_4},$$

$$b_4 = \frac{V_5}{(V_1-V_4)V_1},$$

$$b_5 = \frac{V_6}{(V_1+V_7)V_7},$$

$$b_6 = \frac{V_6}{(V_1+V_7)V_1},$$

$$b_7 = \frac{V_6}{V_1 V_7},$$

$$b_8 = \frac{V_8}{V_7},$$

$$b_9 = b_1 - b_3,$$

$$b_{10} = b_7 - b_1 - b_2 - b_8,$$

$$b_{11} = b_3 - b_1,$$

$$b_{12} = b_1 + b_2,$$

$$b_{13} = b_4 + b_6,$$

$$b_{14} = b_5 - b_8,$$

$$b_{15} = b_8 - b_7.$$

$$c_1 = V_1 + Kr,$$

$$c_2 = \frac{V_2}{V_1},$$

$$c_3 = V_4 + a_5,$$

$$c_4 = V_1 + a_5,$$

$$c_5 = -V_7 + Kr,$$

$$c_6 = -V_7 + a_5.$$

$$I_1 = \frac{1}{2}\left( \ell^{y\sqrt{c_3 a_1}} erfc\left( \frac{y}{2}\sqrt{\frac{a_1}{t}} + \sqrt{c_3 t} \right) + \ell^{-y\sqrt{c_3 a_1}} erfc\left( \frac{y}{2}\sqrt{\frac{a_1}{t}} - \sqrt{c_3 t} \right) \right)$$

$$I_2 = \frac{1}{2}\left( \ell^{y\sqrt{a_1 a_5}} erfc\left( \frac{y}{2}\sqrt{\frac{a_1}{t}} + \sqrt{a_5 t} \right) + \ell^{-y\sqrt{a_1 a_5}} erfc\left( \frac{y}{2}\sqrt{\frac{a_1}{t}} - \sqrt{a_5 t} \right) \right)$$

$$I_3 = \frac{1}{2}\left( \ell^{y\sqrt{V_4 a_6}} erfc\left( \frac{y}{2}\sqrt{\frac{a_6}{t}} + \sqrt{V_4 t} \right) + \ell^{-y\sqrt{V_4 a_6}} erfc\left( \frac{y}{2}\sqrt{\frac{a_6}{t}} - \sqrt{V_4 t} \right) \right)$$

$$I_4 = erfc\left( \frac{y}{2}\sqrt{\frac{a_6}{t}} \right)$$

$$I_5 = \frac{1}{2}\left( \ell^{y\sqrt{V_1 a_6}} erfc\left( \frac{y}{2}\sqrt{\frac{a_6}{t}} + \sqrt{V_1 t} \right) + \ell^{-y\sqrt{V_1 a_6}} erfc\left( \frac{y}{2}\sqrt{\frac{a_6}{t}} - \sqrt{V_1 t} \right) \right)$$

$$I_6 = \frac{1}{2}\left( \ell^{y\sqrt{c_4 a_1}} erfc\left( \frac{y}{2}\sqrt{\frac{a_1}{t}} + \sqrt{c_4 t} \right) + \ell^{-y\sqrt{c_4 a_1}} erfc\left( \frac{y}{2}\sqrt{\frac{a_1}{t}} - \sqrt{c_4 t} \right) \right)$$

$$I_7 = \frac{1}{2}\left( \ell^{y\sqrt{c_5 Sc}} erfc\left( \frac{y}{2}\sqrt{\frac{Sc}{t}} + \sqrt{c_5 t} \right) + \ell^{-y\sqrt{c_5 Sc}} erfc\left( \frac{y}{2}\sqrt{\frac{Sc}{t}} - \sqrt{c_5 t} \right) \right)$$

$$I_8 = \frac{1}{2}\left( \ell^{y\sqrt{c_6 Sc}} erfc\left( \frac{y}{2}\sqrt{\frac{Sc}{t}} + \sqrt{c_6 t} \right) + \ell^{-y\sqrt{c_6 Sc}} erfc\left( \frac{y}{2}\sqrt{\frac{Sc}{t}} - \sqrt{c_6 t} \right) \right)$$

$$I_9 = \frac{1}{2}\left( \ell^{y\sqrt{Krsc}} erfc\left( \frac{y}{2}\sqrt{\frac{Sc}{t}} + \sqrt{Krt} \right) + \ell^{-y\sqrt{Krsc}} erfc\left( \frac{y}{2}\sqrt{\frac{Sc}{t}} - \sqrt{Krt} \right) \right)$$

$$I_{10} = \frac{1}{2}\left( \ell^{y\sqrt{c_6 a_1}} erfc\left( \frac{y}{2}\sqrt{\frac{a_1}{t}} + \sqrt{c_6 t} \right) + \ell^{-y\sqrt{c_6 a_1}} erfc\left( \frac{y}{2}\sqrt{\frac{a_1}{t}} - \sqrt{c_6 t} \right) \right)$$

$$\left.\frac{\partial I_1}{\partial y}\right|_{y=0} = \sqrt{\frac{a_1}{\pi t}}\ell^{-c_3 t} + \sqrt{a_1 c_3}\, erfc\left(\sqrt{c_3 t}\right)$$

$$\left.\frac{\partial I_2}{\partial y}\right|_{y=0} = \sqrt{\frac{a_1}{\pi t}}\ell^{-a_5 t} + \sqrt{a_1 a_5}\, erfc\left(\sqrt{a_5 t}\right)$$

$$\left.\frac{\partial I_3}{\partial y}\right|_{y=0} = \sqrt{\frac{a_6}{\pi t}}\ell^{-V_4 t} + \sqrt{a_6 V_4}\, erfc\left(\sqrt{V_4 t}\right)$$

$$\left.\frac{\partial I_4}{\partial y}\right|_{y=0} = \sqrt{\frac{a_6}{\pi t}}$$

$$\left.\frac{\partial I_5}{\partial y}\right|_{y=0} = \sqrt{\frac{a_6}{\pi t}}\ell^{-V_2 t} + \sqrt{a_6 V_2}\,erfc\left(\sqrt{V_2 t}\right)$$

$$\left.\frac{\partial I_6}{\partial y}\right|_{y=0} = \sqrt{\frac{a_1}{\pi t}}\ell^{-c_4 t} + \sqrt{a_1 c_4}\,erfc\left(\sqrt{c_4 t}\right)$$

$$\left.\frac{\partial I_7}{\partial y}\right|_{y=0} = \sqrt{\frac{Sc}{\pi t}}\ell^{-c_5 t} + \sqrt{c_5 Sc}\,erfc\left(\sqrt{c_5 t}\right)$$

$$\left.\frac{\partial I_8}{\partial y}\right|_{y=0} = \sqrt{\frac{Sc}{\pi t}}\ell^{-c_6 t} + \sqrt{c_6 Sc}\,erfc\left(\sqrt{c_6 t}\right)$$

$$\left.\frac{\partial I_9}{\partial y}\right|_{y=0} = \sqrt{\frac{Sc}{\pi t}}\ell^{-Krt} + \sqrt{KrSc}\,erfc\left(\sqrt{Krt}\right)$$

$$\left.\frac{\partial I_{10}}{\partial y}\right|_{y=0} = \sqrt{\frac{a_1}{\pi t}}\ell^{-c_6 t} + \sqrt{c_6 a_1}\,erfc\left(\sqrt{c_6 t}\right)$$

**HADRONIC JOURNAL 44**, 67 - 96 (2021)
DOI 10.29083/HJ.44.01.2021



# NEW THERMODYNAMICS: INELASTIC COLLISIONS, LOST WORK, AND GASEOUS INEFFICIENCY

**Kent W. Mayhew**
68 Pineglen Cres.
Ottawa, Ontario, Canada, K2G 0G8
kent.mayhew@gmail.com

Received January 5, 2021
Revised April 7, 2021

## Abstract

**Abstract**: This paper examines scientific "certainties" established during the 19th and 20th centuries regarding entropy and the second law. Indoctrinated thermodynamics is structured around elastic collisions. The realization that molecular collisions tend to be inelastic brings into question the validity of accepted thermodynamics. Boltzmann's inspired and brilliant mathematical edifices based upon elastic collisions remain a good approximation for many systems, especially those where the illusion of elastic collisions exists, e.g., most gaseous experimental systems. But, the laws of thermodynamics cannot be built around approximations which this author believes is currently the case. Explanations based upon lost work, friction and drag can explain why perpetual motion is an unrealistic notion. Gaseous inefficiency also occurs when one tries to use a gaseous system to perform work. An improved understanding based upon inelastic collisions alters how one views our universe. The possibility of using Hadronic mathematics to describe a world undergoing inelastic collisions will be briefly discussed.

**Keywords:** Inelastic collisions, lost work, gaseous inefficiency, latent heat, kinematic heat transfer, radiative heat transfer, Hadronic mathematics

Copyright © 2021 by Hadronic Press, Inc., Palm Harbor, FL 34684, USA

## 1. Introduction

Thermodynamics saw its 19th century creators include the likes of Sadi Carnot, Rudolf Clausius and Lord Kelvin. Ludwig Boltzmann in the 1890's provided a mathematical link between the atomic nature of matter and thermodynamics [1] with his statistical probability-based mathematics, whose ensembles were based upon elastic collisions, e.g., Boltzmann distribution a.k.a. Gibbs distribution.

The resulting mathematical genius has not enunciated thermodynamics with clarity. As stated by Sommerfield [2]: "Thermodynamics is a funny subject. The first time you go through it, you do not understand it all. The second time you go through it, you think you understand it, except for one, or two points. And the third time you go through it, you don't know you don't understand it, but by that time you are so used to it, it doesn't bother you anymore"

More recently, Haddad [3] has conveyed a similar sentiment: "In fact, no other discipline in mathematical science is riddled with so many logical and mathematical inconsistencies, differences in definitions, and ill-defined notation as classical thermodynamics. With few notable exceptions, more than a century of mathematicians have turned away in disquietude from classical thermodynamics, often overlooking its grandiose unsubstantiated claims and allowing it to slip into an abyss of ambiguity."

A goal of this paper is to provide thermodynamics with more clarity, starting with realistic collisions being inelastic collisions.

## 2. Elastic Collision

The following analysis for the consideration of an elastic collision is based upon consideration described in this author's book [4]. Consider that mass ($M_1$) moving with initial velocity ($\vec{v}_{1i}$) experiencing an elastic collision with mass ($M_2$) moving at velocity ($\vec{v}_{2i}$). To simplify the analysis, further consider that the trajectory of the two masses is along a solitary plane that passes through their centers of mass. Based upon conservation of kinetic energy for such an elastic collision, one could write:

$$\frac{M_1\vec{v}_{1i}^{\,2}+M_2\vec{v}_{2i}^{\,2}}{2}=\frac{M_1\vec{v}_{1f}^{\,2}+M_2\vec{v}_{2f}^{\,2}}{2} \qquad 1$$

Multiplying both sides of Eq. 1 by 2 and rearranging the variables gives:

$$M_1(\vec{v}_{1i}{}^2 - \vec{v}_{1f}{}^2) = M_2(\vec{v}_{2f}{}^2 - \vec{v}_{2i}{}^2) \qquad 2$$

In terms of difference of squares Eq 2 becomes:

$$M_1(\vec{v}_{1i} + \vec{v}_{1f})(\vec{v}_{1i} - \vec{v}_{1f}) = M_2(\vec{v}_{2f} + \vec{v}_{2i})(\vec{v}_{2f} - \vec{v}_{2i}) \qquad 3$$

For any collision, conservation of momentum means:

$$M_1\vec{v}_{1i} + M_2\vec{v}_{2i} = M_1\vec{v}_{1f} + M_2\vec{v}_{2f} \qquad 4$$

Rearranging Eq. 4 gives:

$$M_1(\vec{v}_{1i} - \vec{v}_{1f}) = M_2(\vec{v}_{2f} - \vec{v}_{2i}) \qquad 5$$

Dividing Eq. 3 by Eq. 5 yields:

$$\vec{v}_{1i} + \vec{v}_{1f} = \vec{v}_{2i} + \vec{v}_{2f} \qquad 6$$

Rearranging Eq. 6 gives an interesting result:

$$\vec{v}_{1i} = \vec{v}_{2f} + \vec{v}_{2i} - \vec{v}_{1f} \qquad 7$$

Eq. 7 states that the relative velocity before the collision equals the negative of the relative velocity after any elastic collision. For example, a super ball will bounce upwards with the same speed it had just before striking the floor.

Inserting Eq. 7 into Eq. 4 gives:

$$M_1(\vec{v}_{2f} + \vec{v}_{2i} - \vec{v}_{1f}) + M_2\vec{v}_{2i} = M_1\vec{v}_{1f} + M_2\vec{v}_{2f} \qquad 8$$

Rearranging the terms gives:

$$M_2/M_1 = (\vec{v}_{2f} + \vec{v}_{2i} - 2\vec{v}_{1f})/(\vec{v}_{2f} - \vec{v}_{2i}) \qquad 9$$

Eq. 9 does not readily determine what an elastic collision looks like. Accepting its validity renders an elastic collision into a rather rare event. Other equally complex solutions can be found [5,6].

However, setting $M_1$=$M_2$, does provide the simple solution for Eq. 9:

$$\vec{v}_{1f} = \vec{v}_{2i} \qquad 10$$

The simple solution for an elastic collision requires two identical masses with all the momentum being transferred from $M_1$ to $M_2$, where $M_2$ has an initial velocity of zero in a head on collision. A classic example takes place in a game of billiards. When the cue ball ($M_1$) hits another ball ($M_2$) through their centers of mass transferring all the momentum from $M_1$ to $M_2$.

A more interesting example of an elastic collision occurs in Newton's Cradle, where a series of balls hung by equal lengths of string, collide through their centers of mass with one another. Each ball and string act as an independent pendulum, which after colliding passes its momentum and its kinetic energy onto the ball with which it collides. Interestingly, if two balls are lifted and then released, it will be two balls that swing/oscillate, and if three balls are lifted (in a five-ball cradle), three of the five balls will swing/oscillate.

The above implies that an elastic-collision-criteria is that solid spheres of equal mass must collide through the centers of their masses, which seemingly validates Eq. 10. Energy is only lost by the drag of a moving ball in its surrounding atmosphere.

### 3. Inelastic Collisions

A simple example of an inelastic collision is a bullet hitting and then lodging itself into a piece of wood. In this inelastic collision, energy is conserved only because of the deformation of the bullet and wood, and any created collisional heat. For such an inelastic collision where the two masses become one, based upon Eq. 4, one obtains:

$$M_1\vec{v}_{1i} + M_2\vec{v}_{2i} = (M_1 + M_2)\vec{v}_f \qquad 11$$

Eq. 11 signifies a "completely inelastic collision" where the two colliding objects stick together after impact. Other inelastic collisions where the two

colliding objects do not stick together are next to impossible to model with any clarity.

## 4. The Question

If traditional statistical mechanics/thermodynamics is based upon elastic collisions and molecular collisions are inelastic, then why do the brilliant distributions of Boltzmann (a.k.a. Gibbs) and Maxwell, seemingly correlate with accepted experimental results?

The illusion of elastic collisions exists in most experimental systems [7-10]. Specifically, all inelastic molecular collision (inter and intra) must result in collision induced thermal energy (thermal photons or phonons), in order for energy to be conserved. This induced thermal energy is:

1) reflected back into the system off of reflective coatings often used in experimental apparatus; and/or

2) adsorbed by the experimental system's walls becoming phonons that may eventually be recirculated back into that system as photons.

In other words, many experimental systems suffer from the illusion of elastic collisions. And due to such illusions, the elastic collision based traditional thermodynamics becomes a valid approximation for experimental results.

Furthermore, the total energy associated with thermal phonons in most gaseous systems is often infinitesimal when compared to the total energy associated with the system's gaseous molecule's kinematics, e.g., translational, rotational and vibrational energies.

Moreover, one must keep in mind that photons travel at the speed of light, so their effects can be more significant than one would suspect based solely upon their total energy at a given instant. Effects include heat transfer, and thermal energy lost by open systems, i.e., if experimental walls are removed, the illusions of elastic collisions quickly disappear as most of the collision-induced thermal photons vanish into one's horizons.

It is inarguable that elastic collision-based conjecture enables mathematical simplification. However, a science structured around completely inelastic collisions, also elicits mathematical simplification. Questions arise, such as:

1) How accurate are the approximations of an elastic collision structure, to one's analysis?

2) Does strict adhesion to an elastic collision structure, cause over-complications of one's science?

No matter one's answers, it must be accepted that the sciences based upon the probability function whose basis is elastic collisions, often remains a reasonable approximation especially for systems where the illusion of elastic collisions exists.

## 5. Real World Elastic Collisions

A thermal photon associated with an inelastic intermolecular collision generally is infinitesimal when compared with the kinematics of a gaseous system. However, an ensemble of such collisions would lend itself to a spectrum of thermal photons. Where would one find such a spectrum?

This author concluded that a good candidate for such a spectrum is a blackbody radiation spectrum [4, 8-10]. Certainly, a cavity surrounded by condensed matter would be filled with such thermal photons from either (or both) inelastic intermolecular or intramolecular collisions. Moreover, the contents within such a cavity would be shielded from much of the wizardry that is generally witnessed here on Earth's surface [4,9,10]. And the placement of a hole into that cavity (e.g., Jean's cube) would expose those very thermal photons, as has been witnessed in the blackbody experiments of the late $19^{th}$ century [4,9].

Based upon an association of blackbody radiation with collision induced thermal photons, one attains an enlightened explanation for the light emanating from both tungsten lightbulbs, and our Sun [9]. Furthermore, much of the blackbody radiation witnessed in our cosmos could readily be explained in terms of inelastic collisions, e.g., both cosmic microwave blackbody radiation and Hawking's radiation [10].

It is accepted that electron-photon collisions are inelastic [11-12], as well as electron-electron collisions [13,14]. Models for inelastic molecular collisions have even been formulated [15]. Presented with all this, why would one even consider that the vast majority of intermolecular collisions are anything but inelastic? Unlike traditional kinetic theory, inelastic intermolecular collisions fit exceptionally well with this author's kinetic theory [4,16,17], which is a superior match to empirical findings. Moreover, this author's kinetic theory does not require any of the hordes of exceptions that plague traditional kinetic theory.

Unfortunately, most of accepted physics has its foundation vested in elastic collisions. The illusion of elastic collisions extends beyond kinetic theory into

the ideal gas law, Avogadro's hypothesis, and even the Navier-Stokes Equation [18]. Inelastic collisions challenges accepted dogma.

Finally, an interesting question facing physics arises: Why are elastic collisions limited to hard spheres of equal mass, whose collision occurs along a plane through their centers of mass [4]?

## 6. Traditional Mathematics and Inelastic Collisions

For simplicity's sake, point particles and electromagnetic (EM) waves propagating are traditionally treated as if they are in some homogeneous and isotropic vacuum, e.g., empty space. Such systems can be referred to as "exterior dynamical systems" [19,20], which consists "of particles at sufficiently large distances to [permit their point-like approximation under sole-action-at-a-distance interactions" [21].

Exterior dynamical systems include those that constantly place of all of a gaseous system's energy solely upon the gas molecules' kinematics, i.e., gaseous systems of elastic collisions. Such elastic collision-based systems conveniently ignore any radiation (residing or generated) within a system. Systems witnessing elastic collisions can be thermodynamically described using statistical thermodynamics, or be dynamically described using either the Hamilton or Lagrange equations.

The Hamiltonian is founded upon conservation energy that being the conservation of a system's kinetic plus potential energy. Here point particles (with kinetic energy) interact with potentials as action-at-a-distance. Certainly, both elastic and inelastic collisions (contact interactions) have zero range hence neither should be strictly Hamiltonian. However, dynamical systems where kinetic plus potential energy is conserved within that system, are really limited to systems undergoing elastic collisions, hence like statistical mechanics is troublesome when applied to real systems undergoing inelastic collisions.

The Lagrange equation considers the generalized forces upon particles/objects (dynamically speaking), hence are sometimes applied to reversible systems (thermodynamically speaking). Like the Hamilton equation, dealing with inelastic collisions within a system would not be ideally suited to the Lagrange equation, except for as a rough approximation. Furthermore, an ensemble of such inelastic collisions results in a thermal spectrum (e.g., a blackbody spectrum), and dealing with a thermal spectrum will add even more complexity to the problem.

Both the Hamilton and Lagrange equations may remain as approximations for systems where the illusion of elastic collisions exists, i.e., systems that recycle photons (or phonons) created by inelastic collisions, back into the system. As was the case of statistical mechanics this requires the blatant oversight of any radiation (thermal or otherwise) residing with a gaseous system.

The generally applied 20th century Hamilton and Lagrange equations are truncated equations i.e., neither considers forces that are not derivable from potentials, e.g., dissipative forces. [20,21]. Real world dynamics do not occur in isotropic vacuums, nor can they all be calculated using such truncated equation.

The above does raise the question: Is the 20th century acceptance of the truncated Hamiltonian and Lagrange equations primarily due to the illusion of elastic collisions in gaseous experimental systems?

It certainly explains why "all known potentials... and therefore all known Hamiltonians, are reversible" [21]. No matter one's acceptance, real world systems remain irreversible, therefore other considerations are obviously required.

## 7. Hadronic Mathematics and Inelastic Collisions

Santilli examined Lie's algebra in his Ph.D thesis (1960's) [21]. The reality that particles/objects generally experience non-conservative forces, which thermodynamically results in irreversible processes that can be considered using Lie's algebra. This led to the construction of "Lie-admissible" statistical mechanics [22,23]. Which eventually led to Hadronic mathematics [20,21,24], whose name is based upon the Hadron which is a subatomic composite particle. Note that Lie-admissible algebra is considered to be algebra in its most general form.

Rather than limiting thought to exterior dynamical systems, Hadronic mathematics is structured to deal with the more complex "interior dynamical systems", where "extended and deformable particles at mutual distances of the order of their size under action-at-a-distance interactions as well as contact nonpotential interactions". [21]

Interior dynamical systems include non-spherical deformable particles (extended particles) and EM waves that propagate inside of some non-homogeneous anisotropic physical medium. Solutions require unconventional math that is neither linear nor local.

So that there is no misunderstanding, Santilli considered exterior dynamical systems in terms of isomathematics, which dynamically speaking considers "time reversal invariant systems of extended and deformable particles" [20]. This allows for the existence of reversibility in thermodynamic systems undergoing elastic collisions.

Interior dynamical systems are dealt with in genomathematics, which dynamically speaking are intended for "time irreversible systems" [20], e.g., energy releasing processes in open systems. Promising applications for genomathematics has been found in both chemistry and nuclear physics, where resultant discrete energy is released. The benefits in describing the generalities of irreversible thermodynamic systems, is not so clear.

This author is the first to admit that he may not be the best suited to fully understand Hadronic mathematics, hence I recommend that others more qualified at dealing with such conceptualizations, read what has been written herein and then seek the brilliant writings of Santilli and others.

Particles undergoing inelastic collisions could be thought of as extended particles. The witnessed radiation from an ensemble of inelastic collisions results in a spectrum of photons (or phonons) that is non-linear, e.g., a complete blackbody spectrum is not mathematically linear. Part of the explanation for this might lay in the fact that molecules are not spherical balls. However, placing lack of sphericality as the sole explanation is premature, especially in light of the facts witnessed at larger scales, namely concerning Newton's cradle, where elastic collisions were limited to equal masses colliding along a path through their centers of mass.

Although this author believes that there may be promise with Hadronic mathematics (e.g., genomathematics in particular) when dealing with irreversible thermodynamic systems undergoing real inelastic collisions, the transformations currently used may be too linear, (e.g., eq. 3.65 in Santilli's paper [20] is for a linear velocity dependent dissipative force). Mind you, dragging an object along the ground can be approximated by a linear velocity dependent dissipative force, although at the molecular level it would be significantly more complex.

Perhaps one could approximate a complete radiated thermal spectrum (blackbody?), due to inelastic collisions, by some linear temperature dependent approximation (along the lines of Wein's approximation). This then could render Hadronic mathematics into a more suitable approximation for thermodynamic reality than the traditionally accepted mathematics can ever achieve.

Two issues remain. Firstly, when one reasons how thermal radiation results from inelastic collisions. If it concerns is in terms of extended particles undergoing deformations at the atomic scale, then what exactly is deforming? Could it be:

- charge distributions in atoms/molecules?: or
- associated nuclear magnetic moments?

Secondly, deformation during inelastic collisions at larger scales implies permanence. At all scales this may not be the case. Therefore, a basic premise may be to envision:

- an inelastic intramolecular collision as resulting in a loss of vibrational energy within molecules, and
- an inelastic intermolecular collision as resulting in the loss of kinetic energy by molecules in motion

Thermal equilibrium remains meaning that as much thermal energy is lost in creating thermal photons, as is gained in their absorption. Note that this considers that thermal equilibrium is purely radiative in nature.

All energy releasing processes in open systems remain irreversible, unless a mechanism exists that can recycle that energy back into the system. Hence some version of Hadronic mathematics may be determined as a superior mathematical fit when compared to the more traditionally accepted mathematics.

## 8. Lost Work

Irreversibility found in systems undergoing inelastic collisions, has been discussed. However, irreversibility also exists in expanding systems that experience lost work [4,7,9,17,25,26]. This occurs irrelevant of whether the expanding system undergoes elastic or inelastic molecular collisions.

Lost work provides insights into why entropy and the second law are ill-advised beyond being based upon misguided statistical thermodynamics, which is structured around elastic collisions.

For those not familiar with lost work, consider that one compresses a monatomic gas in a non-insulated piston-cylinder by placing a pair of identical masses ($M_1$ and $M_2$) on top of the piston as shown in Fig. 1. All movement will be considered as being frictionless, hence ideal.

The compressed gas can be defined in terms of its mechanical parameters, i.e., pressure ($P$) and volume ($V$). Such a $PV$ closed system can often be

modeled in terms of the number of molecules ($N$), Boltzmann's constant ($k$) and temperature ($T$), that being the ideal gas law:

$$PV = NkT \qquad 12$$

How much work was required to compress the gas? For infinitesimal compression, in terms of the gas inside of the piston-cylinder, the isothermal work required for compression [ $W_{(A\rightarrow B)}$] is an integral of increasing pressures change ($dP$) over decreasing incremental constant volumes.

$$W_{(A\rightarrow B)} = \int dw = \int_{P_A}^{P_B} V dp = (NkT) In\left(\frac{P_B}{P_A}\right) \qquad 13$$

As the monatomic gas' pressure increases ($P_A \rightarrow P_B$), an increasing amount of infinitesimal work ($dw$) is required to compress the gas another incremental volume ($V$). This explains why in terms of the gas inside the piston-cylinder, the work required is a natural logarithmic function, i.e., Eq. 13.

Consider that both the masses on top of the piston are removed. In terms of the gas inside of the piston-cylinder the isothermal work done [ $W_{(B\rightarrow A)}$] is again an integral but this time one contemplates it as incremental pressures ($P$) multiplied by infinitesimal volume increases ($dV$), i.e. ($V_B \rightarrow V_A$), hence:

$$W_{(B\rightarrow A)} = \int dw = \int_{V_B}^{V_A} P dv = (NkT) In\left(\frac{V_A}{V_B}\right) \qquad 14$$

Eq 14 is based upon the fact that as the gas' incremental pressure ($P$) decreases, the amount of work that an infinitesimal volume ($dV$) of gas can do, decreases.

The work required to lift [$W_{(\text{lift})}$] those masses a height [$dh_{(B\text{-}A)}$] , i.e., back to their original position is:

$$W_{(lift)} = (M_1 + M_2)\vec{g} dh_{(B\rightarrow A)} \qquad 15$$

The energy described by $W_{(lift)}$ was performed by someone or something external to the piston-cylinder, therefore that work remains external to the system's energy.

Whether considering infinitesimal compression or expansion, one often thinks that work is either being done onto the compressed gas, or being done

by the expanding gas. However, if work is actually done onto the compressed gas, or by the expanding gas, why has its temperature not changed?

In order to answer that question, one must realize that the piston-cylinder is a system inside of another system with the second system being our atmosphere. As the gas was infinitesimally compressed, any heat generated was allowed to escape out through the piston-cylinder walls, thus keeping the process isothermal., i.e., our atmosphere behaved as a heat sink.

Conversely, during infinitesimal expansion any heat lost by the expanding monatomic gas is replaced with thermal energy entering the gas through the piston-cylinder's walls, i.e., our atmosphere behaves as a heat bath. Obviously, one cannot simply consider work done by a system (e.g., piston-cylinder) without considering its interactions with the surrounding atmosphere.

As an open system, our atmosphere's pressure is really determined by its overlying weight (mass in gravitational field), thus it does not constitute a $PV$ closed system in the same manner that a closed system does. At a given elevation, the work is volume change ($dV$) multiplied by the pressure at that elevation. On Earth's surface work done onto our atmosphere is defined by:

$$W_{atm} = (PdV)_{atm} \qquad 16$$

Reconsider the monatomic gas' expansion, surrounded by the atmosphere. As the gas inside of the piston-cylinder expands, it must lift upwards the surrounding atmosphere's overlying mass, as is defined by Eq 16. This work results in a potential energy increase of our atmosphere.

Conversely, a piston-cylinder's volume decreases results in the atmospheric potential energy transform into atmospheric kinetic energy which is a form of heat as defined by kinetic theory (both the traditional and this author's). In other words, a contracting system witnesses an increase in the surrounding atmosphere's kinetic energy. The compression was due to the placement of the masses on top of the piston-cylinder, rather than any work from the atmosphere itself. Just as the lifting of those masses back to their original position required work, that was external to the system as defined by Eq 15.

## 9. Boiling

Consider what happens if one boils a liquid, as illustrated in Fig 2. The Hot System provides thermal energy ($dQ_{in}$) which heats the liquid and surrounding gas ($dE_{sys}$) that being System 1. Hence in terms of number of moles of liquid

($n_{liq}$), number of moles of gas ($n_{gas}$), their isometric molar heat capacities ($C_v$) and temperature change ($dT$):

$$dQ_{in} = dE_{sys1} = (n_{liq}C_{v_{liq}} + n_{gas}C_{v_{gas}})dT \qquad 17$$

Eq. 17 assumes that both the gas and liquid experience the same temperature changes and that their relative quantities remain constant.

At the liquid's boiling point, steam/vapours rapidly form inside of the piston-cylinder, i.e., a mass transfer from the liquid to gaseous state. The piston-cylinder now expands, hence does work onto the surrounding atmosphere ($W_{atm}$). Therefore:

$$dQ_{in} = dE_{sys1} + W_{atm} \qquad 18$$

There is no thermal energy from the surrounding atmosphere entering the insulated piston-cylinder during its expansion, i.e., all input thermal energy comes from the Hot System. Accordingly, no thermal energy leaves the atmosphere even though the atmosphere's potential energy is continually increasing, as the piston-cylinder expands. Now, the work done onto the atmosphere ($W_{atm}$) becomes lost work ($W_{lost}$), i.e., an irreversible energy lost into the surrounding atmosphere resulting in an irreversible atmospheric potential energy increase.

Therefore, the expansion of any heated enclosed system can now be rewritten in a more general form:

$$dQ_{in} = dE_{sys} + W_{lost} = dE_{sys} + (PdV)_{atm} \qquad 19$$

With the Hot System and any insulation around System 1 removed (see Fig. 3), heat radiates out through System 1's walls ($Q_{out}$) into the surrounding atmosphere, hence System 1 cools down. As System 1 cools there is also a mass transfer from the vaporous state back into the liquid state. This lowers the pressure inside the piston-cylinder, allowing the atmosphere to drive the piston back into the piston.

Some might argue that the atmosphere is doing work onto the contents in the piston-cylinder but this is not the case. If the atmosphere is doing work onto System 1, either its pressure or temperature must increase. Since, the pressure is atmospheric, while its temperature is decreasing, then no work is being done onto System 1.

The equation that describes what is happening to System 1 is simply:

$$dQ_{out} = dE_{sys1} \qquad 20$$

Eq. 20 could be rewritten in terms of heat capacities and number of moles, as Eq. 17 is written.

As the piston-cylinder's volume decreases, some of our atmosphere's potential energy is transformed into kinetic energy, which as was previously stated, is a form of heat.

**10. Vaporization vs Condensation**

Based upon Eq. 19, the latent heat of vaporization can be rewritten as [4]:

$$L_{(l\rightarrow g)} = dU + (PdV)_{atm} = dU + W_{lost} \qquad 21$$

Where "$L$' signifies the latent heat, "$(l \rightarrow g)$" indicates that the change is from liquid to gas, (i.e., vaporization), and "$dU$" is the change in bonding energy.

Since lost work is irreversible, the latent heat of condensation becomes [4]:

$$L_{(g\rightarrow l)} = -dU \qquad 22$$

Where "$(g \rightarrow l)$" signifies condensation.

Traditionally, it was incorrectly asserted that the latent heat of condensation is equal and opposite to the latent heat of vaporization, i.e., negative of Eq 21. Since no work can be done in condensation, it is logical to conclude that Eq 22 is correct. Why was this not previously realized?

One never actually measures the latent heat of condensation. Instead, the latent heat of vaporization is measured in an isobaric calorimeter, and then it is incorrectly assumed that the magnitude of latent heat of condensation is equal and opposite. Note that in 1887, John Joly [27] discussed using a gravimetric calorimeter for measuring condensation, but to this author's knowledge such a line of thought has not been rigorously applied.

The fact that many expanding systems perform lost work, while all contracting systems do not, broadens one's understandings. Many useful

systems that power our devices involve expansion, e.g., the steam engine. Irreversible lost work inevitably ends up heating our atmosphere, whether the end result is direct or indirect. This can be taken as part of one's analysis for debunking the second law. Before that is done, entropy must be discussed.

## 11. Entropy

Accepting the Equation written on Boltzmann's tombstone, which defines entropy in terms of the number of microstates ($\Omega$), i.e., the Boltzmann-Planck entropy Equation [4,28]:

$$S = kIn\Omega \qquad 23$$

Eq 23 relates entropy to statistical ensembles that are based upon elastic collisions, whose validity is limited to experimental systems where the illusions of elastic collisions reside.

The notion of entropy ($S$) began with Rudolf Clausius, as something which when multiplied by temperature ($T$) gives energy, i.e., $TS$=Energy.

Entropy increases (e.g., entropy production) is traditionally accepted as the explanation for thermodynamic irreversibility. Mathematically, discussion of entropy increases can become complex, as demonstrated by Hasegawa [29]. Herein, it has been argued that simpler explanations exist for irreversibility. Accordingly, simpler enlightenment for entropy increases is also needed.

Consider the traditionally accepted Equation for the isothermal entropy change in an expanding system. Let "$dE$" be the internal energy change, then one would write [4,28]:

$$TdS = dE + PdV \qquad 24$$

Eq 24 lacks clarity. Specifically, one might incorrectly infer that $PdV$ represents work done in terms of the expanding system [4,30,31], when in fact it is work done by the expanding system onto the surrounding atmosphere. Therefore, clarity is only obtained by rewriting Eq 24 as:

$$(TdS)_{sys} = dE_{sys} + (PdV)_{atm} = dE_{sys} + W_{atm} \qquad 25$$

Although Eq 25 possesses clarity, it is not founded upon sequential logic. The isothermal entropy change has been equated to the expanding system's

energy change plus work done by that expanding system onto the surrounding atmosphere. Since no one really knows what entropy is, this has to be the beginnings of circular logic [4].

Specifically, to claim that something equals something measured, and then to claim that something now proves why the something measured actually exists is circular logic. To then bury this logic in an ever increasing complicated array of probability-based statistical mathematics, does not alleviate the fact that it is now fully circular logic.

For a better understanding consider what $TdS$ represents beyond Clausius's assertion. Consider Eq 25 as a version of Eq 19, except now a heat bath is providing the required energy. Now consider Fig.4 where a heat bath drives the expansion of a fully insulated piston-cylinder.

The heat transferred from the heat bath into System 1 in terms of its isometric heat capacity ($C_v$) and number of molecules ($n$) is $[(nC_vdT)_{\text{bath}}]$. The heat bath's temperature decreases, hence assuming no phase change ($dU$=0) a first law equation describing this process is:

$$(nC_vdT)_{bath} = -[(nC_vdT)_{gas} + (PdV)_{atm}] \qquad 26$$

Consider that the thermal energy associated with the heat bath is orders of magnitude greater than the thermal energy required to increase System 1's temperature plus perform lost work. One understands why the heat bath's temperature remains constant, i.e., $dT_{\text{bath}}$=0, as measured by a thermometer. Just because the temperature decrease is immeasurable, does not mean that thermal energy did not exit the heat bath, i.e., the temperature drop is infinitesimal.

Upon observing this process, one might incorrectly conclude that the process, is an infinitesimal isothermal process, hence $T_{\text{gas}}$=$T_{\text{bath}}$. Obscure rationality may lead to the claim that this process can be explained in terms of the expanding gas' isothermal entropy change ($TdS$), i.e.:

$$(TdS)_{gas} = (nC_vdT)_{gas} + (PdV)_{atm}] \qquad 27$$

Eq. 27 is based upon the fact that the temperature change is immeasurable, rather than it did not occur. Hence, Eq. 27 becomes erroneous. Yes, Eq. 27 does allow for natural logarithmic functionality, but so too does Eq. 28, as will be discussed.

Emphasizing the above point. The heat bath has so much thermal energy in comparison to the expanding system, that the heat bath (and expanding system) seemingly remains isothermal throughout the process of expansion. Just because one's thermometer is not accurate enough to measure the heat bath's temperature change does not mean that the heat bath did not experience an infinitesimal temperature change [4,32].

In other words, the notion of isothermal entropy change, associated with a heat bath experiments, is a misguided supposition that further buries entropy's misguided circular logic origins. No wonder that entropy actually falters when perceived in terms of adiabatic processes [4,32]. No wonder, no one really knows what thermodynamic entropy means [33,34]. How could anyone? Of note, others have also questioned entropy's conscripts [34,35].

All aspects of heat transfer into an expanding system can be dealt with using Eq 19 (or Eq. 26). The bold misguided employment of Eq. 25 (or Eq. 27), hides the fact that one really does not know, and the over-complication hidden behind a mathematics contrived for elastic collisions is the icing on the cake. This was all backed by experimental systems that gave the illusion of elastic collisions.

## 12. The Second (so-called) Law

The origin of the second law was described in the 19th century, by Lord Kelvin: "It is impossible to transform an amount of heat completely into work in a cyclic process in the absence of other effects" [36]. This fundamental realization concerning the irreversibility of certain systems, basically describes perpetual motion, as an unrealistic notion. The 20th and 21st century conscripts of the second law are upheld in Reif's [28] statement: "In any process in which a thermally **isolated system** changes from one macrostate to another, its entropy tends to increase, i.e., $\Delta S \geq 0$".

This author has challenged the above statistical based assertion, with the realization that no expanding system here on Earth's surface can be an isolated system [4,25,26]. Specifically, the fact that all expanding systems must do work onto the surrounding atmosphere tells us with absolute certainty that any notion of an isolated expanding system must be limited to systems that are not surrounded by matter in a gravitational field, e.g., our atmosphere. Perhaps an isolated system remains applicable to a closed expanding system in outer space.

How does one now explain Lord Kelvin's inarguable statement? Lost work clearly explains why the running of a useful expanding system, such as an engine (steam or petroleum powered), is an irreversible process. Therefore, useful expanding systems cannot power a perpetual motion device. To the condition of not having perpetual motion, one can further add friction (both internal and external) to a mechanical system, resulting in the production of heat, which ultimately ends up in our heat sink e.g., our atmosphere and oceans. One could further add drag, a combination of resistance to motion and frictional heat generated by inelastic collisions, between a moving object and its surrounding atmosphere. This helps to explain why perpetual motion cannot occur here on Earth's surface.

Another interesting second law-based statement is Haddad's [3] "the usable energy in an adiabatically isolated dynamical system is always diminishing in spite of the fact that energy is conserved". Realizing that useful expanding systems that do work onto their surrounding atmosphere also diminishes the notion of an "adiabatic isolated dynamical system". Moreover, one can envision that, as an expanding system does work onto the surrounding atmosphere, its ability to do more work diminishes as its pressure decreases, even if the expanding gas remains isothermal. And this may be deemed a degradation of the system's energy, as Haddad implies.

A more pragmatic understanding may be deduced by considering two systems in thermal and physical contact, e.g., System A is at both a higher temperature and pressure than System B, i.e., $T_A > T_B$ and $P_A > P_B$. Then:

1) hotter System A can pass thermal energy onto System B, i.e., $dQ_{(A\rightarrow B)}$.
2) higher-pressure System A can do work onto System B, i.e., $dW_{(A\rightarrow B)}$.

Importantly, the rate of heat transfer will decrease as $T_A \rightarrow T_B$,, hence in terms of some constant "C":

$$\frac{dQ_{(A\rightarrow B)}}{dt} = -CIn\left(\frac{T_B}{T_A}\right) \qquad 28$$

If System A was a heat bath, then $T_A$ would be considered as being constant. Similarly, the rate of work will decrease as $P_A \rightarrow P_B$, hence in terms of some constant "A":

$$\frac{dW_{(A\rightarrow B)}}{dt} = -AIn\left(\frac{P_B}{P_A}\right) \qquad 29$$

If System B was our atmosphere, then $P_{atm}$ would be considered as constant.

The above formulas lead to two important considerations. Firstly, choosing to use the entropy based second law to explain a system's energy degradation is another over-complication. Certainly, a system's capability to transfer thermal energy, or do work, can be explained in simpler terms. Secondly, the natural logarithmic functionality that is so often associated with entropy in thermodynamics, can now be explained with a superior clarity allowing for the dismissal of Clausius' notion of entropy.

## 13. Gaseous Inefficiency

There is still one more issue that is plain to see yet not so obvious. It concerns the inherent "gaseous inefficiency" when a gas's kinetic energy is transformed into work. Compare the ideal gas law (Eq 12) to the total kinetic energy ($E_{k_{tot}}$) of a gas:

$$E_{k_{tot}} = 3NkT/2 \qquad 30$$

As defined by the ideal gas law, the $PV$ space of a gas is 2/3 a gas' total kinetic energy. This is counter-intuitive, but it is our reality.

This author is inclined to believe that the explanation lay in the total molecular "flux" ($\Phi_{\text{work}}$) of an enclosed gas that strikes a unit surface area per unit time that can do work. That being:

$$\Phi_{\text{work}} = \left(\frac{1}{4}\right) n\bar{v} \qquad 31$$

Note Eq 31 is obtained by the summation over all possible speeds ($0< \upsilon < \infty$), over all possible azimuth angles ( $0 < \varphi < 2\pi$) and over all possible angles ( $0 < \theta < \pi$), [4,28].

In kinetic theory, the flux of energy imposed upon an enclosed gas, is from the system's six orthogonal walls. The energy flux ($\Phi_{\text{energy}}$) from any one of those orthogonal walls, in any one of the six plausible directions is:

$$\Phi_{\text{energy}} = \left(\frac{1}{6}\right) n\bar{v} \qquad 32$$

Eq 31 and Eq 32 imply that two thirds of a gas' kinetic energy can be used for work. It must be emphasized that this is most likely limited to gases in enclosed systems, where the structured rigid wall molecules impose their energetics onto the gas molecules that they enclose, e.g., most gaseous experimental systems.

## 14. Limitations of the Accepted Sciences

It should be stated that kinetic theory, Avogadro's hypothesis and the ideal gas law are all limited to closed systems of gases that are sufficiently dilute. Sufficiently dilute means that the primary intermolecular inelastic collision is between the gas molecules and their surrounding walls [4,16,17]. Furthermore, a sufficiently dilute system would also be a system where the illusion of elastic collisions can exist.

When the intermolecular collisions are dominated by gas-gas molecule collisions, many accepted fundamentals of the sciences falter, in part because the illusion of elastic collisions is lost [4]. A prime example of systems dominated by gas-gas molecular collisions is the stars, for which the polytropic equations were devised to define their $PV$ space.

Importantly, when the illusion of elastic collisions is lost, Boltzmann's statistical probability-based math falters. This will be the toughest pill of them all for the physics community to even fathom, yet alone swallow.

## 15. Enhancing One's Understanding of Work

For clarification purposes, consider that an enclosed system's $PV$ space, as defined by the ideal gas law, is actually a representative of a system's ability to do work, i.e., a system's ability to do work ($W_{abi}$) is:

$$W_{abi} = d(PV) = NkdT \qquad 33$$

The system's ability to do work is in relation to a system of zero pressure. So, when differentiated the ideal gas law represents the ability of a system of gas to do work. Another way of looking at this is that the accretion of the dust and particles that formed Earth and its surrounding atmosphere, took work. Therefore, $d(PV)$ becomes a comparison to that result.

On the other hand, a higher-pressure system's potential ($W_{pot}$) to do work onto our atmosphere becomes:

$$W_{pot} = V(P_{sys} - P_{atm}) \qquad 34$$

The potential to do work is the work that can be done in terms of the surrounding atmosphere.

As a final consideration, re-examine Fig. 1 here the compressed piston-cylinder B becomes lower pressure compressed-cylinder C. When $M_2$ is removed then the work done by the gas [ $W_{(B\to C)}$] in going from B to C, is onto both $M_1$ and the surrounding atmosphere. Therefore:

$$W_{(B\to C)} = (PdV)_{atm} + M_1\vec{g}dh_{(B\to C)} \qquad 35$$

Eq 35 reinforces the understanding that the compressed gas lifts both the surrounding atmosphere and mass ($M_1$), increasing both their potential energies. And both the work onto the surrounding atmosphere and in raising $M_1$ are external to the expanding closed system.

Furthermore, this work can be isothermal when thermal energy enters an expanding system through the system's walls from the surrounding walls, or the system is heated infinitesimally from some heat source. Of course, such understanding forgoes the necessity of some isothermal entropy entwined arguments.

Importantly, when the illusion of elastic collisions is lost, Boltzmann's statistical probability-based math falters. This will be the toughest pill of them all for the physics community to even fathom, yet alone swallow.

## 16. Kinetic vs Radiative Heat Transfer and Coatings

Seim and Olsen [39] hung two folded (envelope shaped) pieces of aluminum foil in a box, whose walls were clear plastic. One folded piece was painted black while the second was untouched. The box was first heated with a tungsten-halogen lamp (500W). As expected, the temperature of the black piece increased faster than the untouched aluminum foil. They then heated the box with a hot plate and found the reverse occurred, i.e., the aluminum piece heated faster than the black piece. No explanation for this unexpected result was provided.

A tungsten-halogen lamp is dominated by radiative heat (thermal photons) from a blackbody radiation spectrum (T=3,200 K) [40], which is somewhat redder than our hotter Sun's blackbody spectrum (T = 5,800 K). Behaving as a

classical blackbody, the black foil adsorbs most of the thermal radiation, thus explaining why the black foil heated faster. Note that the shiny aluminum foil should reflect 90% (or more) of the incident radiation for the visible through the infrared spectrum (wavelengths: 248 nm to 100 μm [41]). Thus, one can assume that the aluminum foil is primarily heated due to "kinematic heat transfer" from the inelastic collisions with surrounding gas molecules, i.e., heat transfer explained by this author's kinetic theory of gases [16, 17].

Conversely, when heated by the hot plate, one expects that the thermal energy transfer is primarily due to kinematic heat transfer, i.e., radiative heat transfer becomes a secondary process. This author speculates that the paint must have had a rubber component to it, therefore the surrounding gas molecules bounced off, rather than transferring their kinetic energy onto the blackened foil.

Although unintended, Seim and Olsen [39] have demonstrated that heat transfer into and/or by gases should often be separated into two parts, such as "radiative" and "kinematic heat transfer".

One can also extend the above findings to experimental systems with thermal reflective coatings, as previously discussed. It becomes apparent that an experimental system with reflective coatings, reflects most thermal photons back into an experimental system, thus enhancing the illusion of elastic collisions.

## 17. Understanding Radiative Heat Transfer

Radiative heat transfer suffers from similar over-complication as kinematic heat transfer. This is perhaps best demonstrated by discussing the input from our Sun.

Consider Haddad [3] discussing that "the photons absorbed by Earth from the Sun have a much higher frequency... than those dissipated to space by the Earth, it follows from Planck's formula relating the energy of each photon of light to the frequency of the radiation it emits that the average energy flow into the Earth from the Sun by each individual photon is far greater than the dissipated energy by the Earth to dark space."

There is nothing wrong with the above consideration. Our Sun emits a blackbody spectrum whose peak is in the visible spectrum (as defined by Wein's law). Part of our Sun's incoming visible spectrum is reflected back out into space, therefore not all of our Sun's visible spectrum is transformed into thermal energy. Furthermore, other parts of our Sun's visible spectrum is

absorbed and then radially radiated as heat, that being lower frequency photons. Hence, conservation of energy tells us that the number of radially radiated thermal photons must be at a greater number than the absorbed visible photons from our Sun.

It should be emphasized that the above absorption and ensuing radial radiation as heat, is performed by both condensed matter and polyatomic gases, whose temperatures are closer to 300 K than that of our Sun (5,800 K). Condensed matter and/or an ensemble of polyatomic gases, near 300 K radiate a blackbody spectrum whose peak is in the infrared spectrum, which is generally considered as heat.

Furthermore, although our Sun emits a blackbody spectrum whose peak is in the visible spectrum, a significant portion of our Sun's irradiance is in the infrared [8,9,10,42]. And this significant infrared portion of our Sun's blackbody spectrum will be absorbed, and then radially radiated as blackbody spectrum, whose peak is also in infrared spectrum (T near 300 K).

The above understanding is relatively simple. It does become an over-complication when one tries to then explain this in terms of entropy and the second law. This is demonstrated by the following continuation of Haddad's [3] statement (after "Earth to dark Space"). "This implies that the number of different photon microstates is far greater than the number of microstates carrying the same energy from the Sun to the Earth. Thus, it follows from Boltzmann's entropy formula that the incident energy from the Sun is at considerably lower entropy level than the entropy produced by the Earth through energy dissipation"

Haddad's consideration was easy to deal with up until he felt the indoctrinated need to bring Boltzmann's entropy formula (Eq 23) into it. Haddad continues the overcomplication by discussing how the Earth maintains entropy and uses the free energy argument to support his discussion. Is this all necessary? The answer is no, but only if one question's our indoctrination. Note that this author has previously challenged the conscripts behind free energy.[30]

**Conclusions**

Traditional thermodynamics is based upon a mathematical conscript that incorrectly strictly adheres to the notion of elastic molecular collisions. This has been reinforced by experiments in gaseous systems where the illusion of elastic collisions exists. Gaseous systems displaying such illusions tend to be

those where the intermolecular collisions between gas molecules and the system's walls dominate, and where the walls can adsorb and then recirculate any thermal energy created by molecular inelastic collisions, e.g., collisional induced thermal photons.

""Science" requires a mathematical treatment producing numerical values that can be confirmed by experiments" [21]. One understands the obscurantism, i.e., the overlooking of the illusion of elastic collisions in experimental systems, concluding that experiments back the elastic collisional based mathematics, e.g., statistical mechanics, as well as the truncated Hamilton and Lagrange equations.

Certainly, a thermal photon from an inelastic collision signifies an infinitesimal amount of energy in comparison to that of most systems. However, an ensemble of such collisions forms a spectrum of thermal radiation. It has been postulated that blackbody radiation spectrum could be a thermal spectrum from such an ensemble of inelastic collisions.

Even as a spectrum, the instantaneous energy associated with thermal photons often is infinitesimal when compared to the energies associated with gaseous molecules. However, the speed of gaseous molecules is infinitesimal when compared to the speed of light. Therefore, the rates of heat transfer in closed systems due to thermal photons and/or the rate of thermal energy (heat) loss due to photon (thermal and otherwise) emission from an open system can be significant.

The energetics of many systems may be approximated by mathematics based upon elastic collisions, which simplifies the math. Certainly, rewriting the sciences based upon inelastic collisions at the molecular scale is a monumental task, one that may have no end, especially when dealing with fully open systems, where simple approximations may not exist. The mathematical understanding may start with Hadronic mathematics, but that has been left for others to determine.

In order to appreciate all the dynamics associated with work and energy, one cannot focus upon a given system, rather one must look at most systems as a system within a second system, with the second system being the first system's surroundings, e.g., our atmosphere.

Lost work is irreversible work, that occurs when energy is transferred from most useful expanding systems into the surrounding atmosphere. Realizing that our atmospheric pressure is defined in terms of the overlying weight of the atmosphere at a given elevation, the lost work done onto our atmosphere is defined by: $W_{lost} = W_{atm} = (PdV)_{atm}$.

Lost work signifies a potential energy increase of our atmosphere. Some of our atmosphere's potential energy is readily transformed into atmospheric kinetic energic (heat) when a system's volume decreases. This also means that the latent heat of condensation does not involve work, hence it is not equal in magnitude to the latent heat of vaporization, which involves lost work.

Many useful systems, that power mankind's machinery, involve systematic volume increases hence lost work. This in part helps to explain why the second law based upon increasing entropy, is no longer required when explaining why perpetual motion is not a realistic notion. Other reasons for perpetual motion's vincibility include friction and drag, with drag being a combination of resistance and friction (heat from inelastic collisions) between a moving object and its surrounding atmosphere.

Thermodynamic irreversibility in terms of an isothermal entropy increase is an unnecessary over-complication. Energy losses such as those associated with inelastic collisions and lost work, are better logic-based explanations for irreversibility in systems.

Another reason for inefficiencies is that only 2/3 of a gas's kinetic energy can be used for work. This can be ascertained by comparing a gas' kinetic energy to its ability to perform work. The reasoning most likely has to do with the fluxes of gases, and this means that the maximum efficiency when using a gas' kinetic energy to perform work is 66.667%.

Furthermore, using the second (so-called) law to explain a degradation of a system's energy is another over-complication. Explaining a degradation of a systems energy in terms of lost work, or changes to the rate at which a system can exchange energy, or perform work, elicits a simpler understanding.

Thermodynamics is not the mature science once thought, as it is in need of a rethink. Boltzmann's, Maxwell's and others' distributions that subscribe to elastic collisions remains beneficial, but only as approximations to idealized systems. Real-world approximations should be determined, e.g., modified Hadronic mathematics. Formulating laws, namely the second law, based upon elastic collision approximations, is not great science. Finally, entropy's status, in all of its guises, needs to be re-examined.

**Figures**

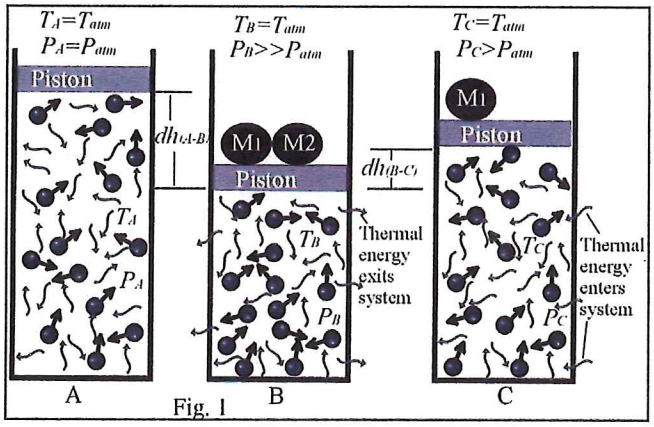


Fig. 1

Fig. 1 shows a piston-cylinder at atmospheric pressure and temperature in A. Then at a higher compressed pressure in both B and C, while still remaining at atmospheric temperature ($T_{atm}$).

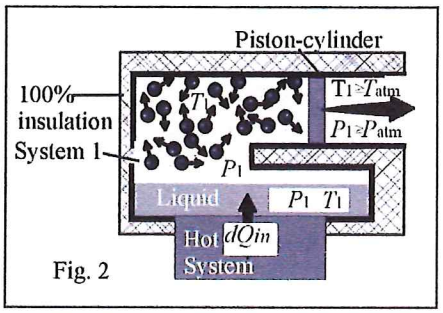


Fig. 2

Fig. 2 shows a Hot System heating a liquid in fully insulated System 1, which eventually leads to boiling and the System 1's isobaric expansion using a piston-cylinder apparatus.

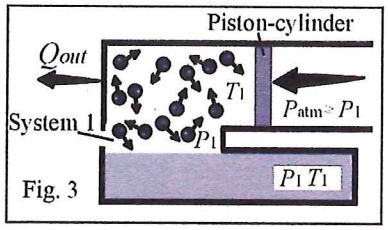


Fig. 3 shows the apparatus of Fig. 2, but now with both the Hot System and with System 1's insulation removed.

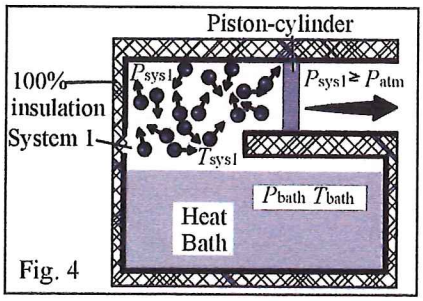


Fig. 4 shows a heat bath driving the expansion of a fully insulated piston-cylinder

**Acknowledgements**

I would like to thank Lloyd and Gail Mayhew for their assistance in putting this paper together

**References**

1) Gyftopoulos, E.; Beretta, G. "Thermodynamics. Foundations and Applications", Macmillan, N.Y., USA, 1991.
2) https://www.goodreads.com/quotes/7149061-thermodynamics-is-a-funny-subject-the-first-time-you-go-through
3) Haddad, W.M., "Entropy Thermodynamics: The Unique Universal Science" Entropy, 19 (2017) pg 1-70

4) Mayhew K.W, "New Thermodynamics: Untangling Entropy's Web, Includes treatise on Global Warming" (2020) https://www.amazon.ca/New-Thermodynamics-Untangling-Entropys-Treatise/dp/B087SGS55J
5) http://hyperphysics.phy-astr.gsu.edu/hbase/elacol2.html, Dec., 26, 2020
6) Sears, F., Young, H., Zemansky, M., "University Physics", Addison Wesley Publishing company, Reading Massachusetts, 1987
7) Mayhew, K.W., "New thermodynamics: Illusions of Elastic Collisions in the Sciences", EJERS, Vol. 5, 1, (2020), pg 87-90
8) Mayhew K.W., "New Thermodynamics: New Thermodynamics: Temperature, Sun's Insolation, Thermal, and Blackbody Radiation", EJERS, Vol. 5, 3(2020) pg 264-270
9) Mayhew, K.W., "New Thermodynamics: Inelastic Collisions, Blackbody Radiation, Entropy and Light", Vol 2, 6, pg 1-6
10) Mayhew, K.W., "New Thermodynamics: Inelastic Collisions and Cosmology", E-J Phys. Vol 2, 6, (2020) pg 1-7
11) J. M. Jauch and F. Rohlich, "The theory of Photons and Electrons" Cambridge, MA:Addison-Wesley,1955
12) H. A. Bethe and E. E. Salpeter, "Quantum Mechanics of One and Two electron Atoms", New York: Springer-Verlag, 1957.
13) Eliashberg, G.M. "Inelastic Electron Collisions and NonEquilibrium Stationary States in Superconductors" Sov. Phys. JETP Vol 34, 3, (1972)
14) Schramm et. al. "Vibrational resonance and threshold effects in inelastic electron collisions with methyl iodide molecules" J of Phys. B: Atomic, Molecular and Optical Physics Vol 32, 9, (1999)
15) Plass, W., R., Cooks, R.G., "A model for energy transfer in inelastic molecular collisions applicable at steady state or non-steady state and for an arbitrary distribution of collision energies" J of Am. Soc, for Mass Spectr. Vol 14, 12 (2003) 1348-1359.
16) Mayhew, K.W., "A New Perspective for Kinetic Theory and Heat Capacity", Prog. in Phys., Vol. 13, 4 (2017) pg 166-173
17) Mayhew, K.W. "Kinetic Theory: Flatlining of Polyatomic Gases", Prog. in Phys., Vol. 14, 2 (2018) pg 75-79
18) Mayhew, K.W., "New thermodynamics: Illusions of Elastic Collisions in the Sciences", EJERS, Vol. 5, 1, (2020), pg 87-90
19) Muktibodh, A. S., "Foundations of Isomathematics": https://www.researchgate.net/publication/260829382_Foundations_of_Isomathematics

20) Santilli. R.M. "An Introduction to New Sciences for a New Era" Clifford Algebras and their Applications Vol. 6, No. 1, (2017) p. 1-119,
21) Santilli, R.M., "Hadronic Mathematics, Mechanics and Chemistry Vol 1" International Academic Press (2008)
22) Fronteau, J., Tellez-Arenas, A. and Santilli, R.M., ``Lie-admissible structure of statistical mechanics," Hadronic J., Vol. 3, p. 130-176 (1979)
23) Santilli,R.M., "An Introduction to Lie-Admissible Algebra" Supplemento al Nuovo Cimento 1, 6 (1968) pg 1225-1249
24) Anderson, R., "Outline of Hadronic Mathematics, Mechanics and Chemistry by R.M. Santilli" Am. J. of Modern Phys. 4,5:1 (2015)
25) Mayhew, K.W., "Second law and lost work", Phys. Essays **28**, vol 1,152 (2015)
26) Mayhew, K.W., "New Thermodynamics: Inefficiency of a Piston-Cylinder", EJERS Vol 5, 2, (2020) pg 187-191
27) Joly, John, "On the method of condensation in calorimetry" Proceedings of Royal Society London (1887)
28) Reif, F., "Fundamentals of Statistical and Thermal Physics", McGraw-Hill, New York, 1965
29) Hasegawa, H, "Thermodynamic properties of Non-Equilibrium states subject to Fokker-Planck equations", Prog. Of Theor. Phys. 57, 5 (1977) pg 143-157
30) Mayhew, K.W., "Resolving Problematic Thermodynamics", Hadronic Journal, vol 41, 3, (2018) pg 259-272
31) Mayhew, K.W., "New Thermodynamics: Reversibility and Free Energy", Hadronic Journal, Vol 43, 1, 2020 pg. 51-60
32) Mayhew, K.W., "New Thermodynamics: Reversibility, Entropy and Adiabatic Processes" E-J Physics, Vol 2 Issue 2, (2020)
33) Mayhew, K.W., "Entropy an ill-conceived mathematical contrivance" Phys. Essays **28** vol 3, 352 (2015)
34) Ben-Naim, A., "A Farewell to Entropy: Statistical thermodynamics Based on Information." World Scientific Publishing Co Hackensack NJ 2011
35) Aguirre, J. and Hernandez, H. (2020). "Entropy: A Physical Entity or a Mathematical Construct?" ForsChem Research Reports, 5, 2020-10. doi: 10.13140/RG.2.2.34938.93124.
36) Dunning-Davis, Jeremey "A Cautionary Note on the Second Law of Thermodynamics" Presented in 2010
37) Wikipedia: https://en.wikipedia.org/wiki/Boltzmann_constant Dec., 27, 2020
38) Feynman, R. (1970). *The Feynman Lectures on Physics Vol I*. Addison Wesley Longman. ISBN 978-0-201-02115-8.

39) Seim, T.O. and Olsen B.T. "Unexpected relationships between thermal and radiative transfer" Atm. and clim. Sci. vol 10 no 4 (2020)
40) http://zeiss-campus.magnet.fsu.edu/articles/lightsources/ tungstenhalogen.html Dec., 2, 2020
41) https://laserbeamproducts.wordpress.com/2014/06/19/reflectivity-of-aluminium-uv-visible-and-infrared/, Dec., 2, 2020
42) https://www.ncbi.nlm.nih.gov/pmc/articles/PMC4841185/ Nov., 22, 2020

**HADRONIC JOURNAL 44**, 97 - 108 (2021)
DOI 10.29083/HJ.44.01.2021


# CALCULATION OF THE EXACT RANGE OF THE MASS OF HIGGS BOSON IN THE LARGE HADRON COLLIDER (LHC) ON THE BASIS OF THE QUANTIZED SPACE AND TIME THEORY.

**Hamid Reza Karimi**
Electrical Engineering Department
Islamic Azad University, South Tehran Branch
Tehran, 17776-13651, Iran
hr.karimy@gmail.com

Received May 19, 2020
Revised February 20, 2021

**Abstract**

In this paper by applying the Quantized space and time theory, the speed limit of protons has been determined and consequently the Lorentz factor has been calculated with a high degree of accuracy. Eventually the mass equivalent to energy of Higgs boson which is created by collision of two proton beams (This experiment has been performed in LHC) has been calculated. .

Key words: Higgs boson, speed limit, quantized space and time

Copyright © 2021 by Hadronic Press, Inc., Palm Harbor, FL 34684, USA

**1-Introduction:**

By considering the speed limit under the rules of quantized space and time rules, Lorentz factor will be equal to 1722.9[1]
Exact determination of Higgs boson mass by using quantum relativity is difficult. According to the ultra-high voltage applied on each particle of protons (13Tev)in LHC[2], the Lorentz factor with current relativity rules and field of 13Tev is equal to: $\gamma = \frac{1}{\sqrt{1-\frac{v^2}{c^2}}} = 6930$: Lorentz factor[2](1)

Regarding to relativity, if the speed of particles increase to speed of light then the energy of them should be infinitive, so the energy of Higgs boson in the produced radiation of collision two beams of proton to each other in LHC cannot be calculated precisely [3].
On the basis of the Quantized space and time theory, which has been defined by the author, all of the charged elementary particles have a speed limit equal to: $V_{max}$=299792407.5m/s [1].
Existing of speed limit, which makes the precise calculation of the Higgs boson mass possible, is a strong proof of the quantized baryonic universe.
Assuming the space and time quantized, help us to prevent of making infinitive amounts in special relativity and uncertainty of Heisenberg principle.
**1-1:** Why the speed is not quantized meanwhile the space and time are quantized? This is the main question. This question is burst because of the time and space considered abstract, and then the movement add to them. The Mach principle says the geometry will be collapsed without the material [4]. This fundamental principle leads us to find out the elementary particles makes their own internal space, time and movement. The triangle of movement. Time and space creates the baryonic universe. In the following a relation will be presented which express the external speed of elementary particles.

1-2: by using two axioms in baryonic universe we will have the minimum possible length not separable to smaller lengths which still contains motion and it is equal to $l_0$ : Length quanta $= 1.409\times10^{-15}m$. (2) [1]
The minimum possible time which there is no smaller time interval than it, is equal to,

$\Delta T_0$ : Time quanta $= \frac{l_0}{c} = 0.47\times10^{-23}$ (3)[1]

Where c = 299,792,458 m/s is the speed of light
There are a lot of samples of these two amounts of quantas, in the baryonic universe. Such as the nuclear power range, the life time of vector mesons and...
1-3: There are some problems in assuming the time and space quantized with above mentioned axioms, the first one is; the Plank's length and time are much smaller than our axiom.

$$\ell_p = \sqrt{\frac{\hbar G}{c^3}} = 1.616252 \times 10^{-35} m \qquad (4)\ [1]$$

$$t_p = \frac{l_p}{c} = 5.39124 \times 10^{-44} s \qquad (5)\ [1]$$

And the second one is how beginning and the end of each length and time quanta can be separated from the next one?
The third problem is how the energy is limited in these quantas and wouldn't radiated entirely?

**2- Super dimension:**

To solve the problems of previous section, another axiom is needed, that is a super dimension [1]. The super dimension is a compressed ladder string by the width of Plank's length which doesn't have any baryonic movement individually. It is illustrated in the Fig.1 as the black spiral and its vertical axis [1].
The figure 1 shows the creation of the frequent time and space sequences of electron on his own. The sequence of time and length quanta of an electron in super dimension is shown as $\overrightarrow{S_n}$. The electron has positive spin angular momentum with a relative velocity with respect to a local frame.

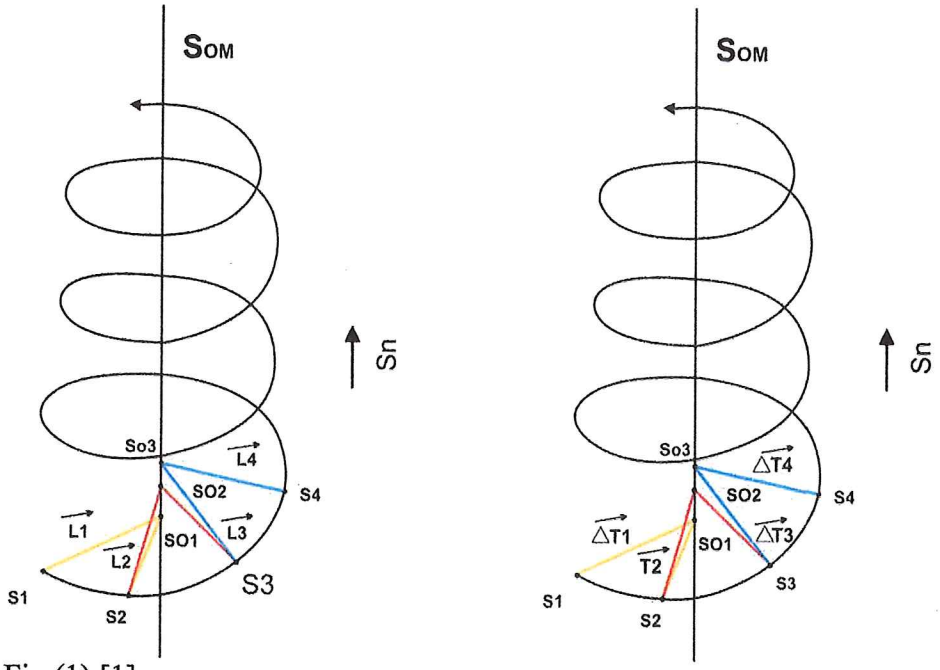


Fig (1) [1]

When the moton is purred in the string of super dimension due the time and length of colored lines in the figure 1 , it finds same measurable dimension

**3- The relative velocity:**

We can find the relative velocity of a particle with respect to a reference frame using Figures1 [1]

$$\vec{V}^2 = \left(\frac{\vec{l}_{1(so1)}}{\Delta\vec{T}_{1(so1)}} \times \frac{\vec{l}_{2(so1)}}{\Delta\vec{T}_{2(so1)}}\right) - \left(\frac{\vec{l}_{2(so2)}}{\Delta\vec{T}_{2(so2)}} \times \frac{\vec{l}_{3(so3)}}{\Delta\vec{T}_{3(so3)}}\right), \qquad (6)\ [1]$$

$$\vec{l}_0 = \vec{l}_1 = \vec{l}_{2\ (S_{o1})} = 1.409\times10^{-15}\text{m}, \qquad (7)\ [1]$$

$$\Delta\vec{T}_0 = \Delta\vec{T}_1 = \Delta T_{2\ (S_{o1})} = 0.47\times10^{-23}\text{s}, \qquad (8)\ [1]$$

$$\vec{l}_{3\ (S_{o2})} = \frac{\vec{l}_0}{\gamma}, \qquad (10)\ [1]$$

$$\Delta\vec{T}_{3\ (S_{o2})} = \Delta\vec{T}_0\gamma, \qquad (11)\ [1]$$

$$V^2 = C^2 - \frac{C^2}{\gamma^2}, \qquad (12)\ [1]$$

$$\gamma = \frac{1}{\sqrt{1-\frac{v^2}{c^2}}}: \text{ Lorentz coefficient} \qquad (13)\ [3]$$

$$\vec{l} = \frac{\vec{l}_0}{\gamma}, \qquad \Delta T = \Delta \vec{T}_0 \gamma, \qquad (15)[3] \qquad (14)[3]$$

$$|V| = \sqrt{c^2 - \frac{c^2}{\gamma^2}}: \text{ Relative velocity of the particle} \qquad (16)\ [1]$$

By using of the speed equation the internal movement of the elementary particles with external appearance, can be modeled and it can show that the movement in the outside of the elementary has a continuous graph.
This explains movement of particles by using the de Broglie wavelength relation ( $\lambda = \frac{h}{p} = \frac{h}{mv}$) the following equation will be obtained. $p_{max} = \frac{h\sqrt{1-\frac{v_{max}^2}{c^2}}}{l_0\sqrt{1-\frac{v^2}{c^2}}}$,

(17) [1]
By using the equation (17) and knowing that quarks are divided to moton in the case of quantized space and time. [1] The limit momentum and maximum speed of protons can be calculated in LHC.
Maximum speed limit : regarding to quantized space and time theory there is a maximum speed limit for charge subatomic particles is equal to $V_{max}$=299792407.5m/s this speed express that the internal time and length quanta elementary particles have a limited capacity for transferring and momentum the extra energy applied to charged particles will be relatively radiated.[1]

**4-Relativity charge formula**

This formula shows that how the nuclear, electrical and magnetic field of charged subatomic particles bond to each other at speed limit.
We define charge as the energy radiated by a particle and we have:

$$E_{max} = \frac{p_{max}c^2}{v} \qquad (18)\ [1]$$

The amount of effect of the internal energy of particles on the surrounding space that is one length quanta or more is defined as electric charge. We calculate the charge using the electromagnetic interaction of positive and negative charges which are at least one length quanta apart together, with using equation 18, we have:[1]

$$q = \sqrt{(8\pi\varepsilon_0 mc^2 l_0)}C \qquad (19)[1]$$

Here $l_0$ is the length quanta, q and m are the charge and active mass and $\varepsilon_0$=8.854×10$^{-12}$ F/m is the vacuum permittivity. By applying the special relativity principles in Equation 19, we will get the following equation:

$$q = \frac{\sqrt{8\pi\varepsilon_0 m_0 c^2 l_0}}{4\sqrt{1-\frac{v^2}{c^2}}}C = \frac{1.602\times10^{-19}}{4\sqrt{1-\frac{v^2}{c^2}}}C \qquad (20)[1]$$

Where $m_0$ =9.109×10$^{-31}$ kg, $m_0$ is the initial active mass, and $l_0$=1.409×10$^{-15}$ m, $l_0$ is length quanta around the particle.
In this formula the active mass protected by the energy momentum limit relation and as a result the absolute value of the basic charge of parting became equal of each other in low speeds and different masses.

## 5- Decay of protons in LHC accelerator

Proton decay performed when two beams of protons radiate to each other in opposite direction at the speed limit .With calculating the Lorentz coefficient for speed limit we will have:

$$\gamma = \frac{1}{\sqrt{1-\frac{299792407.5^2}{c^2}}} = 1722.9 \qquad \sqrt{\gamma} = \frac{1}{4\sqrt{1-\frac{299792407^2}{c^2}}} = 41.51$$

(21)

And it considers The LHC as an electrical field (by relation (20))

$$E\frac{1}{q_0 \times \sqrt{\gamma}} = V \qquad (22) \qquad [1]$$

$$Y = (x \times (m_p \times c^2) \times \frac{1723.9}{41.51} \times \frac{1}{1.602 \times 10^{-19}})$$
$$+ (z \times Egluon \times \frac{1}{1.602 \times 10^{-19}}) - E2 = Yev \quad (23)$$

Y: Energy equivalent mass of The Higgs boson

E2: energy of electromagnetic between protons.

$$E2 = x \times (\frac{8\pi\varepsilon_0 m_0 c^2 l_0}{4 \times 2\pi \times \varepsilon_0 \times L} \times \frac{1}{4\sqrt{1 - \frac{v^2}{c^2}}})$$

In relation (24) x is the number of protons which form a Higgs boson

To determine x the proton structure is applied

$$gluon_{1_1} + u_1 + gluon_{2_1} + d_1 + gluon_{3_1} + u_1 \xrightarrow{\overline{s_{p1}}}$$

$$gluon_{1_2} + u_2 + gluon_{2_2} + d_2 + gluon_{3_2} + u_2 \xrightarrow{\overline{s_{p2}}} \quad (24)\ [1]$$

As said before X is equal to sum of the integer numbers that indicating the number of protons which are sticked to each others with minimum electromagnetic force .These protons form a ultra hot layer of motons and super dimension. Neither the super dimension nor the time and space quanta can absorb or carry that energy.

According relation (24) we have:

The energy of proton is sum of the energy of three quarks and three gluons:

$$E_p = Egluon \times 3 + Eu + Eu + Ed \quad (25)$$

$$Egluon = E_{\max} = \frac{p_{\max} c^2}{v} = 0.88Gev \quad (26)[1]$$

$$E_p = Egluon \times 3 + Eu + Eu + Ed = (3 \times 0.88Gev) + (Mproton \times C^2) = 41.59Gev$$

(27) [1]

**6-Determinations of X:**

After determination of the binding energy of the gluon which are produced in the collision of proton to each other and separation them from electromagnetic energy between protons the x will be obtained

$$x=2 \rightarrow \quad Y=(2\times E_p)+(z\times E_{p-p}gluon)-(\frac{8\pi\varepsilon_0 m_0 c^2 l_0}{4\times 2\pi\times\varepsilon_0\times L}\times\frac{1}{4\sqrt{1-\frac{v^2}{c^2}}})$$

$$=83.18Gev+(z\times 0\bullet 88Gev)-(0\bullet 02Gev\times\frac{l_0}{L}) \qquad (28)$$

$$x=3 \rightarrow \quad Y=(3\times E_p)+(z\times E_{p-p}gluon)-(3\times(\frac{8\pi\varepsilon_0 m_0 c^2 l_0}{4\times 2\pi\times\varepsilon_0\times L}\times\frac{1}{4\sqrt{1-\frac{v^2}{c^2}}}))$$

$$=124.77Gev+(z\times 0\bullet 88Gev)-(3\times 0\bullet 02Gev\times\frac{l_0}{L}) \qquad (29)$$

$$x=4 \rightarrow \quad Y=(4\times E_p)+(z\times E_{p-p}gluon)-(6\times(\frac{8\pi\varepsilon_0 m_0 c^2 l_0}{4\times 2\pi\times\varepsilon_0\times L}\times\frac{1}{4\sqrt{1-\frac{v^2}{c^2}}}))$$

$$=166.36Gev+(z\times 0\bullet 88Gev)-(6\times 0\bullet 02Gev\times\frac{l_0}{L}) \qquad (30)$$

$$Y=xE_p+(\pm z)E_{p-p}gluon)-(x\times(\frac{8\pi\varepsilon_0 m_0 c^2 l_0}{4\times 2\pi\times\varepsilon_0}\times\frac{1}{L})\times\frac{1}{4\sqrt{1-\frac{v^2}{c^2}}}) \qquad (31)$$

L: the distance of active mass to gather protons which shows that length (space) quanta acs like a flexible spring and this is a very fundamental issue. Our function is too sensitive to length decrease and it has a continuous rate because of the continuity of the charge graph.

When x=2 then the resultant impulse of momentum of two protons is in the smallest end and the repulsive force of electromagnetism is the greatest so x=2 will be impossible

If x=4 it means that the square chord is equal to the sides of the square and it is impossible.

So x=4 and bigger amount are impossible because length is quantized.

In relation (31) we heave $3 \geq z \geq -3$ and $z \in Z$ that is the uncertainty of the production of gluon by the relation (26) following amounts are obtained and Statistical calculations must be:

$$E_p = Egluon \times 3 + Eu + Eu + Ed = (3 \times 0.88Gev) + (Mproton \times C^2) = 41.59Gev$$

$x = 3$ (31)

The amount of mass equivalent to energy of Higgs boson without considering the energy of gluons which contains some level of uncertainty, calculates equal to 124.77 Gev

And when the gluons create. For X=3 will be as following:

Z= -1 Y=123.89Gev z=1 Y=125.65Gev
Z= -2 Y=123.01Gev z=2 Y=126.53Gev
Z= -3 Y=122.13Gev z=3 Y=127.41Gev

The range of changes is equal to Equivalent to electromagnetic energy changes:

$\Delta Y = 0 \bullet 02Gev$ (32) $\sigma = 0.88Gev$ Standard deviation (33)

The frequency of dates can be found from testing in LHC (Cern) and the decay graph can be drowning. The result of the CMS detector in Cern is shown in

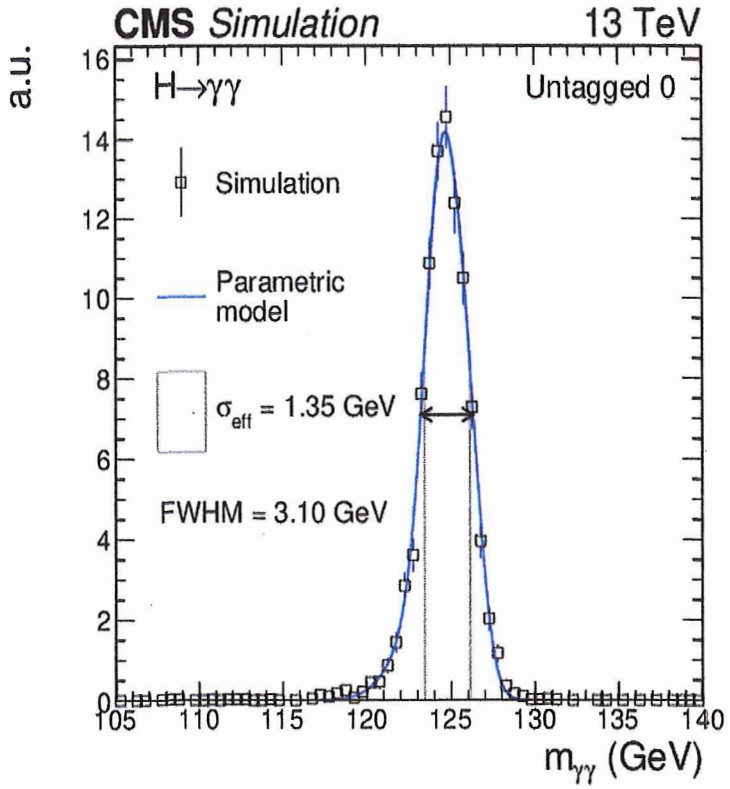


the graph 2. [5]
in the graph 2 the function(Y) of Higgs boson decay energy is calculated by Z measures. In this graph the produced force by gluon are shown as the weak interaction force between protons and the electromagnetice force as repulsive, respectively and.the diffrentiation between theses two, indicates the energy of the gamma readiation.

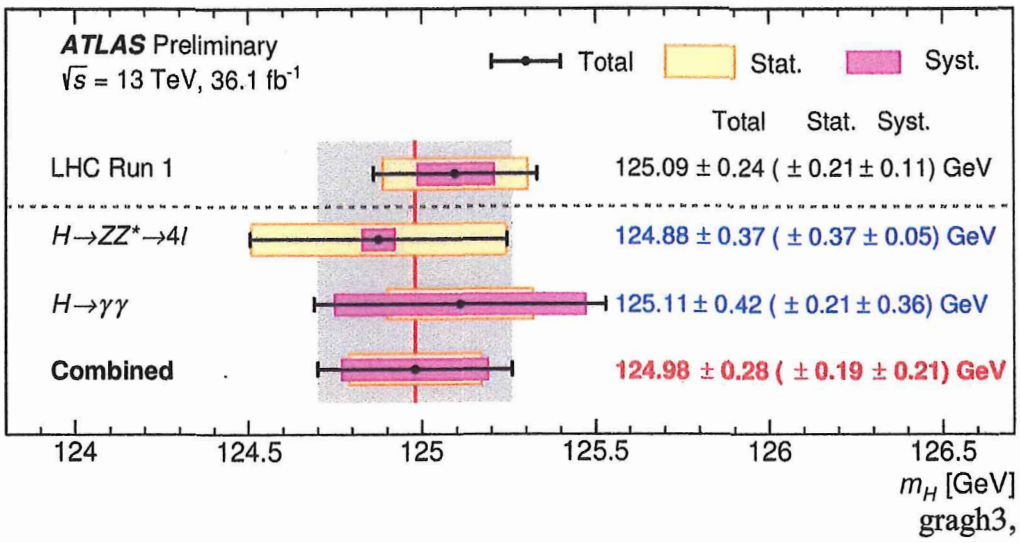


gragh3,

In the gragh 3 ,[6] the decay of Higgs boson to gamma radiation and $ZZ^*$ particle has been shown in Gamma decay, the function is:
Z=1

$$Y = 3E_p + (1 \times E_{p-p} gluon) - ((\frac{8\pi\varepsilon_0 m_0 c^2 l_0}{4 \times 2\pi \times \varepsilon_0} \times \frac{1}{L}) \times \frac{1}{4\sqrt{1-\frac{v^2}{c^2}}}) \quad (34)$$

$$Y = 124.77Gev + 0.88Gev - (3 \times 0.02Gev \frac{l_0}{L}) \quad (35)$$

In the equation (34), the electromagnetic force works until the gluon energy reaches to zero. The Gamma decay Energy range in the graph 3 is because of this issue

**7-Conclusion:**

By using the theory of quantized space and time the mass if Higgs boson calculated precisely to $124.77Gev \pm 02Gev$ Due to the ability of determination of maximum speed of charged particeles in accelator LHC by considering the time and space quantized the caculated amont is completey being consistent to experimental data gaddering for determinating the mass of Higgs boson in LHC .This being consistent

can be considered as a proof of the grate potentials of the theory of quantized space and time to explains, predict and calculate the more various physical phenomena.

References

[1]Hadronic journal volume 33, Number3, June 2010 Quantized space a- Time and internal structure of elementary particles: A new model 249 Hamid Reza Karimi Electrical engineering Department Azadof south of Tehran 17776-13651, Iran hr.karimy@gmail.com.

[2].study of the simulation of the ATLAS fast Tracker system –LH accelerator (pag13).by Aristoole university of Thessaloniki Faculty of Scinces School of physics

[3] . Robert Resnick, Introduction to Special Relativity, Wiley Fastern Private Limited, 1972.

[4]The Fermi Solution: Essays on Science,Hans Christian Von Baeyer Courier Corporation, Dey 12, 1379 AP - Science - 172 pages

[5].A measurement of the Higss boson mass in the diphoton decay channel the CMS collaboration .contact:cms-pag-convenesrs-higgs@cern.ch /2019/09/30

[6] Measurement of the Higgs boson mass in the $H\rightarrow ZZ^{*}\rightarrow 4\ell$ and $H\rightarrow\gamma\gamma$ channels with $s\sqrt{}=13$TeV pp collisions using the ATLAS detector/ATLAS-CONF-2017-046 5 July 2017/*Figure 12*
https://atlas.web.cern.ch/Atlas/GROUPS/PHYSICS/CONFNOTES/ATLAS-CONF-2017-046/